AD-A049 499 ILLINOIS UNIV AT URBANA-CHAMPAIGN DEPT OF AERONAUTICA--ETC F/G 21/9.2
MODELING OF CONVECTIVE MODE COMBUSTION THROUGH GRANULATED PROPE--ETC(U)
OCT 77 H KRIER, J A KEZERLE AFOSR-77-3115

UNCLASSIFIED AAE-77-17 AFOSR-TR-78-0007 NL

OF 2
AD A049499

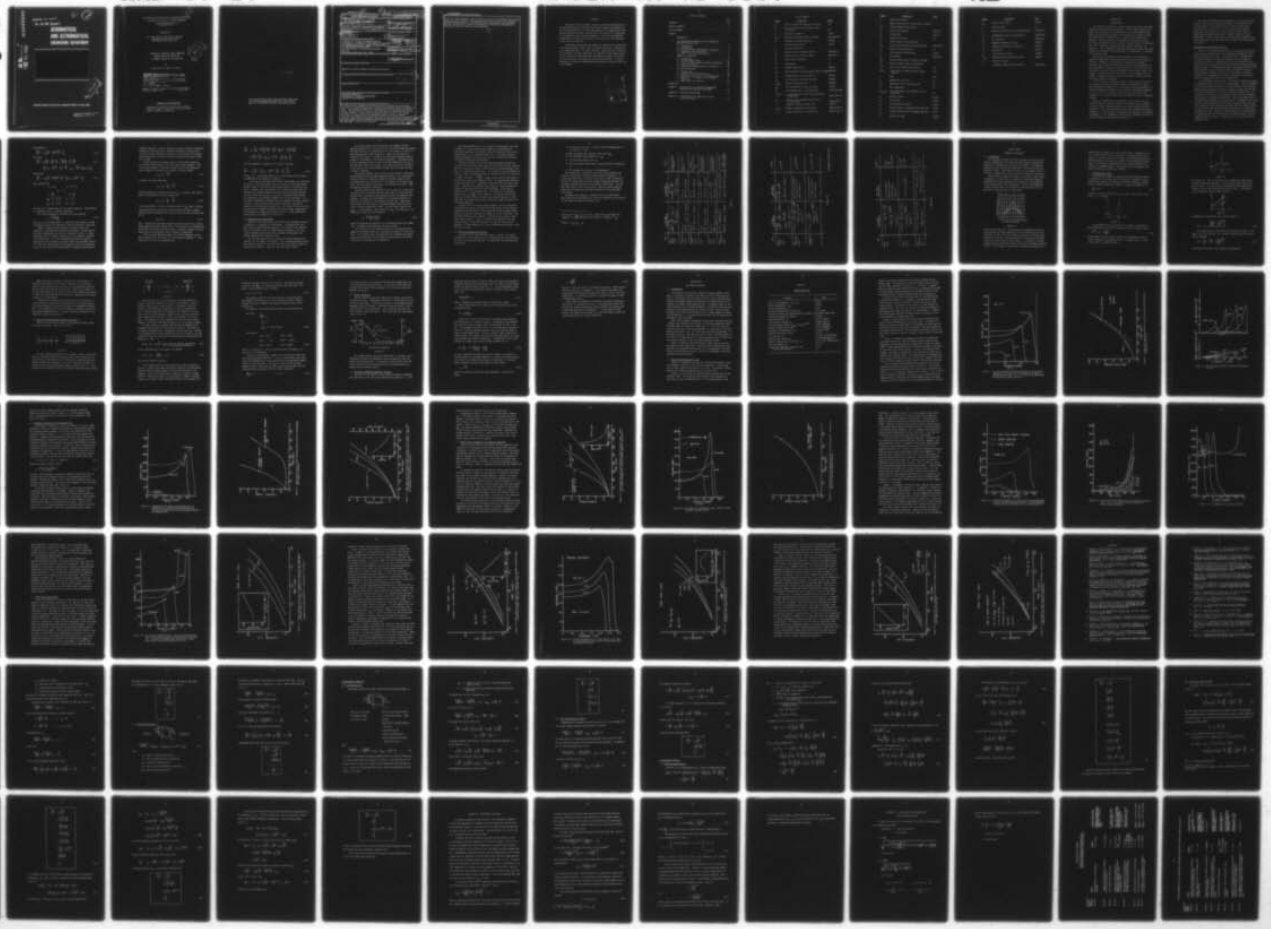

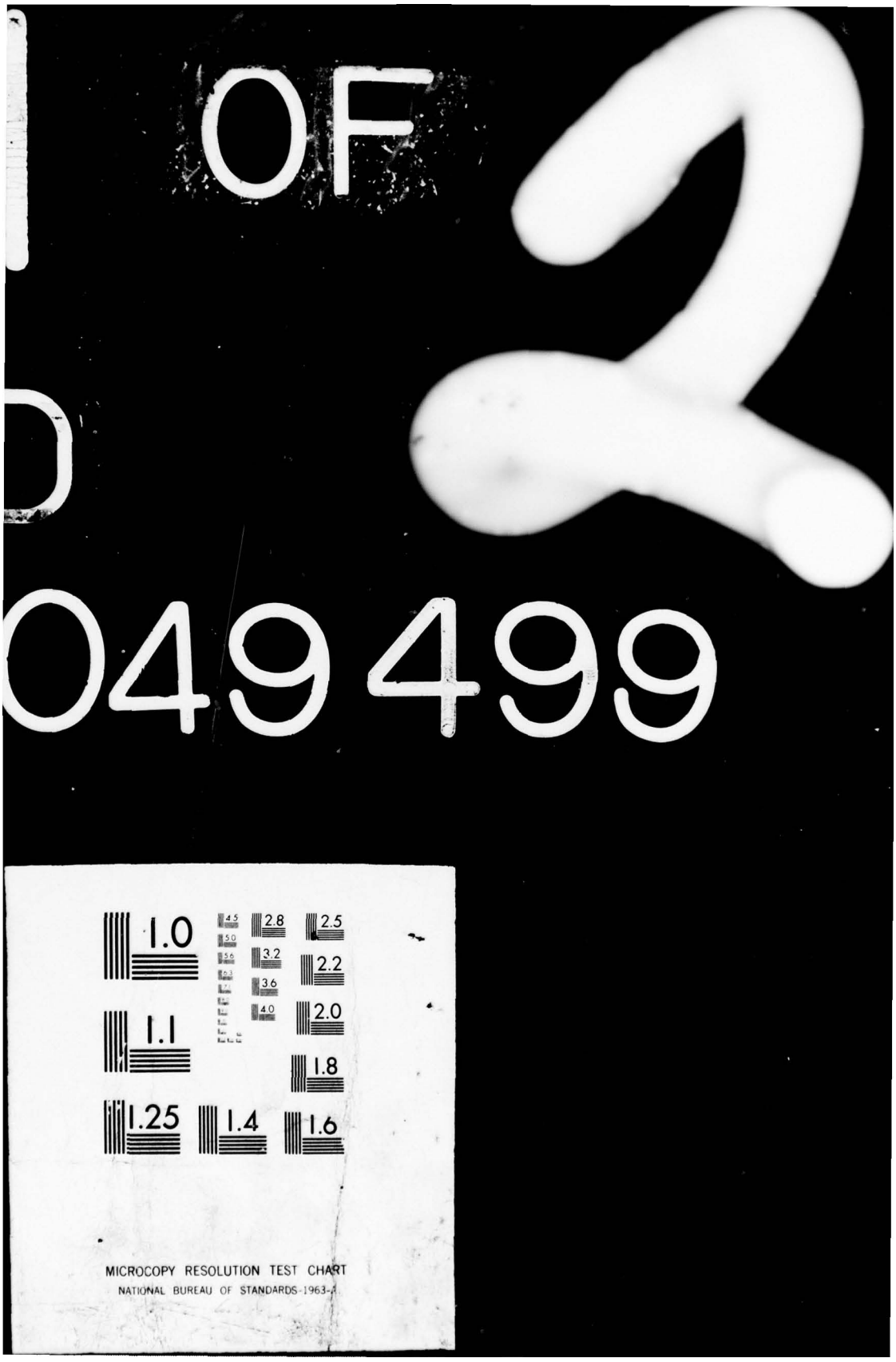
OF
049499
1.0
1.1
1.25
1.4
1.6
1.8
2.0
2.2
2.5
2.8
3.2
3.6
4.0
4.5
5.0
5.6
6.3
MICROCOPY RESOLUTION TEST CHART
NATIONAL BUREAU OF STANDARDS-1963-A

AFOSR-TR- 78-0007

AAE

AERONAUTICAL AND ASTRONAUTICAL ENGINEERING DEPARTMENT

ENGINEERING EXPERIMENT STATION, COLLEGE OF ENGINEERING, UNIVERSITY OF ILLINOIS, URBANA

Aeronautical and Astronautical Engineering Department
University of Illinois at Urbana-Champaign

Technical Report AAE-77-17
UILU-Eng 77 0517

Prepared for

Air Force Office of Scientific Research
Aerospace Sciences Directorate
Bolling Air Force Base, D.C.

MODELING OF CONVECTIVE MODE COMBUSTION THROUGH GRANULATED PROPELLANT TO PREDICT TRANSITION TO DETONATION

by

Herman Krier and James A. Kezerle

Approved for public release; distribution unlimited
Grant No. AFOSR 77-3115 October 1977

Qualified requestors may obtain additional copies from the Defense Documentation Center; all others should apply to the National Technical Information Service.

UNCLASSIFIED

SECURITY CLASSIFICATION OF THIS PAGE (When Data Entered)

AAE-77-17 UILU-ENG-77-0517

REPORT DOCUMENTATION PAGE

READ INSTRUCTIONS BEFORE COMPLETING FORM

1. REPORT NUMBER: AFOSR-TR-78-0007	2. GOVT ACCESSION NO. / 3. RECIPIENT'S CATALOG NUMBER
4. TITLE (and Subtitle): MODELING OF CONVECTIVE MODE COMBUSTION THROUGH GRANULATED PROPELLANT TO PREDICT TRANSITION TO DETONATION	5. TYPE OF REPORT & PERIOD COVERED: FINAL rept. 1 Oct 76 - 30 Sep 77 / 6. PERFORMING ORG. REPORT NUMBER
7. AUTHOR(s): HERMAN KRIER, JAMES A. KEZERLE	8. CONTRACT OR GRANT NUMBER(s): AFOSR-77-3115 new
9. PERFORMING ORGANIZATION NAME AND ADDRESS: UNIVERSITY OF ILLINOIS AT URBANA-CHAMPAIGN, AERONAUTICAL & ASTRONAUTICAL ENGINEERING DEPARTMENT, 101 TRANSPORTATION BLDG, URBANA, ILLINOIS 61801	10. PROGRAM ELEMENT, PROJECT, TASK AREA & WORK UNIT NUMBERS: 2308A1 / 61102F / A1
11. CONTROLLING OFFICE NAME AND ADDRESS: AIR FORCE OFFICE OF SCIENTIFIC RESEARCH/NA, BLDG 410, BOLLING AIR FORCE BASE, D C 20332	12. REPORT DATE: Oct 77 / NUMBER OF PAGES: 90 / 105 p.
14. MONITORING AGENCY NAME & ADDRESS (if different from Controlling Office)	15. SECURITY CLASS. (of this report): UNCLASSIFIED / 15a. DECLASSIFICATION/DOWNGRADING SCHEDULE

16. DISTRIBUTION STATEMENT (of this Report)

Approved for public release; distribution unlimited.

17. DISTRIBUTION STATEMENT (of the abstract entered in Block 20, if different from Report)

DDC JAN 31 1978 F

18. SUPPLEMENTARY NOTES

19. KEY WORDS (Continue on reverse side if necessary and identify by block number)

PROPELLANT COMBUSTION
DEFLAGRATION TO DETONATION TRANSITION
TWO-PHASE FLUID MECHANICS

20. ABSTRACT (Continue on reverse side if necessary and identify by block number)

Derivation of the two-phase (reactive particle) unsteady-flow conservation equations are presented based upon the generally accepted concept of separated-flow. The resulting formulation is compared with those equations derived by others, and questions are raised as the correctness or interpretation made by previous modelers. Details of the numerical method chosen to solve these equations (an explicit two-step MacCormack scheme) are also presented. Solutions are presented that predict the pressure wave build-up and accelerating ignition (flame) front for highly loaded beds of granulated solid propellant → over

DD FORM 1 JAN 73 1473 EDITION OF 1 NOV 65 IS OBSOLETE

UNCLASSIFIED 176 005

SECURITY CLASSIFICATION OF THIS PAGE (When Data Entered)

fixed in a rigid container. Some discussion is given of the sensitivity of these predictions as a function of the assumed constitutive relations for interphase heat and momentum transfer, for particle-particle resistance, and propellant burning rate functions. As yet no unambiguous criterion for deflagration-to-detonation transition (DDT) has been presented.

ABSTRACT

Derivation of the two-phase (reactive particle) unsteady-flow conservation equations are presented based upon the generally accepted concept of separated-flow. The resulting formulation is compared with those equations derived by others, and questions are raised as the correctness or interpretation made by previous modelers. Details of the numerical method chosen to solve these equations (an explicit two-step MacCormack scheme) are also presented.

Solutions are presented that predict the pressure wave build-up and accelerating ignition (flame) front for highly loaded beds of granulated solid propellant fixed in a rigid container. Some discussion is given of the sensitivity of these predictions as a function of the assumed constitutive relations for interphase heat and momentum transfer, for particle-particle resistance, and propellant burning rate functions. As yet no unambiguous criterion for deflagration-to-detonation transition (DDT) has been presented.

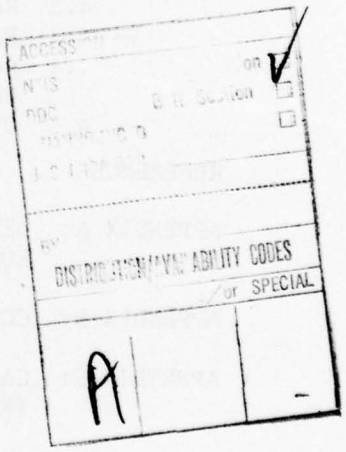

TABLE OF CONTENTS

LIST OF SYMBOLS

Symbol	Definition	Units
A_g	Cross sectional area occupied by the gas	in^2
A_p	Cross sectional area occupied by solid particles	in^2
b_1	Burning rate constant	in/sec
b_2 B_2	Burning rate proportionality constant	$in/sec\text{-}psia)^n$
B_V	Covolume of burning propellant	in^3/Lbm
c	Mixture speed of sound	in/sec
C_f	Friction Coefficient	
C_p	Specific heat at constant pressure	BTU/Lbm-°R
C_V	Specific heat at constant volume	BTU/Lbm-°R
d_p	Solid particle diameter	in
D_B	Bed diameter	in
E_g	Thermal energy of gas	BTU/Lbm
E_{g_o}	Total energy of the gas(includes kinetic energy)	BTU/Lbm
E_p	Thermal energy of solid particles	BTU/Lbm
E_{p_o}	Total energy of the solid particles	BTU/Lbm
E_{chem}	Chemical energy released	BTU/Lbm
f_{gp}	Gas-solid particle interaction drag	Lbf/in^3
g_c	Gravitational unit conversion factor	$Lbm\text{-}in/Lbf\text{-}sec^2$
h_c,HTC	Gas-solid particle convective heat transfer coefficient	$BTU/in^2\text{-}sec\text{-}°R$
h_{c_e}	Convective heat transfer coefficient to the end walls	BTU/in-sec-°R
K	Constant in particle stress term	Lbf/in^2
k_g,K_g	Thermal conductivity of gas phase	$BTU/in^2\text{-}sec\text{-}°R$
K_w	Thermal conductivity of solid walls	$BTU/in^2\text{-}sec\text{-}°R$

Symbol	Definition	Unit
n	Burning rate index	
N	Number of grid points in which data is stored	
Nu_w	Nusselt number of solid walls	
P_i	Initial gas pressure	Lbf/in^2
P_g	Gas pressure	Lbf/in^2
$\overline{P}_w$	Perimeter of the bed	in
Pr	Prandtl number of the gas phase	
Q_{pg}	Heat transfer from gas to solid particles	BTU/in^3-sec
r_p	Radius of solid particles	in
$\dot{r}$	Solid particles burning rate	in/sec
$\overline{R}_g$	Gas constant	BTU/Lbm-°R
Re_p	Reynolds number based on particle diameter	
Re_D	Reynolds number based on bed diameter	
S,A	Total cross sectional area of bed	in^2
$(S/V)_p$	Surface area to volume ratio for single particle	in^{-1}
t	Time	μsec
T_g	Temperature of the gas	°R
T_p	Temperature of the solid particles	°R
T_w	Wall temperature	°R
T_{ign}, T_{ig}	"Bulk temperature" for ignition of solid particles	°R
u_m	Mixture velocity	in/sec
u_g	Gas velocity	in/sec
u_p	Solid particles velocity	in/sec
u_w	Mixture velocity evaluated at the end walls	in/sec
u_{w_p}	Particle velocity due to breakage from wall	in/sec
V_f	Flame front speed	in/msec

Symbol	Definition	Unit
V_{p_w}	Pressure front speed	in/msec
x	Linear distance	in
Γ_g	Production rate of gas from solid particles	Lbm/in^3-sec
Γ_p	Disappearance rate of solid particles	Lbm/in^3-sec
μ_g	Gas viscosity	Lbm/in-sec
ρ_1	Apparent gas density ($= \rho_g\phi$)	Lbm/in^3
ρ_2	Apparent solid density ($= \rho_p(1-\phi)$)	Lbm/in^3
ρ_g	Gas density	Lbm/in^3
ρ_p	Solid particles density	Lbm/in^3
τ_s, τ_p	Particle-particle interaction force	Lbf/in^3
ϕ	Porosity ($= A_g/S$)	
Φ	Interphase convective heat transfer	BTU/in^3-sec

CHAPTER ONE

INTRODUCTION

The ability to calculate the fluid dynamics that result from flame spreading and pressure wave formation in a bed of highly loaded, small grain, solid propellant is the motivation for the work reported here. There have been previous efforts at the University of Illinois, under the direction of Dr. Herman Krier, to analyze such transient flow problems. These include the work reported by Van Tassell and Krier [1], Krier and Gokhale [2], Krier, Rajan, and Van Tassell [3], Dimitstein [4], Krier, Dimitstein, and Gokhale [5], and Krier, Gokhale, and Hughes [6]. This considerable background proved quite useful and indeed essential in allowing this detailed work to be completed in a relatively short period of time.

There have been several different approaches in developing the appropriate governing conservation equations to describe the physics of the flow. Although it is difficult to categorize all the models published, one of the main differences stems from the assumptions that (a) the equations of motion be derived based on the center of mass of each phase, versus (b) those derived based on the center of mass of the mixture. In addition to that distinction, there are models that (c) attempt to define rigorous average-flow properties in which one phase does <u>not</u> constitute a continuum.

A brief review was recently prepared by Krier [7] which discusses the concepts resulting in equations based on assumption (a) versus those obtained by assumption (b). Derivations utilizing assumption (a) have been termed the "separated-flow" approach, those using assumption (b) are called the "continuum-mixture" approach, and those using assumption (c) might come under the broad definition of an "averaging" approach.

The work reported here is an attempt to first, derive the conservation equations using the concept of separated flow (as defined in the text by Wallis [8]) and second, to develop an accurate solution technique to solve the problem of unsteady flows through packed beds of propellant. The derivation of the conservation equations is presented in Appendix A. The equations derived here are compared with those of other investigators and discussed in Chapter II.

This work also includes some modeling that will allow the calculations to be utilized at high gas pressures. As discussed in the text that follows, such items as (a) an accurate non-ideal high pressure equation of state, (b) a better value for the mixture sound speed, (c) a model for the axial particle stress, and (d) a temperature dependent viscosity were included. With all of the above inputs it will be shown that this code provides reasonable and consistant pressure wave and flame front histories over widely varied flow regimes.

Deflagration-to-Detonation Transition

Studies of the spontaneous deflagration-to-detonation transition (DDT) in gases indicate that in an accelerated deflagration a shock front runs ahead of the flame. The present work is concerned with such dynamic behavior in granular propellant, with an attempt to elucidate the details of propagation of the flame (ignition) front, pressure fronts and possible shock fronts before development of steady-state detonation. The experimental work of Bernecker and Price[35] with granular explosives and the work of Gipson and Macek[36] with DDT in solid explosives indicate clearly that in the study of buildup to detonation it is important to know the relationship of the pressure (shock or compression) fronts to the flame front.

In the problem of concern here a fraction of the propellant grains are assumed ignited at one end of a closed chamber. The mass generated in the ignition region accelerates the flame forward, with the region behind the flame rapidly increasing in pressure as more and more mass is being generated due to the pressure-sensitive burning rate. Calculations then show that a steep pressure front begins to accelerate and attempts to overtake the flame front. When this happens there is an almost abrupt increase in the flame speed. A detonation can be said to have started when the pressure front proceeds the flame front and they both attain about the same high speed. We are of course limited by our numerical differencing scheme to indicate a true shock front proceeding the flame. But with a rapid transition of the flame front in conjunction with the interaction of the pressure fronts, one can suppose that DDT can occur. A discussion of a criterion for DDT is presented later.

CHAPTER TWO

THE CONSERVATION EQUATIONS FOR ONE-DIMENSIONAL UNSTEADY TWO-PHASE FLOW

2.1 Introduction

The one-dimensional conservation equations for a two-phase reactive mixture have been derived by most investigators through the concept of separated flow as defined in the text by Wallis [8]. This approach considers two distinct flows, each through a separate control volume, such that the sum of the volumes represents an average mixture volume and the sums of the properties of each flow represent average mixture properties of the fluid. With this approach, separate equations for continuity, momentum, and energy are written for each phase and are solved with a state equation to describe the overall flow. Panton [10] has provided the rigorous formulation with the important assumptions required to express these field balance equations. There are, of course, many other analyses that have arrived at similar forms of the equations. Some of these would include the work by Anderson and Jackson [11], Pigford and Baron [12], Green and Naghdi [13], Crowe [14], Solbrig, Mortenson, Lyczkowski [15], Hughes [16], Kuo and Summerfield [17], Gough [18], Nigmatulin [19], Gidaspow [20], and Zuber [21]. Not all of these investigations have treated the two energy equations, as is done here.

2.2 Assumptions

The important assumptions upon which this separated flow model is based are listed below.

1) The two phases are assumed interdispersed, but separate, coupled only by the appropriate interaction terms.
2) Each phase is a continuum and therefore derivatives are uniquely defined.
3) The total cross sectional area is the sum of the gas and solid flow areas. (The problem is quasi-one-dimensional).
4) Solid particles are large compared to molecules and hence do not contribute to the total pressure of the mixture.
5) When combustion of particles causes mass transfer between the phases, the solid phase always loses mass while the gas phase gains it, i.e., $\Gamma_c \geq 0$.

6) The diameter of a typical particle can be thought of as the average diameter of the total number of particles.
7) All gases obey the non-ideal Noble-Abel equation of state with a variable co-volume.
8) Heat transfer to the particles due to conduction and radiation is neglected.
9) The density of the solid phase is constant.
10) The equations are laminar in the sense that turbulent flow due to the two-phase nature of the fluid has been averaged out. (See Panton [10] for additional discussions regarding this assumption.)
11) The gases are inviscid except for their action on the particles through the drag term.
12) The fluid properties C_p and C_v are assumed constant, but gas viscosity and conductivity are generally known functions of temperature.

2.3 The Conservation Field Balance Equations

Some of the details in the derivation of the six field balance equations have been presented in Appendix A. In order to specifically describe the state of a two-phase fluid one needs equations to solve for the following variables: ρ_g, u_g, T_g, P_g, ϕ, u_p, and T_p. The state equation is added to the field balance equations to obtain the seven required equations. Therefore two continuity equations, two momentum equations, and two energy equations will be necessary. These equations are listed below in operator form.*

Gas Continuity

$$\frac{\partial \rho_1}{\partial t} = - \rho_1 \frac{\partial u_g}{\partial x} - u_g \frac{\partial \rho_1}{\partial x} - \frac{\rho_1 u_g}{S} \frac{\partial S}{\partial x} + \Gamma_g \tag{2.1}$$

Solid Continuity

$$\frac{\partial \rho_2}{\partial t} = - \rho_2 \frac{\partial u_p}{\partial x} - u_p \frac{\partial \rho_2}{\partial x} - \frac{\rho_2 u_p}{S} \frac{\partial S}{\partial x} - \Gamma_g \tag{2.2}$$

Gas Momentum

$$\frac{\partial u_g}{\partial t} = - u_g \frac{\partial u_g}{\partial x} - \frac{\phi}{\rho_1} \frac{\partial P}{\partial x} - \frac{(u_g - u_p)}{\rho_1} \Gamma_g - \frac{\bar{F}}{\rho_1} \tag{2.3}$$

---

* See list of nomenclature for definitions of all symbols in equations (2.1) - (2.6).

Solid Momentum

$$\frac{\partial u_p}{\partial t} = - u_p \frac{\partial u_p}{\partial x} - \frac{(1-\phi)}{\rho_2} \frac{\partial \tau_p}{\partial x} + \frac{\bar{F}}{\rho_2} \tag{2.4}$$

Gas Energy

$$\frac{\partial E_g}{\partial t} = -u_g \frac{\partial E_g}{\partial x} - \frac{u_g P}{\rho_1 S} \frac{\partial S}{\partial x} - \frac{u_g P}{\rho_1} \frac{\partial \phi}{\partial x} - \frac{\phi P}{\rho_1} \frac{\partial u_g}{\partial x} \tag{2.5}$$

$$- \frac{\Gamma_g}{\rho_1} (E_g - E_g^{chem}) + \frac{\Gamma_g}{\rho_1} \left(\frac{u_g^2}{2} - u_g u_p + \frac{u_p^2}{2} \right) + \frac{\bar{F}}{\rho_1} (u_g - u_p) - \frac{\Phi}{\rho_1}$$

Solid Energy

$$\frac{\partial E_p}{\partial t} = - u_p \frac{\partial E_p}{\partial x} + \frac{(1-\phi) u_p}{\rho_2} \frac{\partial \tau_p}{\partial x} + \frac{\Gamma_g}{\rho_2} (E_p + E_p^{chem}) + \frac{\Phi}{\rho_2} \tag{2.6}$$

Here, specifically

$$\rho_1 = \phi \rho_g \quad , \quad \rho_2 = (1-\phi)\, \rho_p$$

$$\Gamma_g = - \Gamma_p$$

$$\phi = \frac{A_g}{S} \qquad 1 - \phi = \frac{A_p}{S}$$

$$E_{g_o} = E_g + \frac{1}{2} u_g^2 \qquad E_g = C_v T_g$$

$$E_{p_o} = E_p + \frac{1}{2} u_p^2 \qquad E_p = C_p T_g$$

The subscript "g" denotes gas and "p" denotes particle. The subscript "o" stands for (total) stagnation conditions.

The seventh equation is the Noble-Abel state equation

$$P_g = \frac{\rho_g \bar{R}_g T_g}{1 - \rho_g B_v} \tag{2.7}$$

where B_v is the covolume which is a function of gas density, so that at extreme pressures, an appropriate non-ideal equation is satisfied.

There is currently concern whether the quasi-linear, one-dimensional, separated flow equations listed above, or those derived from other formulations, constitute an hyperbolic system. A recent examination of such systems with regard to this question is carried out by Hughes [6]. It is the contention here that the system of equations must be hyperbolic to provide stable and meaningful results. It is also felt that knowledge of the nature of the roots (characteristics) of the equations can provide much information concerning the

boundary conditions, initial conditions and other auxiliary information required to solve the system. Therefore changes in the form of the six field balance conservation equations (in particular the two momentum balances) may be required in order to provide a well-posed, hyperbolic system.

Another reason for alternate forms of these balance equations arises from the derivation of the solid phase energy equation. There can be some ambiguity concerning the definition of the appropriate total enthalpy of the particles. Equation 2.6 above assumes

$$H_{p_o} = E_p + \frac{u_p^2}{2} \tag{2.8}$$

instead of the usual definition

$$H_{p_o} = E_p + \frac{P_p}{\rho_p} + \frac{u_p^2}{2} \tag{2.9}$$

Since the meaning of a particle pressure, P_p, is unclear, some investigators, like Rudinger [27] have assumed that

$$H_{p_o} = E_p + \frac{P_g}{\rho_p} + \frac{u_p^2}{2} \tag{2.10}$$

is more appropriate. All of these definitions for H_{p_o} imply a possible interchange between the particle internal energy and kinetic energy. Another possible assumption that does not allow for such an energy transfer is

$$H_p = E_p \tag{2.11}$$

only. Assuming that the total stagnation enthalpy is only the internal energy appears plausible because first, the solid phase is incompressible and second, it does not constitute a gas. Therefore a change in kinetic energy should not necessarily imply a change in temperature.

Particle energy equations based on the three assumptions listed above (equations 2.8, 2.10, and 2.11) are derived in Appendix A. Final forms for the latter two assumptions are

$$\frac{\partial E_p}{\partial t} = - u_p \frac{\partial E_p}{\partial x} - \frac{(1-\phi)P_g}{\rho_2} \frac{\partial u_p}{\partial x} - \frac{u_p P_g}{\rho_2} \frac{\partial(1-\phi)}{\partial x} - \frac{(1-\phi)u_p}{\rho_2} \frac{\partial P_g}{\partial x}$$

$$+ \frac{(1-\phi)u_p}{\rho_2} \frac{\partial \tau_p}{\partial x} + \frac{\Gamma_g}{\rho_2} [E_p + E_p^{chem}] - \frac{u_p P_g}{S\rho_p} \frac{\partial S}{\partial x} + \frac{\Phi_p}{\rho_2} \qquad (2.12)$$

for the assumption in equation 2.10, and the following,

$$\frac{\partial E_p}{\partial t} = - u_p \frac{\partial E_p}{\partial x} + \frac{\Gamma_g}{\rho_2} [E_p + E_p^{chem} - \frac{u_p^2}{2}] + \frac{\Phi_p}{\rho_2} + \frac{\overline{Fu}_g}{\rho_2} \qquad (2.13)$$

for $H_{p_o} = E_p$. The systems based on all three variations were studied and differences are reported in Chapter 4.

It has been duly observed that several investigators, in particular Kuo et al., [17,22] and Gough [18], do not write a solid phase energy balance symmetric with the gas phase energy balance, like equation 2.6 above. Instead, these investigators have decided to simply solve the unsteady heat conduction equation for the solid particle and monitor the heat gained from the gas in the form of convective heat transfer. This approach was not deemed acceptable for the work done here. It is considered fundamentally necessary that when adding the energy equations 2.5 and 2.6, the classical mixture energy equation is obtained as required in the discussion by Wallis [8]. This leads to the utilization of an overall or "lumped" parameter for particle energy (temperature) which requires an appropriate ignition criteria. These discrepancies between models are summarized in Table 2-2.

2.4 Comparison with Other Models

Table 2.1 lists both the gas and particle phase momentum equations as reported by six groups of investigators. In preparing the table some work was required because several of the equations were reported only in conservative form. As demonstrated in Appendix A, the continuity equation must be utilized to transform the momentum field balance equations into "operator" form.

The left hand side (L.H.S.) of both field balance equations are identical for all models, as expected. The two momentum equations used here generally agree well with those of other investigators using the separated flow-concept. There are some differences, however.

In the form used by Krier and Kezerle, for example, the gas pressure gradient term is missing from the solid phase momentum equation. The reason for this, as pointed out in the next chapter, is that in so doing the equations become hyperbolic. Hughes [6] has shown that retention of the term $-(1-\phi)\frac{\partial P}{\partial x}$ in the solid phase momentum equation results in the mechanical set being non-hyperbolic. The form derived in this study agrees with the work of Kuo and Summerfield [17] but not with the later work of Kuo, et al., [22] where pressure was included in the term τ_p, nor with the model of Gough [18] or Culick [23] where the term is retained.

The pressure gradient term is also the main source of differences between models in the gas-phase momentum equation. All investigators write this term as the partial gradient of pressure except for Kuo and Summerfield [17], who write it as the gradient of a partial pressure. The later model by Kuo et al., [22] subtracts the term $-P\frac{\partial \phi}{\partial x}$ by redefining the drag coefficient.

The final forms of the equations given in Table 2.1 by Krier and Van Tassell [1] are distinct from the other models in that they were derived from a continuum mixture approach and not the separated flow approach. An additional term appears in each momentum equation as explained in Reference [6] and supported by Soo [24]. These terms arise during the splitting of the mixture momentum equation and are called "inertial interaction" terms. Also the typical source term $\Gamma_g(u_g - u_p)$ now appears in both phases as $\Gamma_g(u_g - u_m)$ and $\Gamma_g(u_g - u_m)$ where u_m is a mean velocity defined as

$$u_m = \frac{(\rho_1 u_g + \rho_2 u_p)}{(\rho_1 + \rho_2)} \tag{2.14}$$

These continuum-derived equations are included here mainly for comparison. In general those equations are more rigorous.

The first five sets of momentum equations, although derived by apparently different means, have essentially arrived at the same final form. It is possible that this means that the averaging and control volume techniques match the separated flow derivation as utilized by Culick and as presented here in Appendix A.

The energy equations of all six groups of investigators are shown in Table 2.2. The gas phase energy equations of both Gough and Culick were reported in convenient "operator" (Eulerian) form and were copied directly. The equations of Kuo and his co-workers required careful manipulation to change them into this form from the conservative form in which they were reported.

Focusing attention first on the gas-phase energy equations one can see that the control volume technique utilized here yields equations which are surprisingly close to those derived by other approaches, with only a few significant differences. In the model of Kuo and Summerfield there is a minor difference in that the pressure work term is written as $-\phi P \frac{\partial u_g}{\partial x}$ instead of $- P \frac{\partial (\phi u_g)}{\partial x}$. Gough, Culick, and the later model by Kuo use this latter, more acceptable form. An unexplainable difference is the additional term $- P_g \frac{\partial \phi}{\partial t}$ used by Gough and Kuo, Koo, Davis, and Coates. Gough also has an extra term $\Gamma_g (P_g/\rho_g)$. Other discrepancies between the work done here and that of Kuo *et al.*, arise from his re-definition of the interphase drag. The result is an additional, unusual term, $u_p P_g \frac{\partial \phi}{\partial x}$ in their equation. The model of Culick correlates well with the model used here, except that he chooses to place some terms in the gas phase equation which more properly belong in the solid phase equation.

Turning to the solid phase energy balances, one sees immediately that neither Kuo and his co-workers nor Gough writes such an equation. Instead they have resorted to calculating the particle surface temperature by solving the unsteady heat conduction in the solid phase. Kuo and Summerfield have made comments in defense of not writing a solid phase energy equation. There is certainly some question as to what mixture energy is being conserved when one does not write such an equation in a form symmetrical to the gas phase energy equation as done here and by Culick.

2.5 Notes on Constitutive Relations

In order to solve the equations listed in section 2.3 several variables must be set through the use of known physical laws governing the critical interaction processes. In particular, the following must be specified.

1) An ignition criterion, in terms of the bulk temperatures of the solid, $T_p = E_p/C_v$.

2)* The inter-phase heat transfer coefficient, $\bar{h}_{gp}$.

3)** The inter-phase drag coefficient, f_{gp}.

4) The propellant burning rate, $\dot{r}_p$.

5) The axial normal stress due to particle-particle interaction, τ_s.

6) The variation of viscosity with temperature.

The constitutive relations as used here, which determine the relations listed above, are given and discussed in Appendix B. It can be noted here that in contrast to the earlier work of Dimitstein [4] only the stated drag laws were changed through multiplication by a variable constant and not the heat transfer coefficient. Also the wall shear forces, heat losses to walls, and mass sources from the walls were not necessary and properly neglected in this one-dimensional model.

Although little emphasis is placed on these relations here, their proper form and function are critically important to the success of this model for reactive two-phase flow.

---

*Note that $\Phi \equiv \bar{h}_{gp} (T_g - T_p) \phi (S/V)_p$, where $(S/V)_p$ represents the surface to volume of the particle, which for a sphere = $3/r_p$.

**Here, $\bar{F} = f_{gp} (u_g - u_p)$

MODEL	GAS PHASE MOMENTUM EQUATION	SOLID PHASE MOMENTUM EQUATION	COMMENTS
Krier/ Kezerle [1977]	$(L.H.S)_g$ $\phi\rho_g(\frac{\partial u_g}{\partial t} + u_g\frac{\partial u_g}{\partial x}) = -\Gamma_g(u_g - u_p)$ $- \phi\frac{\partial P_g}{\partial x} - f_{gp}(u_g-u_p)$	$(L.H.S.)_p$ $(1-\phi)\rho_p(\frac{\partial u_p}{\partial t} + u_p\frac{\partial u_p}{\partial x}) =$ $- (1-\phi)\frac{\partial \tau_s}{\partial x} + f_{gp}(u_g-u_p)$	No pressure gradient in solid phase.
Kuo/ Summerfield [1974]	$(L.H.S.)_g =$ $-\frac{\partial}{\partial x}(\phi P_g) - f_{gp}(u_g - u_p) - \Gamma_g(u_g-u_p)$	$(L.H.S.)_p =$ $-\frac{\partial}{\partial x}[(1-\phi)\tau_s] + f_{gp}(u_g-u_p)$	Gradient of partial pressure
Kuo/Koo/Davis Coates [1976]	$(L.H.S.)_g =$ $-\phi\frac{\partial P_g}{\partial x} - f_{gp}(u_g - u_p) - \Gamma_g(u_g-u_p)$	$(L.H.S.)_p =$ $-\frac{\partial}{\partial x}[(1-\phi)\tau_p] + f'_{gp}(u_g-u_p)$	τ_p includes P_g The f' term includes $- P\frac{\partial \phi}{\partial x}$.
Gough	$(L.H.S._g =$ $-\phi\frac{\partial P_g}{\partial x} - f_{gp}(u_g-u_p) - \Gamma_g(u_g-u_p)$	$(L.H.S.)_p = (1-\phi)\frac{\partial P_g}{\partial x}$ $-\frac{\partial}{\partial x}[(1-\phi)\tau_s] + f_{gp}(u_g-u_p)$	Note, gas pressure gradient accelerates the solid phase.
Culick [1974]	$(L.H.S.)_g =$ $-\phi\frac{\partial P_g}{\partial x} - f_{gp}(u_g - u_p) - \Gamma_g(u_g - u_p)$	$(L.H.S.)_p = -(1-\phi)\frac{\partial P_g}{\partial x}$ $-\frac{\partial}{\partial x}[(1-\phi)\tau_s] + f_{gp}(u_g-u_p)$	Note, gas pressure gradient accelerates the solid phase.
Krier/ Van Tassell [1974]	$(L.H.S.)_g = +\frac{\partial}{\partial x}[\phi\rho_g(u_g-u_m)^2]$ $-\frac{\partial}{\partial x}(\phi P_g) - f_{gp}(u_g-u_p) - \Gamma_g(u_g-u_m)$	$(L.H.S.)_p = +\frac{\partial}{\partial x}[(1-\phi)\rho_p(u_p-u_m)^2]$ $+\Gamma_g(u_p-u_m) - \frac{\partial}{\partial x}[(1-\phi)\tau_s] + f_{gp}(u_g-u_p)$	Continuum Approach $u_m = \frac{\phi\rho_g u_g + (1-\phi)\rho_p u_p}{\phi\rho_g + (1-\phi)\rho_p}$

Table 2.1

MODEL	GAS PHASE ENERGY EQUATION	SOLID PHASE ENERGY EQUATION	COMMENTS
Krier/ Kezerle [1977]	$(L.H.S.)_g$ $\phi \rho_g (\frac{\partial E_g}{\partial t} + u_g \frac{\partial E_g}{\partial x}) = - P_g \frac{\partial}{\partial x}(\phi u_g)$ $- \Gamma_g [u_p u_g - \frac{(u_g^2 + u_p^2)}{2}]$ $+ \Gamma_g (\hat{E}_g - E_g) + f_{pg}(u_g - u_p)^2 - \dot{Q}$	$(L.H.S.)_p$ $(1-\phi)\rho_p (\frac{\partial E_p}{\partial t} + u_p \frac{\partial E_p}{\partial x}) =$ $- \tau_s \frac{\partial}{\partial x} [(1-\phi)u_p] - \Gamma_g (\hat{E}_p - E_p) + \dot{Q}$	$\hat{E}_g \equiv E_g^{chem}$
Kuo/ Summerfield [1974]	$(L.H.S.)_g = - P_g \frac{D\phi}{Dt} - \phi P_g \frac{\partial u_g}{\partial x} + P_g u_p \frac{\partial \phi}{\partial x}$ $+ \Gamma_g [h_{chem} - E_g + (u_g - u_p)^2/2]$ $+ f_{pg}(u_g - u_p)^2 - \dot{Q}$	Uses heat conduction balance to calculate a "particle surface" temperature	$h_{chem} \equiv E_g^{chem} - E_p^{chem}$
Kuo/Koo/Davis/ Coates	$(L.H.S.)_g = - P_g \frac{\partial (\phi u_p)}{\partial x}$ $+ \Gamma_g [h_{chem} - E_g + \frac{(u_g - u_p)^2}{2}]$ $+ f_{pg}(u_g - u_p)^2 - \dot{Q}$	Uses heat conduction balance to calculate a "particle surface" temperature	$h_{chem} = E_g^{chem} - E_p^{chem}$

Table 2.2a

[Continued on Table 2.2b]

MODEL	GAS PHASE ENERGY EQUATION	SOLID PHASE ENERGY EQUATION	COMMENTS
Gough [1974]	$(L.H.S.)_g = - P_g \frac{\partial}{\partial x}(\phi u_g) - P_g \frac{\partial \phi}{\partial t} + \Gamma_g[\hat{E}_g - E_g + \frac{P_g}{\rho_p} + \frac{(u_g-u_p)^2}{2}] + f_{pg}(u_g-u_p)^2 - \dot{Q}$	Uses heat conduction balance to calculate a "particle surface" temperature	The term $- P \frac{\partial \phi}{\partial t}$ is questionable
Culick [1974]	$(L.H.S.)_g = - P_g \frac{\partial}{\partial x}\{\phi u_g + (1-\phi)u_p\} + \Gamma_g[\hat{E}_g - \hat{E}_p - E_g + E_p + \frac{(u_g-u_p)^2}{2}] + f_{pg}(u_g-u_p)^2 - \dot{Q}$	$(L.H.S.)_p = (1-\phi)\tau_s \frac{\partial u_p}{\partial x} + \dot{Q}$	$\hat{E}_g \equiv E_g^{chem}$ $\hat{E}_p \equiv E_p^{chem}$
Krier/ Van Tassell [1974]	$(L.H.S.)_g = - \frac{\partial}{\partial x}[\phi P_g u_m] + \Gamma(\hat{E}_g - E_g) + \frac{\partial}{\partial x}[\phi_{pg} E_g (u_g-u_m)] - \dot{Q}$	$(L.H.S.)_p = - \frac{\partial}{\partial x}[(1-\phi)\tau_p u_m] - \Gamma_g(\hat{E}_p - E_p) + \frac{\partial}{\partial x}[(1-\phi)\rho_p E_p (u_p-u_m)] + \dot{Q}$	Continuum Approach

Table 2.2b

CHAPTER THREE

NUMERICAL INTEGRATION

3.1 Introduction

The two-phase separated flow model generates a set of six non-linear, inhomogeneous, and coupled hyperbolic partial differential equations, as demonstrated in the previous chapter. The numerical method chosen for solving these equations is the explicit two-step MacCormack scheme. This method was chosen for its accuracy and its ability to capture shocks without the use of "artificial viscosity."

With an explicit numerical method it is possible, under certain circumstances, to "march out" a solution to a system of hyperbolic equations on a fixed, rectangular grid instead of a grid composed of the characteristics of the equations. For the "two-dimensional" system of concern here (one dimension in space and one in time) a grid of the following type is constructed.

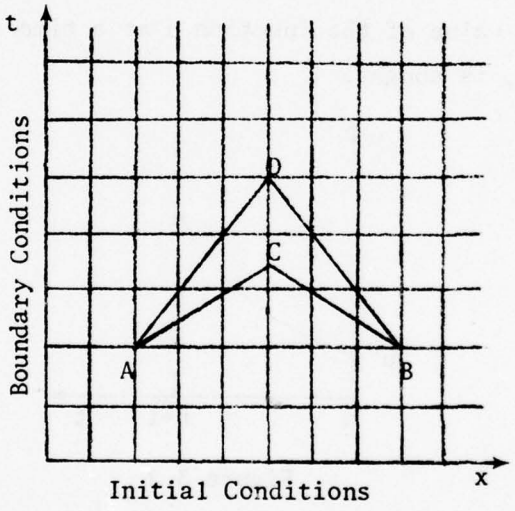

Figure 3.1

As discussed in Ames [25], the solution to the hyperbolic system is known within the triangle formed by the real characteristics, lines AC and BC, in Fig. 3.1 if the solution is known up to the time indicated by the line AB. The point predicted by the numerical computation of one step forward in time, point D, is a product of the grid spacings which determine the slope of the "finite difference characteristics." If the slope of these finite difference characteristics is

greater than the slope of the real characteristics, instability sets in; if equal, the solution is identical to the characteristic solutions; if less than, the system is stable but accuracy decreases with decreasing slope. The idea of an explicit finite difference method, then, is to accurately approximate the real characteristics of the system on a rectangular grid. These points must be considered later when the question of stability is studied.

3.2 The MacCormack Scheme

The MacCormack scheme is a two-step, predictor-corrector method of integration. The basic idea of the method, as applied to partial differential equations can readily be understood through an analogy with an ordinary differential equation. Consider the simple O.D.E.

$$\frac{\partial u}{\partial t} = f(t) \quad . \tag{3.1}$$

Knowing the value of the function u at a time n, the value of a new time, n + 1, is sought.

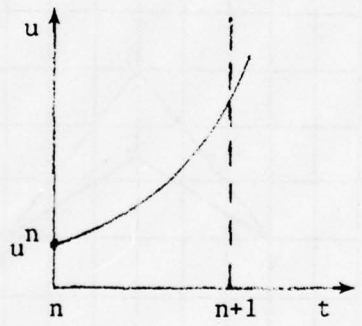

Figure 3.2

An approximate value at the new time is found in the predictor step, knowing only the value of the function and its slope at time n.

$$\overline{u^{n+1}} = u^n + \Delta t\left(\frac{du}{dt}\right)^n \quad . \tag{3.2}$$

The bar above a term is used to indicate the intermediate nature of a value computed in the predictor step. As shown in Fig. 3.3, this value can be in considerable error.

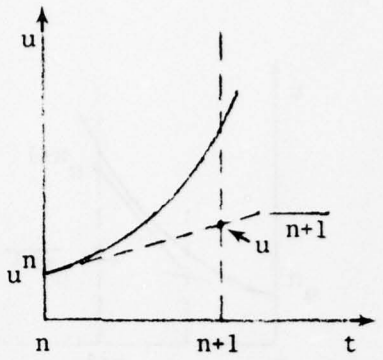

Figure 3.3

The "predicted" value is revised by first finding a new slope of the function at the predicted point. The "corrected" value of the function at time n + 1 is then found by averaging the known slope of the function at time n and the predicted slope of time n + 1 and making a new extrapolation from the known value, u^n.

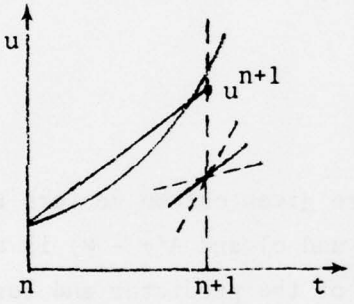

Figure 3.4

The equation for finding this more accurate point is:

$$u^{n+1} = u^n + \Delta t \frac{\left[\left(\frac{du}{dt}\right)^n + \overline{\left(\frac{du}{dt}\right)^{n+1}}\right]}{2} \tag{3.3}$$

If a substitution for the slope of the function at time n + 1 is made in Eq. (3.3) from Eq. (3.2), another common form of the corrector step is obtained.

$$u^{n+1} = \frac{1}{2}\left[u^n + \overline{u^{n+1}} + \Delta t \overline{\left(\frac{du}{dt}\right)^{n+1}}\right] \tag{3.4}$$

This equation describes a new schematic representation.

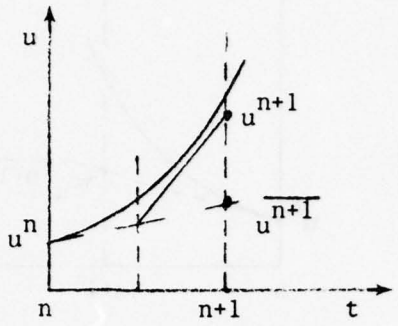

Figure 3.5

The application of the MacCormack scheme to a partial differential equation is a natural extension of the method shown above. In this case, the simple vector form of the equation is:

$$\frac{\partial u}{\partial t} + B \frac{\partial F}{\partial x} = 0 \tag{3.5}$$

or

$$\frac{\partial u}{\partial t} = A \frac{\partial F}{\partial x} \tag{3.6}$$

where u and F are given column vectors representing the parameters of interest (ρ, u, and e) and A(= - B) is a constant matrix of coefficients. The formulation of the predictor and corrector steps is the same as before, but now the time derivatives of the function u can be replaced by special derivatives in the coordinate x as Eq. (3.6) clearly shows. In the simplified case u = F, the following grid system can be constructed.

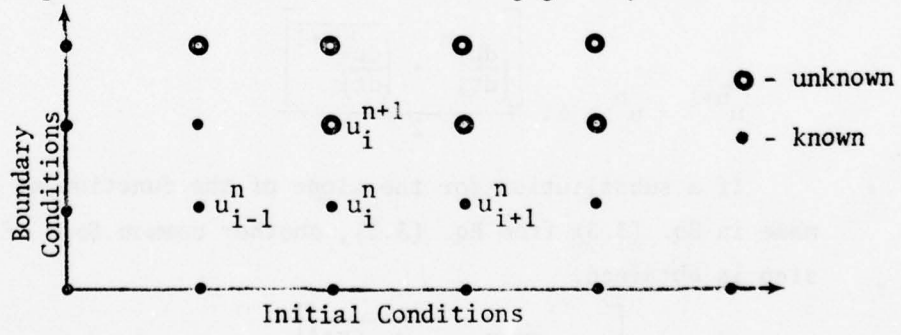

Figure 3.6

The equation for the predictor step is now a revision of Eq. (3.2).

$$u_i^{n+1} = u_i^n + \Delta t \left.\frac{\partial u}{\partial t}\right|_i^n$$

$$= u_i^n + A\Delta t \left.\frac{\partial u}{\partial x}\right|_i^n$$

$$= u_i^n + A \frac{\Delta t}{\Delta x} \left[u_{i+1}^n - u_i^n\right] \tag{3.7}$$

A forward difference in space was chosen to evaluate the spatial derivative, although it was not mandatory. It follows that the equation of the corrector step is a simple revision of either Eq. (3.3) or Eq. (3.4). Choosing Eq. (3.4) yields;

$$u_i^{n+1} = \frac{1}{2}\left[u_i^n + \overline{u_i^{n+1}} + \Delta t \left.\overline{\frac{\partial u}{\partial t}}\right|_i^{n+1}\right]$$

$$= \frac{1}{2}\left[u_i^n + \overline{u_i^{n+1}} + A\Delta t \left.\overline{\frac{\partial u}{\partial x}}\right|_i^{n+1}\right]$$

$$= \frac{1}{2}\left[u_i^n + \overline{u_i^{n+1}} + \frac{A\Delta t}{\Delta x}\left(\overline{u_i^{n+1}} - \overline{u_{i-1}^{n+1}}\right)\right] \tag{3.8}$$

In this instance a backward difference was used to evaluate the spatial derivative.

The equations used in the Illinois Separated Flow Code are forms of Eq. (3.7) and (3.8) when $u \neq F$. In simplified form they are:

Predictor

$$\overline{u_i^{n+1}} = u_i^n + A \frac{\Delta t}{\Delta x}\left[F_{i+1}^n - F_i^n\right] \tag{3.9}$$

Corrector

$$u_i^{n+1} = \frac{1}{2}\left[u_i^n + \overline{u_i^{n+1}} + A \frac{\Delta t}{\Delta x}\left(\overline{F_i^{n+1}} - \overline{F_{i-1}^{n+1}}\right)\right] \tag{3.10}$$

When both steps are completed, the value of the function u is known for a new time at one location. (See Fig. 3.6.) The entire process of both predictor and corrector is then repeated for the next point in the x-direction and the same time. When all the points in the one-dimensional grid are known at the new time another step forward in time can be taken and the entire process is repeated for each point starting at a known boundary.

Although each step (predictor and corrector) of the process is a simple forward or backward finite difference of first order accuracy, the overall process has second order accuracy as explained by Warming [26]. This procedure also acts as an implicit artificial viscosity to help capture embedded shocks. The above completes description of the scheme and reasons for its choice.

3.3 Choice of Mesh System and Boundary Conditions

There are two basic mesh systems to which the MacCormack scheme can easily be applied. (See Fig. 3.7 below).

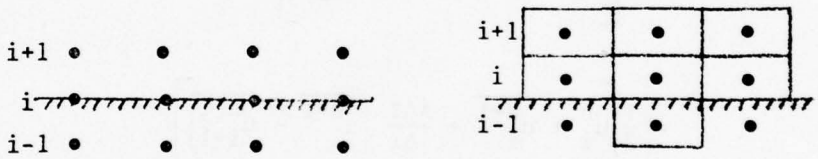

Figure 3.7

The major difference between the two systems is that, in the first, there is a grid point lying on the wall, while in the second there is no such point. The choice of a mesh system has a great bearing on how boundary conditions are employed. For the work done here a mesh system of the first type was used and labeled as shown in Fig. 3.8. This convention must be kept in mind as the boundary conditions are discussed.

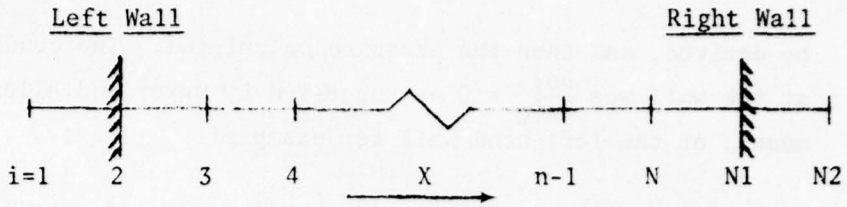

Figure 3.8

Since both ends of the one-dimensional flow were considered closed a solid wall condition was imposed at both places. The only boundary condition that can be stated with certainty is that the velocity of both particles and gas must be zero at the end walls [27]. The most convenient way of applying this condition is to define a row of fictitious points inside the wall and use an anti-symmetric reflection of velocity, u, while also setting u = 0 at the walls. The procedure is very compatible with the first mesh system. Boundary conditions on the other parameters are not as easy to deduce.

In order to derive a boundary condition on gas temperature an assumption must be made as to the nature of the wall. One choice is to assume an adiabatic wall, although that was not done here. Instead it was assumed that the heat conducted by the wall is equal to the heat convected to the wall by the gas as was done by Krier, Dimitstein, and Gokhale [5]. Thus

$$h_c(T_g - T_w) = K_g \frac{\partial T_g}{\partial x} \quad \text{, where the heat transfer coefficient, } h_c \text{, is an assumed given function.} \tag{3.11}$$

At the right-hand wall, for example, this becomes

$$h_c(T_g - T_w) = -\frac{K_g}{\Delta x}(T_{N1} - T_{N2}) \quad . \tag{3.12}$$

This can be solved for $T_w (=T_{N1})$.

Since the Noble-Abel non-ideal equation of state is assumed to hold at all points, the remaining boundary condition on the gas phase need only specify either pressure or density and the other is determined. Because this state equation employs a variable co-volume which is a function of density it was necessary to impose a boundary condition on density so that with density known, the co-volume could

be derived, and then the pressure calculated. The condition imposed at the wall was $\left.\frac{\partial \rho}{\partial x}\right|_w = 0$ as suggested by Dwyer and Allen [28]. This meant, at the left-hand wall for example:

$$\rho(1) = \rho(2) = \rho(3) \quad . \tag{3.13}$$

The boundary values for the solid phase were calculated using anti-symmetric reflection of velocity (as stated earlier), symmetric reflection of other variables, and employing regular interior point differencing.

To summarize, the boundaries were handled in the following way:

Gas Phase:

$$\left.\frac{\partial \rho_g}{\partial x}\right|_w = 0$$

$$\left. u_1 \right|_w = 0$$

$$\left. T_g \right|_w = f \quad \text{(heat balance)} \tag{3.14}$$

Solid Phase:

$$\rho_2(1) = \rho_2(3) \qquad \rho_2(N) = \rho_2(N2)$$

$$u_2(1) = -\, u_2(3) \qquad u_2(N) = -\, u_2(N2)$$

$$e_2(1) = e_2(3) \qquad e_2(N) = e_2(N2) \tag{3.15}$$

where $\rho_1 = \phi\rho_g$ and $\rho_2 = (1-\phi)\rho_p$ as defined earlier, and where $[\ ]_1$ = gas and $[\ ]_2$ = solid phase.

Values for the gas phase variables at the fictitious points were also assigned through reflection. It must be noted however that these values were employed only in the calculation of the MacCormack damping factor, as discussed later. They were not used to find gas phase boundary values. There has been some concern expressed [29] that the reflection principle implies "extra" boundary conditions,

$$\left.\frac{\partial f}{\partial x}\right|_w = 0 \quad , \qquad f = \rho, u, e \quad . \tag{3.16}$$

It is felt that this is not true for the equations studied here, due to the large source and sink terms. It must also be noted that with the mesh system used reflection through a wall does not insure zero gradient at the wall.

3.4 Initial Conditions

Initial conditions specified temperature, pressure, and velocity throughout the grid. Temperatures were set by a linear decay over the first five grid points. Pressure was subject to an exponential decay throughout the entire domain. Velocities of gas and solid at time = 0 were set equal to zero everywhere. Initial porosity was set as desired, usually distributed evenly. These conditions are shown graphically in Fig. 3.9.

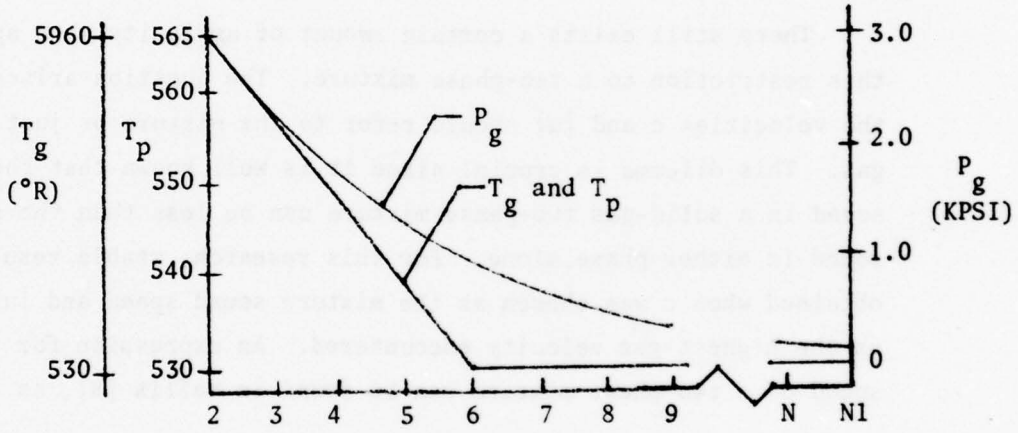

Initialization Profiles

Figure 3.9

The pressure profile initialized above differs from that used by Dimitstein [4] where the exponential decay was applied to only one quarter of the grid points. It was found in the course of this work that a "smooth" initial pressure profile (no discontinuities) was needed to provide stable results.

3.5 Discussions Regarding Numerical Stability

The ability of an explicit finite difference method is dependent upon the grid size and time step as mentioned in Section 3.1. It has

been shown that in order to obtain a stable solution to the hyperbolic system the numerically predicted point must lie within the area formed by the real characteristics (See Fig. 3.1). For the MacCormack scheme this is assured by satisfying the Courant, Friedrichs, Levy criteria [30], i.e.,

$$\frac{\Delta t(c + |u|)}{\Delta x} \leq 1 \quad . \tag{3.17}$$

where c represents the average speed of sound of the system.

With a fixed grid size, a slightly more restrictive form of this criteria was used.

$$\Delta t = \frac{.7*\Delta x}{(c + |u|)} \tag{3.18}$$

There still exists a certain amount of ambiguity when applying this restriction to a two-phase mixture. The question arises whether the velocities c and $|u|$ should refer to the mixture or just to the gas. This dilemma is crucial since it is well known that the speed of sound in a solid-gas two-phase mixture can be less than the speed of sound in either phase alone. For this research, stable results were obtained when c was chosen as the mixture sound speed and $|u|$ was taken as the highest gas velocity encountered. An expression for the sound speed of a two-phase mixture can be found in Wallis [8], as

$$\frac{1}{c^2} = \left[\alpha\rho_2 + (1-\alpha)\right]\left[\frac{\alpha}{\rho_2 c_2^2} + \frac{1-\alpha}{\rho_1 c_1^2}\right] \quad . \tag{3.19}$$

It can be seen that the sound speed of the mixture is a function of the sound speed in each phase separately. Therefore the first priority was to find a value for the sound speed in each phase. For the gas phase, standard isentropic sound speed was used, namely

$$c_1 = \sqrt{\gamma RT} \tag{3.20}$$

where T was chosen as the initial gas temperature. For the solid phase,

$$c_2 = \sqrt{\frac{K_2}{\rho_2}} \tag{3.21}$$

where K_2 is the bulk modulus of a medium hard plastic. These calculations are carried out in Appendix C. With these values known, the sound speed of the mixture was calculated from Eq. (3.16). The value computed was c = 2,708 ft/sec, which was less than the speed of sound in either phase alone.

With c and $|u|$ determined, a desirable time step was calculated from the C.F.L. criteria Eq. (3.15). It was found that, using this restriction, stable solutions were always obtained for those systems of equations believed to be hyperbolic. A recent paper by Krier, Gokhale, and Hughes [6] discusses the concern and manner in which the governing equations are actually hyperbolic.

CHAPTER FOUR

THE PREDICTED RESULTS

4.1 Introduction

As discussed in the previous chapters, the major purpose of this work is to predict the pressure wave fronts relative to the ignition front in a two-phase reactive mixture in order to give some indication whether a high-speed transient deflagration wave might transit to a detonation in a highly loaded propellant bed. To properly study all possible variations in the allowed parameters, the scope of this work would have had to be broadened beyond its original intent. This not being possible in the time period available, only a limited number of results are included here. It is expected that this work will be continued and broadened in the near future.

After several hundred independent calculations a baseline case with standard input conditions was deduced. The governing equations solved are those shown in Chapter Two, namely Eqs. (2.1) to (2.7), with constitutive relations as outlined in Appendix B. Specifically, the solid phase stress tensor in Eq. (2.4) does not include the gas pressure. As mentioned previously, the reason for this is that it has been shown [6] that the set of equations will be totally hyperbolic only if there is no gas pressure gradient in the solid phase momentum equation.

Table 4.1 summarizes the most important input used to carry out the typical results shown below. The main results presented from this analysis are the pressure distributions as time progresses, the flame front locus and pressure front(s), as well as developments in the temperature and velocity fields.

4.2 Results From the Baseline Case

Figures 4.1 through 4.5 present the distribution histories of the fluid dynamic variables in a bed of solid propellant, 3 inches long, with a solids loading at 60 percent (ϕ_o = 0.40). The results in these figures were termed the baseline case, as defined above.

Figure 4.1 outlines the calculated pressure distributions at four different times. As in previous work related to this problem (see Krier *et al.* [3,5], the appearance of a "continental-divide" in the

Table 4.1

TYPICAL INPUT DATA

Parameter	Value
Initial bed temperature, T_g. T_p, T_w	530°R
Ignition temperature, T_{ign}	545°R
Initial bed porosity, ϕ	0.40
Propellant burning rate constant, b_1	0.0 in/sec
Propellant burning rate proportionality constant, b_2	0.00553 in/sec-Psia^n
Propellant burning rate index, n	(0.90)
Propellant density, ρ_p	0.0571 Lbm/in^3
Initial grain diameter, d_p	400μm (200 μm)
Chemical energy released, $E_{chem} = (E_g - E_p)^{chem}$	2360.9 BTU/Lbm
Molecular weight of gas, MW	22.6 Lbm/Lbmole
Covolume of propellant gas, B_v	29.85 in^3/Lbm
Specific heat ratio of gas, γ	1.252
Gas viscosity, μg	0.249 x 10^{-5}lbm/in-sec
Universal gas constant, R	1.9869 BTU/Lbmole-°R
Thermal conductivity of the walls, k_w	0.3 x 10^{-5} BTU/in-sec-°R
Total bed length, L_B	3.0 in.
Percent heat transfer to particle and to wall after ignition	10%

interior of the bed is pronounced and pressure gradients are extremely steep. In addition, the average pressures behind the front are very high, reaching in excess of 0.5×10^6 psia. It appears that for nearly the same constituitive laws, the separated flow model (as derived here) predicts pressure wave mechanics similar to that calculated with the continuum mixture model of Krier et al.[6].

The locus of the flame (ignition) front for the baseline case is presented in Figure 4.2. As expected, the deflagration speed (slope of the x-t locus) accelerates to several mm/μ-sec in this 3-inch long bed. Also shown in this figure is a line labeled the "pressure front." This locus was derived by noting the midpoint of the pressure wave shown in Figure 4.1 at various times. It appears that the pressure front and the flame front are coincident as the flame accelerates to complete ignition.

Figure 4.3 shows both the gas velocity and the propellant particle velocity distributions at the chosen times. As might be expected, the velocity peaks shown are a consequence of the steep pressure front arriving at the various locations. Also worth noting are the extreme gas velocities, often exceeding 5000 ft/sec, and the fact that peaks in particle velocity lag peaks in gas velocity at any given time.

Figure 4.4 presents gas temperature and particle temperature distribution histories. With the chemical energy fixed for this propellant, the gas temperatures are generated at values of roughly 6500°R. These temperatures decay as the gases lose heat to the solid by convection into the bed interior. Later, as the pressure front steepens, the gases are compressed in the interior to values far exceeding their incoming values. The subsequent particle temperatures are increased not only due to the convective heat transfer, but also due to the rapid changes in kinetic energy of these mobile particles.

The last predictions displayed for the baseline case are the porosity distribution histories shown in Figure 4.5. The porosity profiles show that near the front of the bed (which is partially ignited at $t = 0$) the porosity increases fairly rapidly. This is due to both a reduction in volume of the particles due to burning and the forward motion of these particles being dragged along by the gases. Subsequent to this, the particles are compacted somewhere in the bed

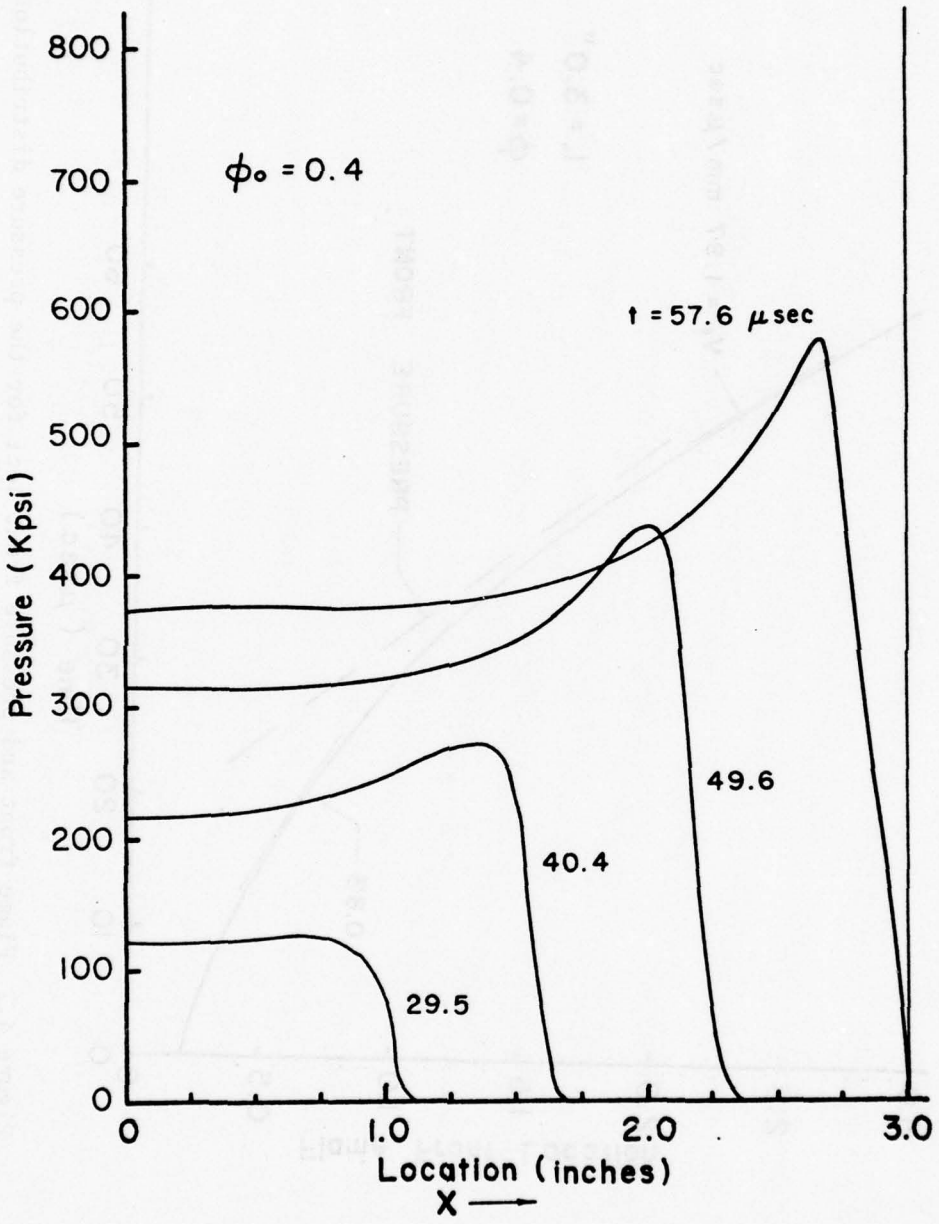

Figure 4.1 Pressure distribution history predicted for a three inch long bed with an initial solids loading of 60 percent. [Predictions for Figs. 4.1 - 4.5 utilized the second-form of the particle energy equation.]

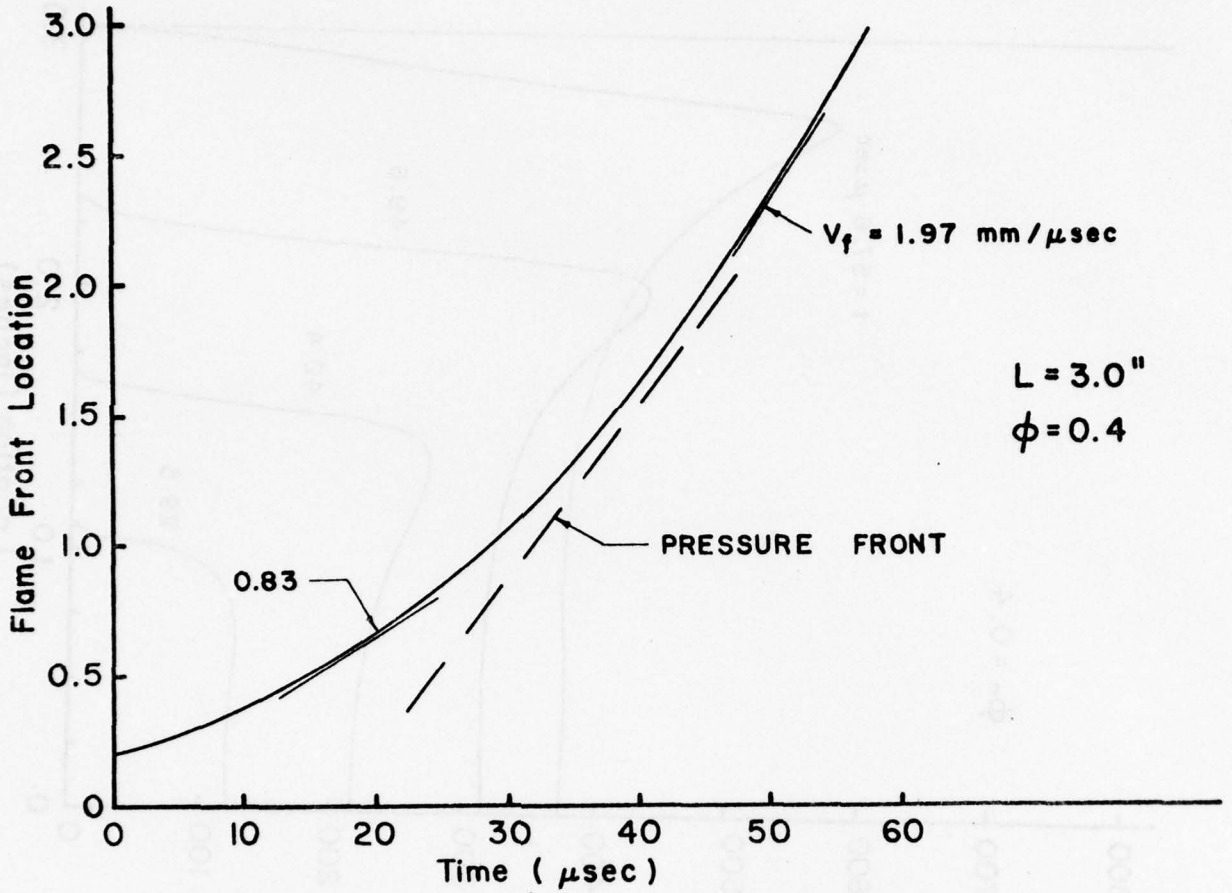

Figure 4.2 Flame front and pressure front loci for the pressure distributions indicated in Fig. 4.1.

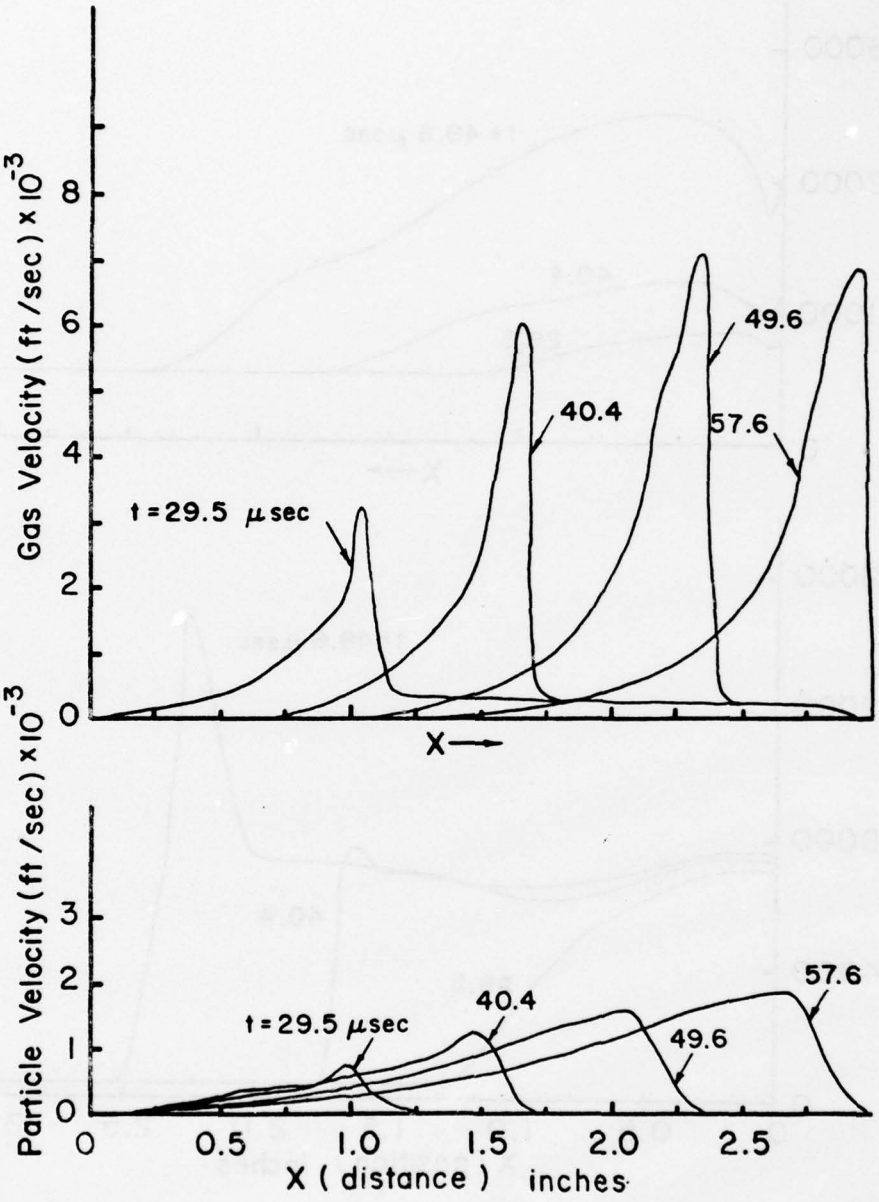

Figure 4.3 Gas velocity and particle velocity distribution history.

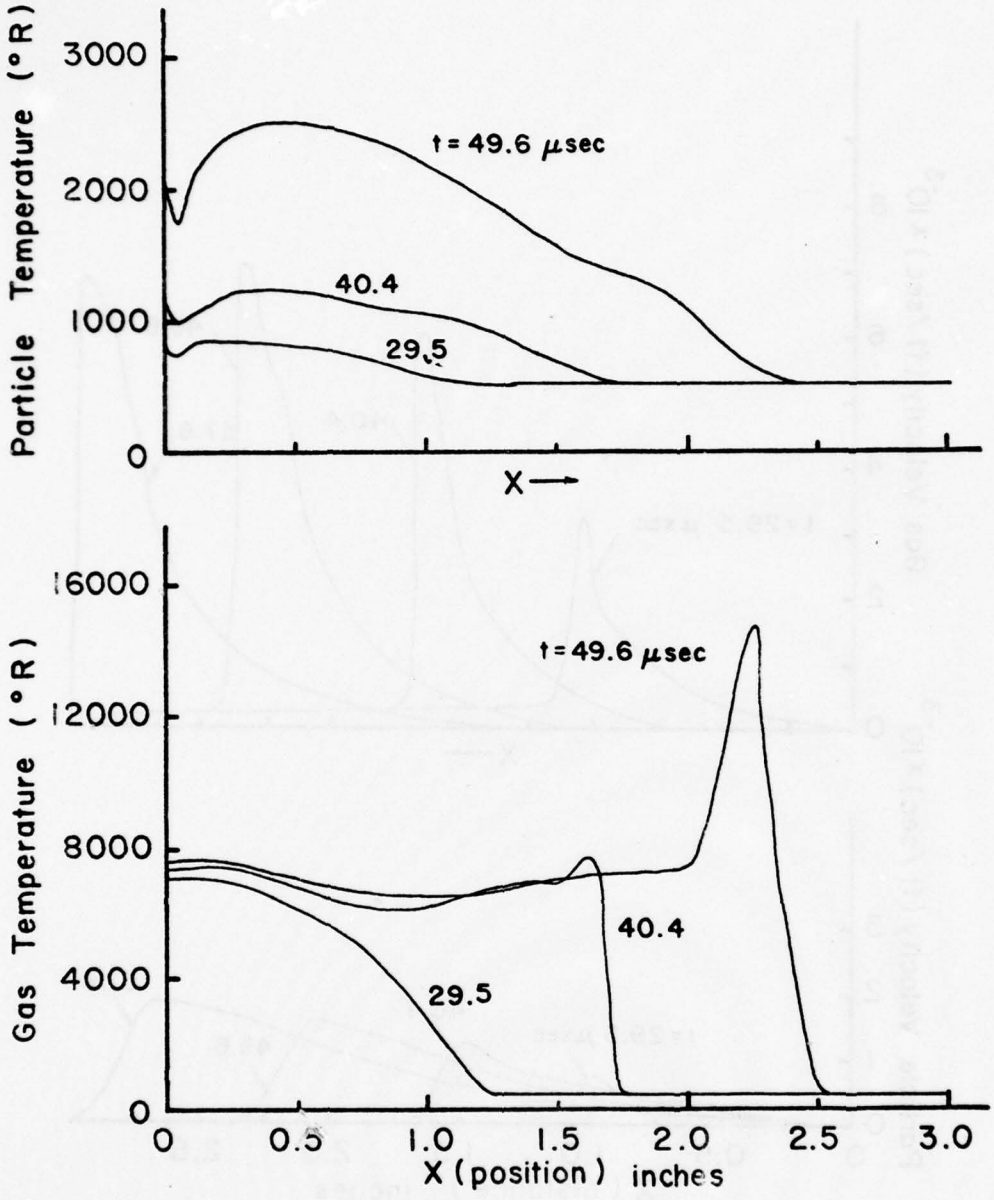

Figure 4.4 Particle temperature and gas temperature distribution history.

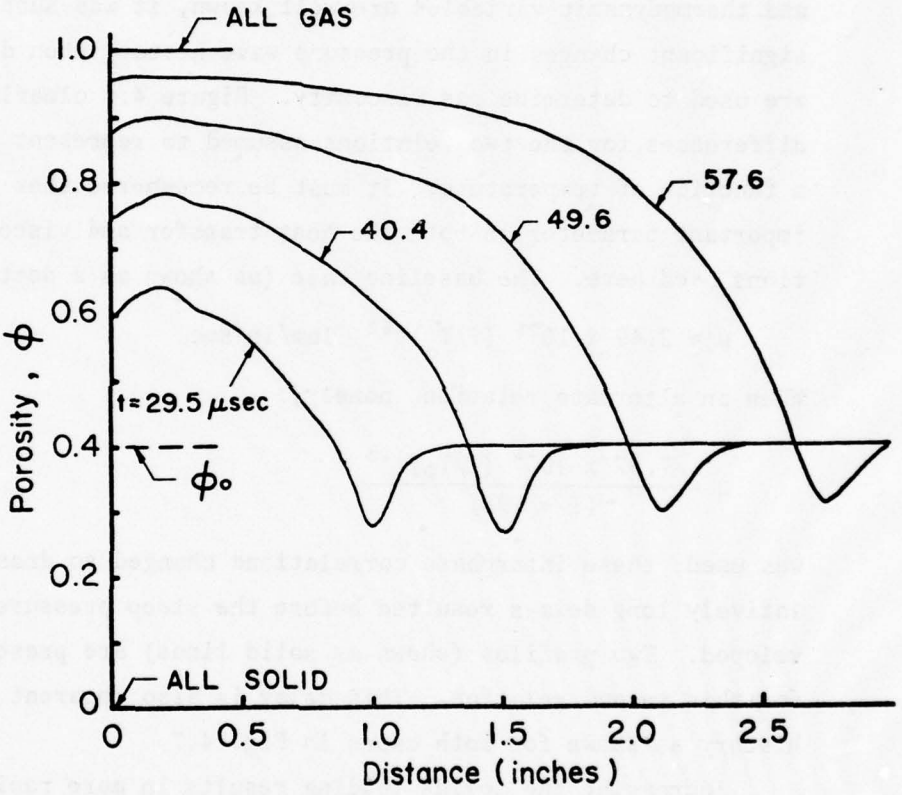

Figure 4.5 Porosity (gas volume fraction) distribution history complementary to predictions in Figs. 4.1 - 4.4.

interior to solids loadings greater than the original 60 percent. (Recall that the solid fraction equals $1-\phi$.) For the results shown here, a significant fraction of the bed has been consumed at a time equal to 50 μ-sec.

4.3 Parametric Variations on the Baseline Case

As discussed in Section 4.1, it was not possible to vary all input parameters or study all possible formulations of the governing equations. The following figures, however, will indicate the sensitivity of the predictions shown in Figs. 4.1 - 4.5 to some of the most important parameters. Although one might generally assume that the gas phase fluid and thermodynamic variables are well known, it was surprising to see the significant changes in the pressure wave history when different relations are used to determine gas viscosity. Figure 4.6 clearly indicates these differences for the two relations assumed to represent gas viscosity as a function of temperature. It must be remembered that viscosity is an important parameter in both the heat transfer and viscous drag correlations used here. The baseline case (as shown as a dotted curve) uses

$$\mu = 2.49 \times 10^{-6} \, (T/T_o)^{.65} \quad \text{lbm/in-sec} \quad . \tag{4.1}$$

When an alternate relation, namely,

$$\mu = \frac{7.57 \times 10^{-4} \, (T/T_o)^{1.5}}{(T + 198)} \tag{4.2}$$

was used, these interphase correlations changed so drastically that relatively long delays resulted before the steep pressure fronts developed. Two profiles (shown as solid lines) are presented in Fig. 4.6 for this second relation. This delay is also apparent in the flame front history as shown for both cases in Fig. 4.7

Increasing the solids loading results in more rapid wave dynamics and greater peak pressures, as expected. Figure 4.8 presents the flame front locus for three solids loadings varying from 70 percent to 50 percent. Had calculations carried past a bed length of three inches, possible transitions to detonation might have been expected in much shorter run-up lengths for the high solids loading. Shown as an insert on Fig. 4.8 is the peak pressure in the bed interior at times just before full bed ignition. Note that increasing the solids loading

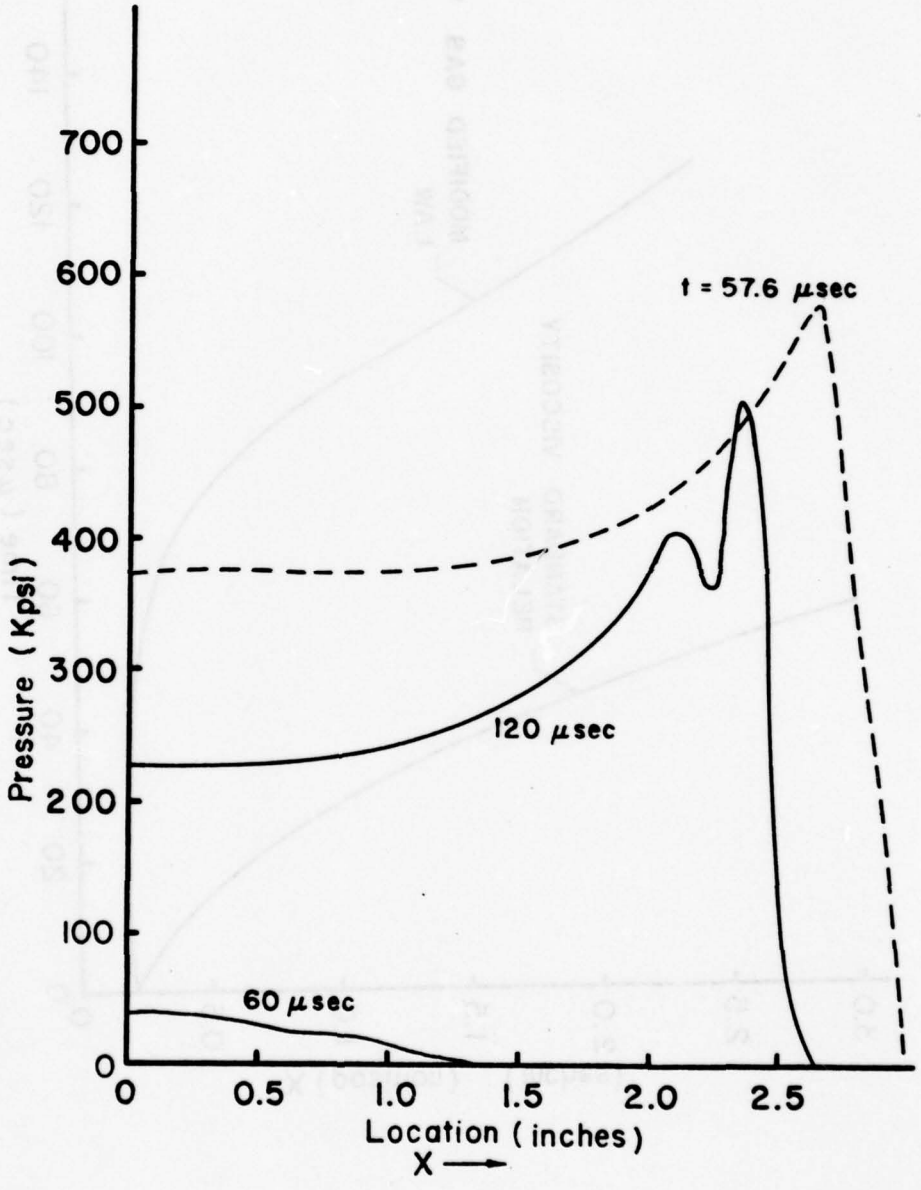

Figure 4.6 Comparison of the pressure distribution for an alternate gas viscosity relation with that predicted at an earlier time for the standard viscosity law (dashed line).

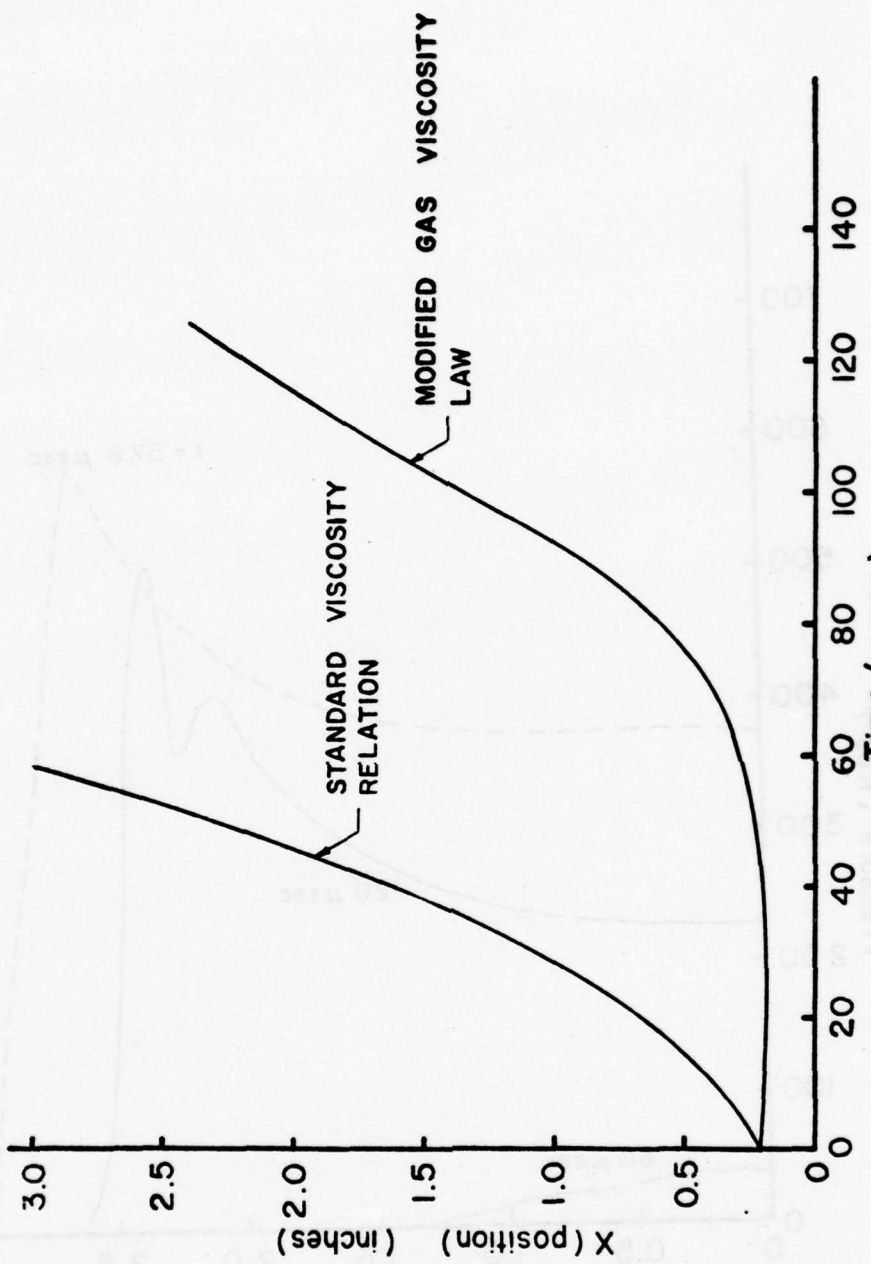

Figure 4.7 Flame front locus in a three inch long bed for cases of two different gas viscosity relations.

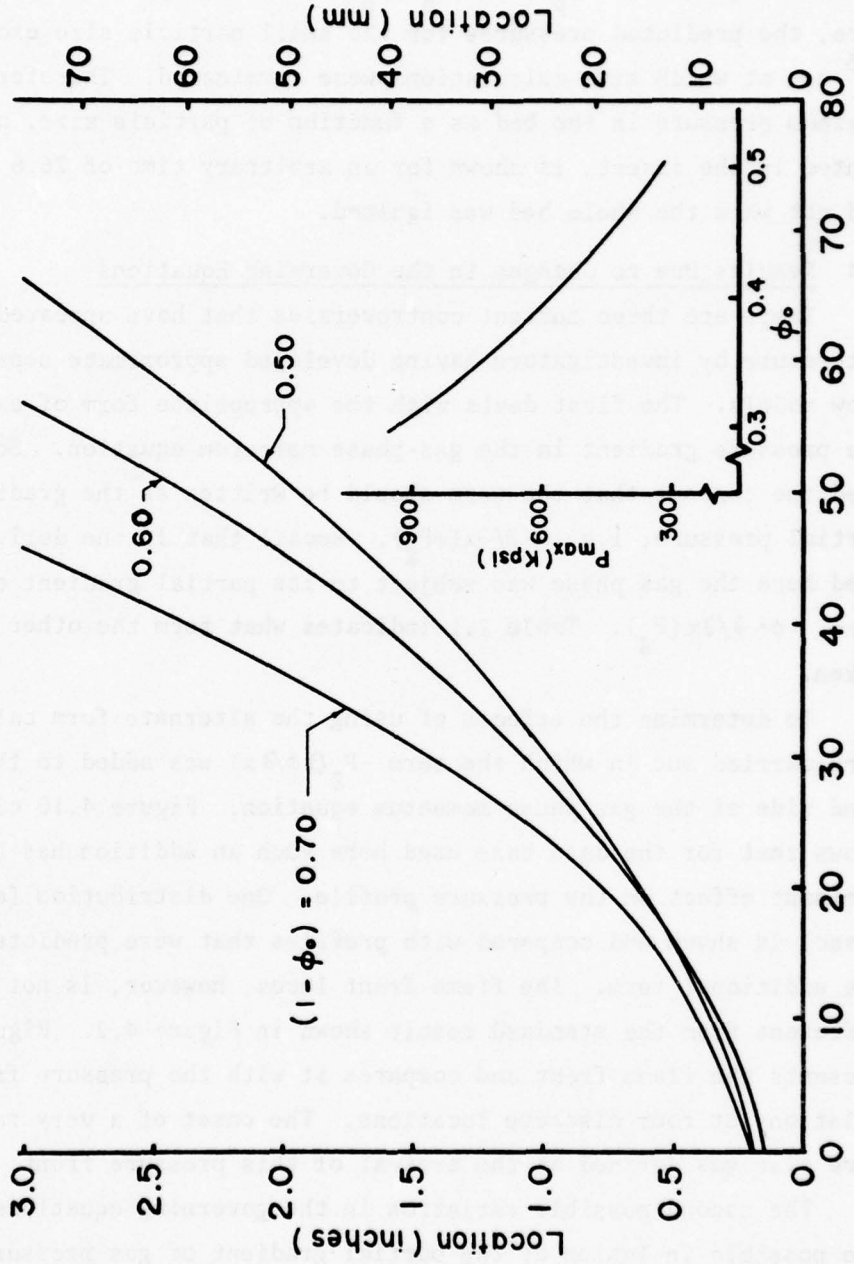

Figure 4.8 Flame front locus for three different initial solids loading. [The insert curve indicates peak pressure in the bed (prior to the time of complete bed ignition) as a function of porosity.]

from 50 percent to 70 percent triples this peak pressure.

Decreasing the particle size from the standard 200 μ diameter (r_p = .004 inches) yields a trend similar to increasing the solids loading. In the case shown in Figure 4.9, decreasing the radius to 100 μ results in an increase in the S/V ratio of the particles at 100 percent. (Since $(S/V)_p = 3(1-\phi_o)/r_p$) For the input data base used here, the predicted pressures for the small particle size exceeded 10^6 psi at which time calculations were terminated. Therefore the maximum pressure in the bed as a function of particle size, as presented in the insert, is shown for an arbitrary time of 26.6 μsec, and not when the whole bed was ignited.

4.4 Results Due to Changes in the Governing Equations

There are three current controversies that have appeared in the literature by investigators having developed approximate separated flow models. The first deals with the appropriate form of expressing the pressure gradient in the gas-phase momentum equation. Some have used the concept that the term should be written as the gradient of partial pressure, i.e., $-\partial/\partial x(\phi P_g)$. Recall that in the derivation used here the gas phase was subject to its partial gradient of pressure, $-\phi \cdot \partial/\partial x(P_g)$. Table 2.1 indicates what form the other models have taken.

To determine the effects of using the alternate form calculations were carried out in which the term $-P_g(\partial \phi/\partial x)$ was added to the right hand side of the gas phase momentum equation. Figure 4.10 clearly shows that for the data base used here such an addition has a very dominant effect on the pressure profile. One distribution (at t = 42.4 μ-sec) is shown and compared with profiles that were predicted without the additional term. The flame front locus, however, is not markedly different from the standard result shown in Figure 4.2. Figure 4.11 presents the flame front and compares it with the pressure front calculations at four discrete locations. The onset of a very rapid pressure rise was defined as the arrival of this pressure front.

The second possible variation in the governing equations concerns the possible inclusion of the partial gradient of gas pressures in the solid phase momentum equation, namely $-(1-\phi)\partial P_g/\partial x$. Hughes [6] has shown that this term in that equation results in a non-hyperbolic system and one that might experience difficulties in numerical

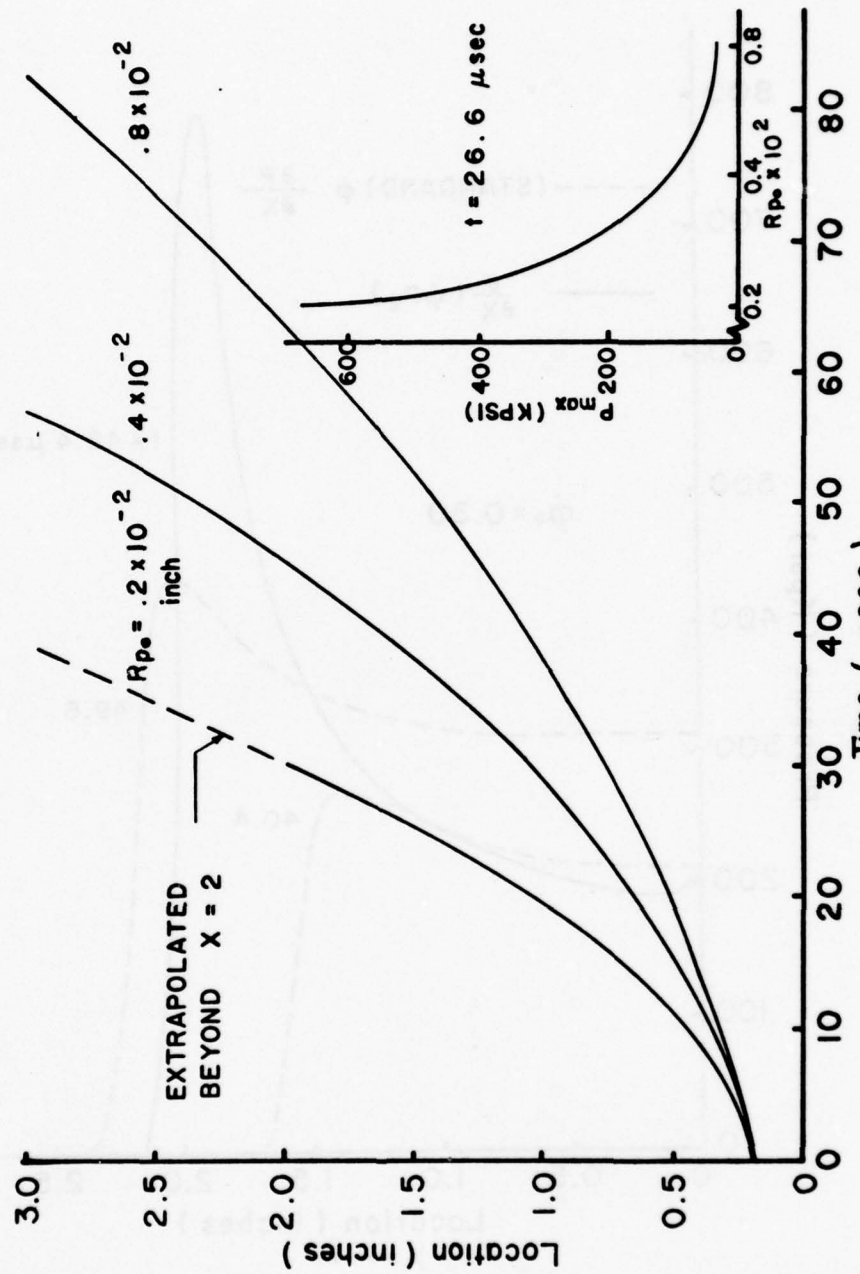

Figure 4.9 Flame front locus for three different initial particle sizes. [Note, R_p = 0.004 corresponds to a 200 μm diameter spherical particles.]

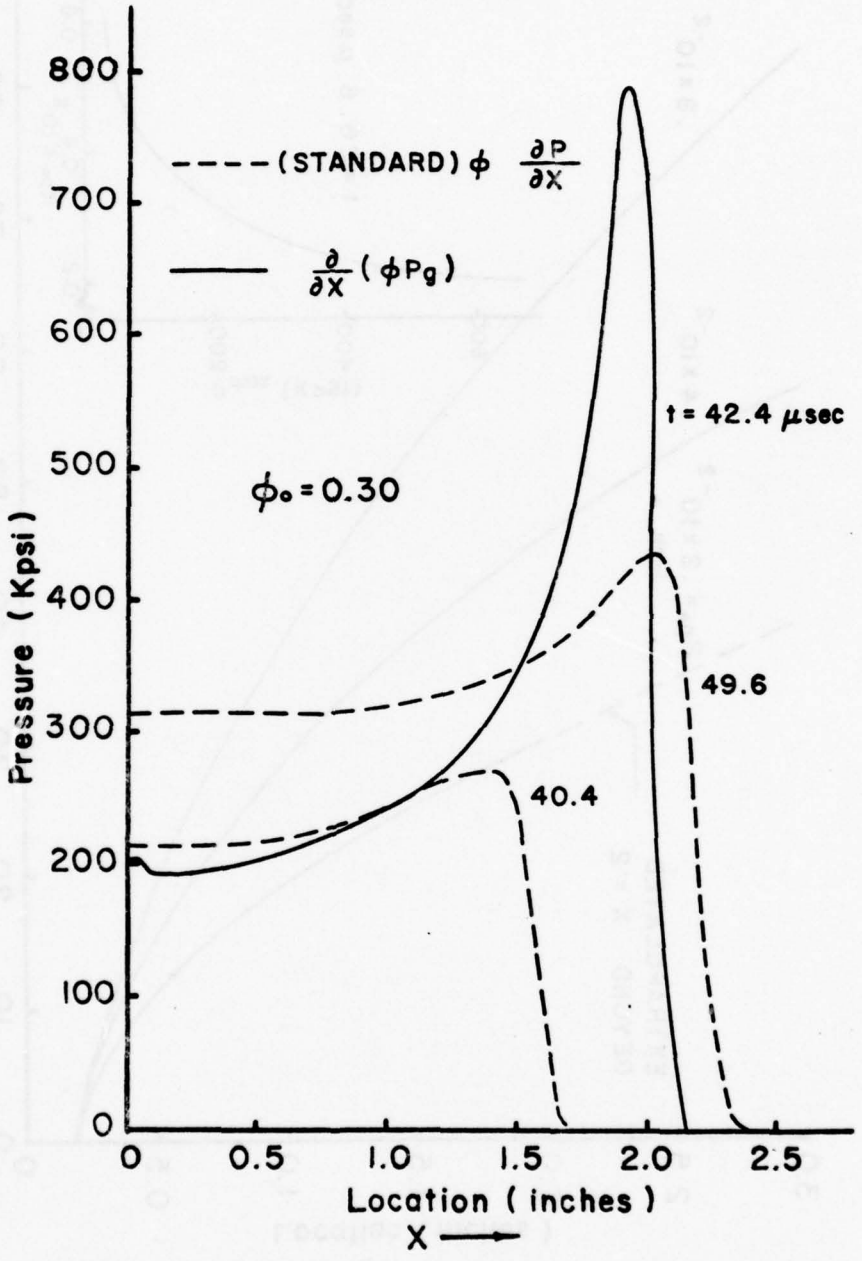

Figure 4.10 The effect of including the term, $-P\partial\phi/\partial x$, in the gas-phase momentum balance.

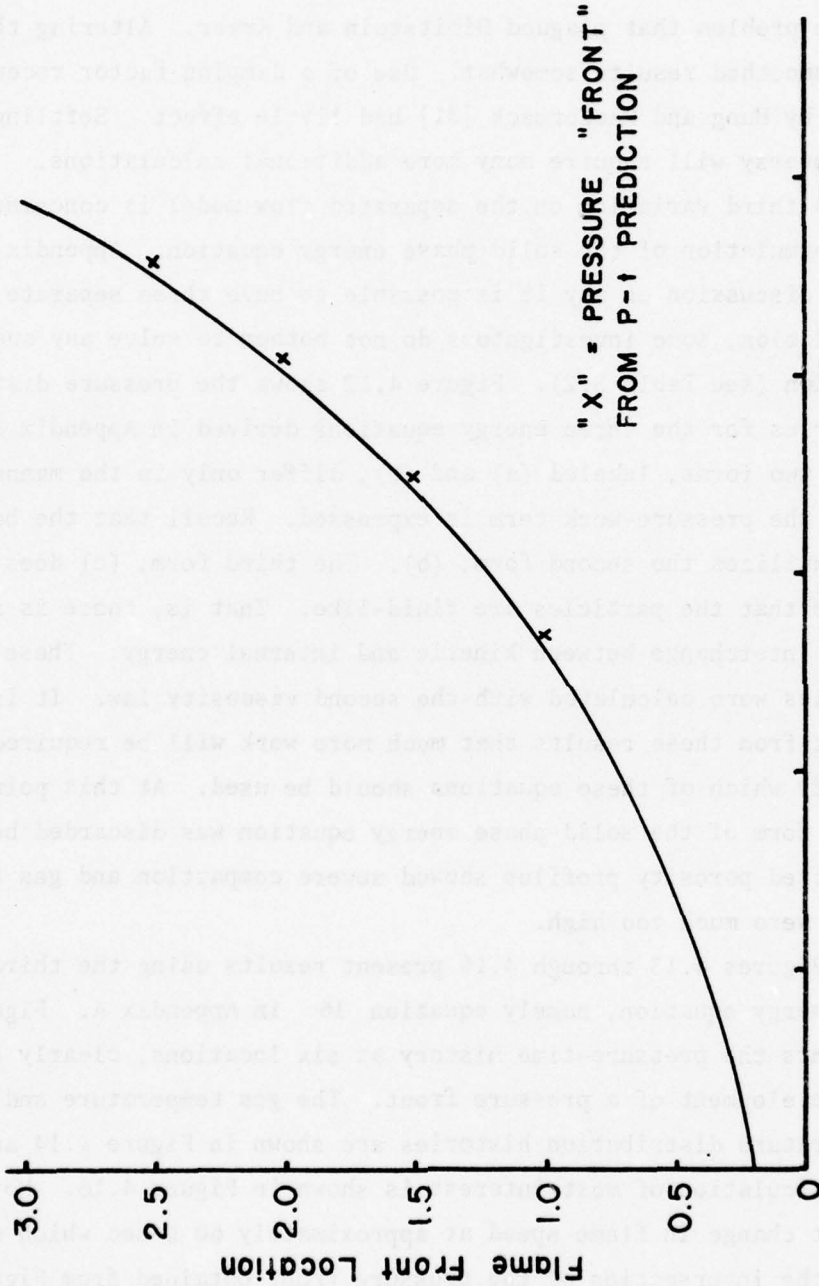

Figure 4.11 The flame front locus predicted for the case when the term, $-\partial/\partial x(\phi P)$, is used in the gas-phase momentum balance.

integration. As shown in Table 3.1, several modelers retain such a term. The calculations to date seem to confirm the concepts of Hughes, although the evidence is not conclusive. Stable and well-behaved results were never really achieved when this term was included. Pressure and velocity oscillations usually occurred similar to the problem that plagued Dimitstein and Krier. Altering the mesh size smoothed results somewhat. Use of a damping factor recently devised by Hung and MacCormack [31] had little effect. Settling this controversy will require many more additional calculations.

A third variation on the separated flow model is concerned with the formulation of the solid phase energy equation. Appendix A presents discussion on why it is possible to have three separate forms. In addition, some investigators do not bother to solve any such equation (see Table 3.2). Figure 4.12 shows the pressure distribution histories for the three energy equations derived in Appendix A. The first two forms, labeled (a) and (b), differ only in the manner in which the pressure-work term is expressed. Recall that the baseline case utilizes the second form, (b). The third form, (c) does not assume that the particles are fluid-like. That is, there is no possible interchange between kinetic and internal energy. These pressure profiles were calculated with the second viscosity law. It is apparent from these results that much more work will be required to justify which of these equations should be used. At this point, the first form of the solid-phase energy equation was discarded because predicted porosity profiles showed severe compaction and gas temperatures were much too high.

Figures 4.13 through 4.16 present results using the third form of the energy equation, namely equation 16 in Appendix A. Figure 4.13 presents the pressure-time history at six locations, clearly showing the development of a pressure front. The gas temperature and particle temperature distribution histories are shown in Figure 4.14 and 4.15. The calculation of most interest is shown in Figure 4.16. Notice the abrupt change in flame speed at approximately 60 μ-sec which coincides with the intersection of the pressure front obtained from Figure 4.13.

The results shown in Figure 4.16 might represent a possible deflagration to detonation transition. Beyond 60 μ-sec the pressure front leads the flame front as one could expect to see in a detonation

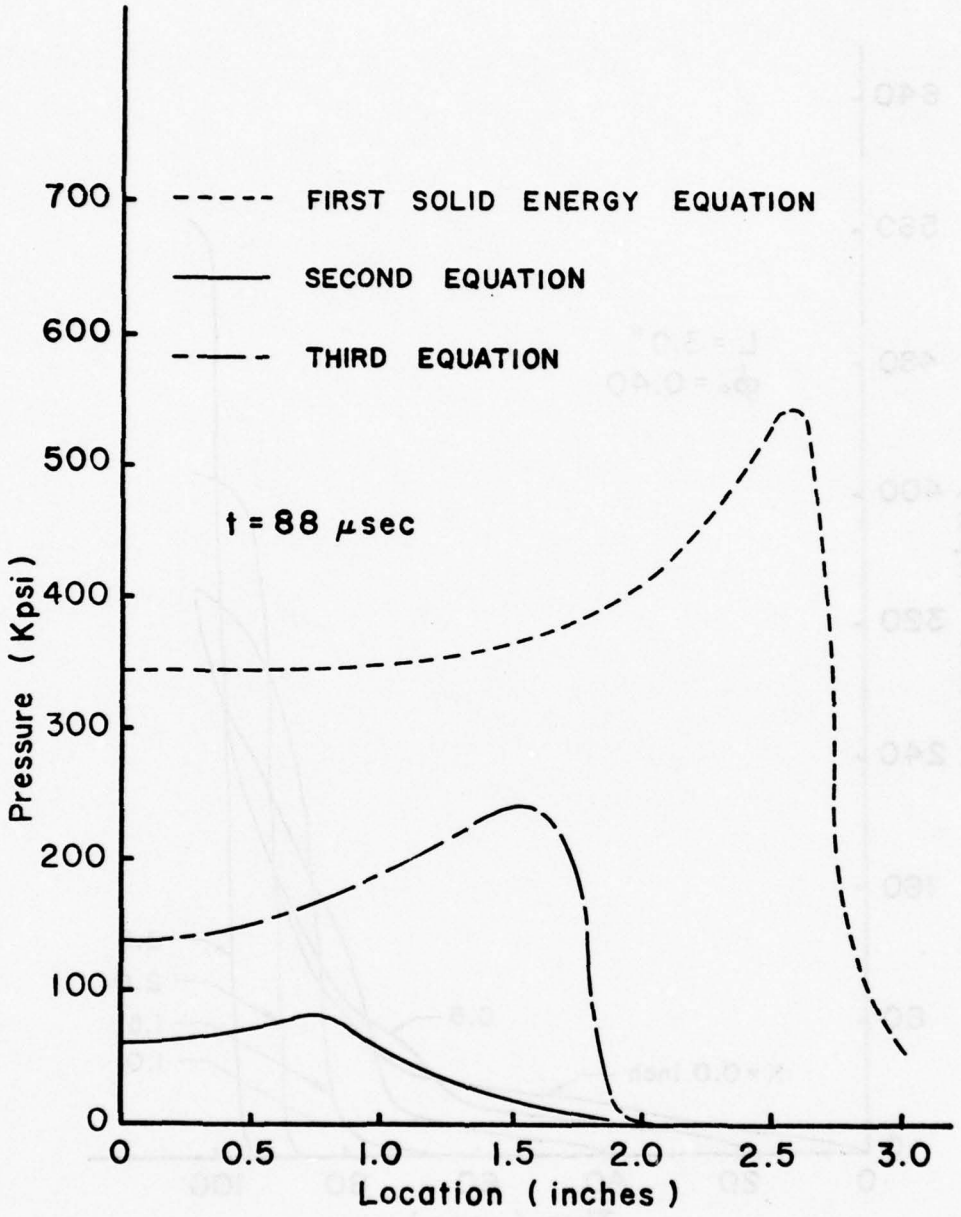

Figure 4.12 Pressure distribution at a given time for three different forms of the particle-energy balance. [The alternate gas viscosity law was utilized for all three calculations.]

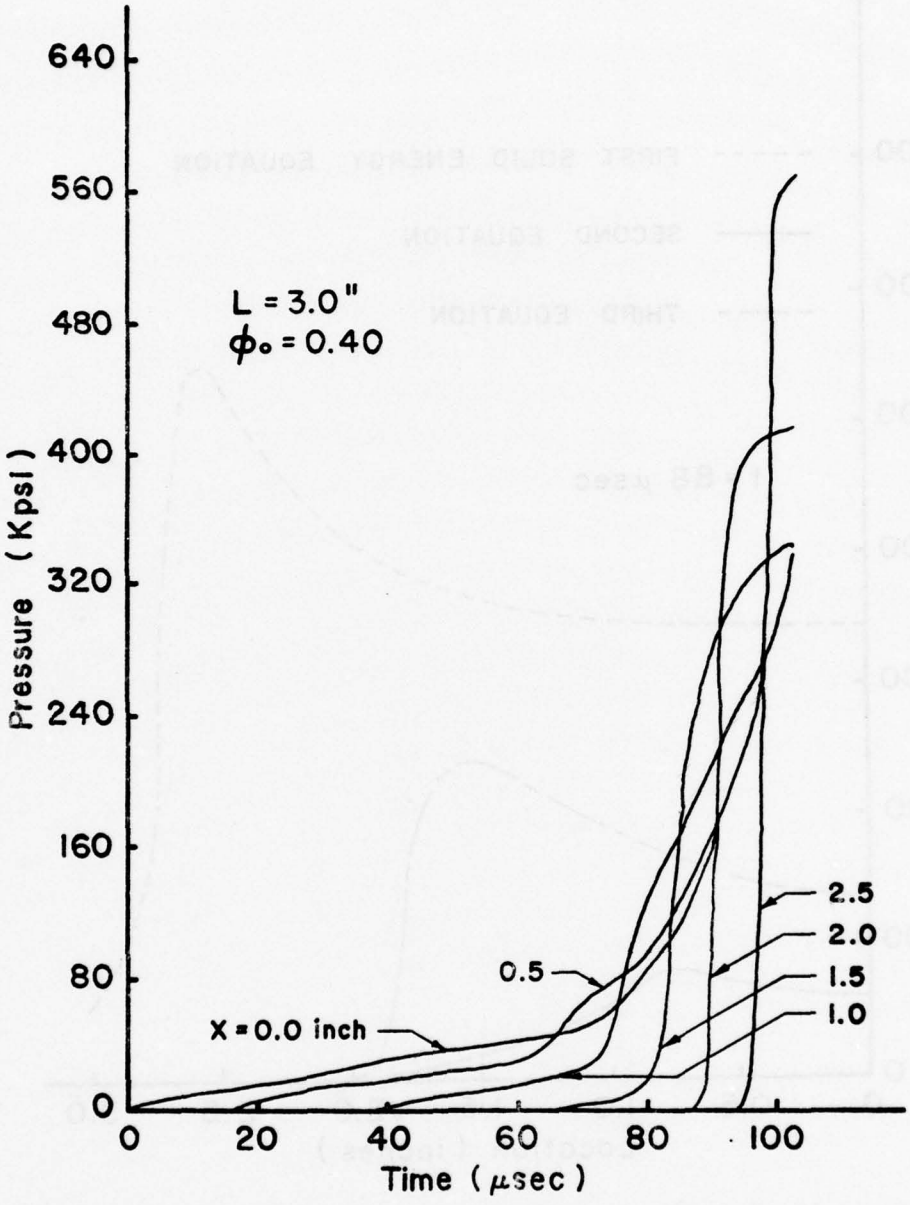

Figure 4.13 The pressure-time variations at six different locations. [Figs. 4.13 - 4.16 utilize the third form of the particle-energy equation.]

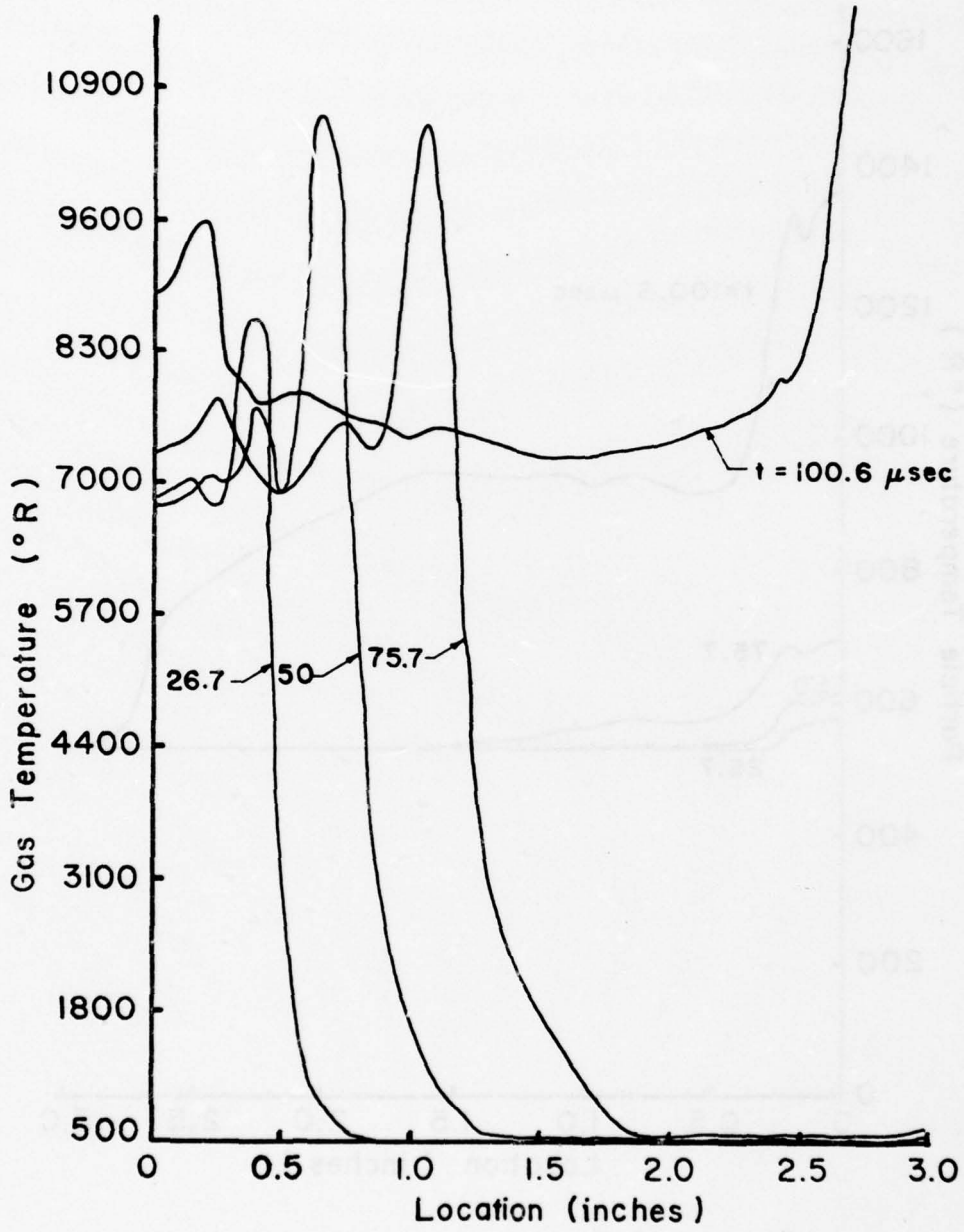

Figure 4.14 Gas temperature distribution history.

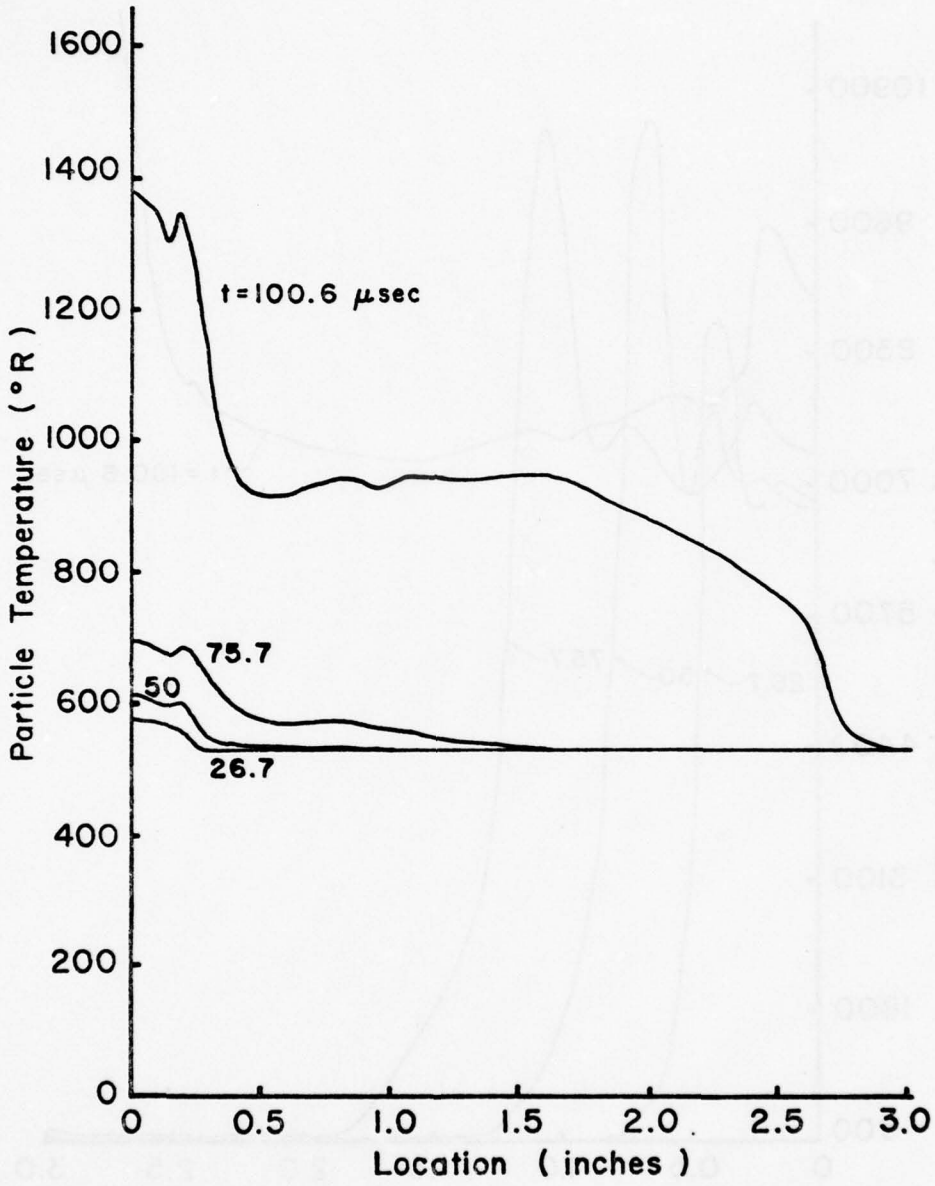

Figure 4.15 Particle temperature distribution history.

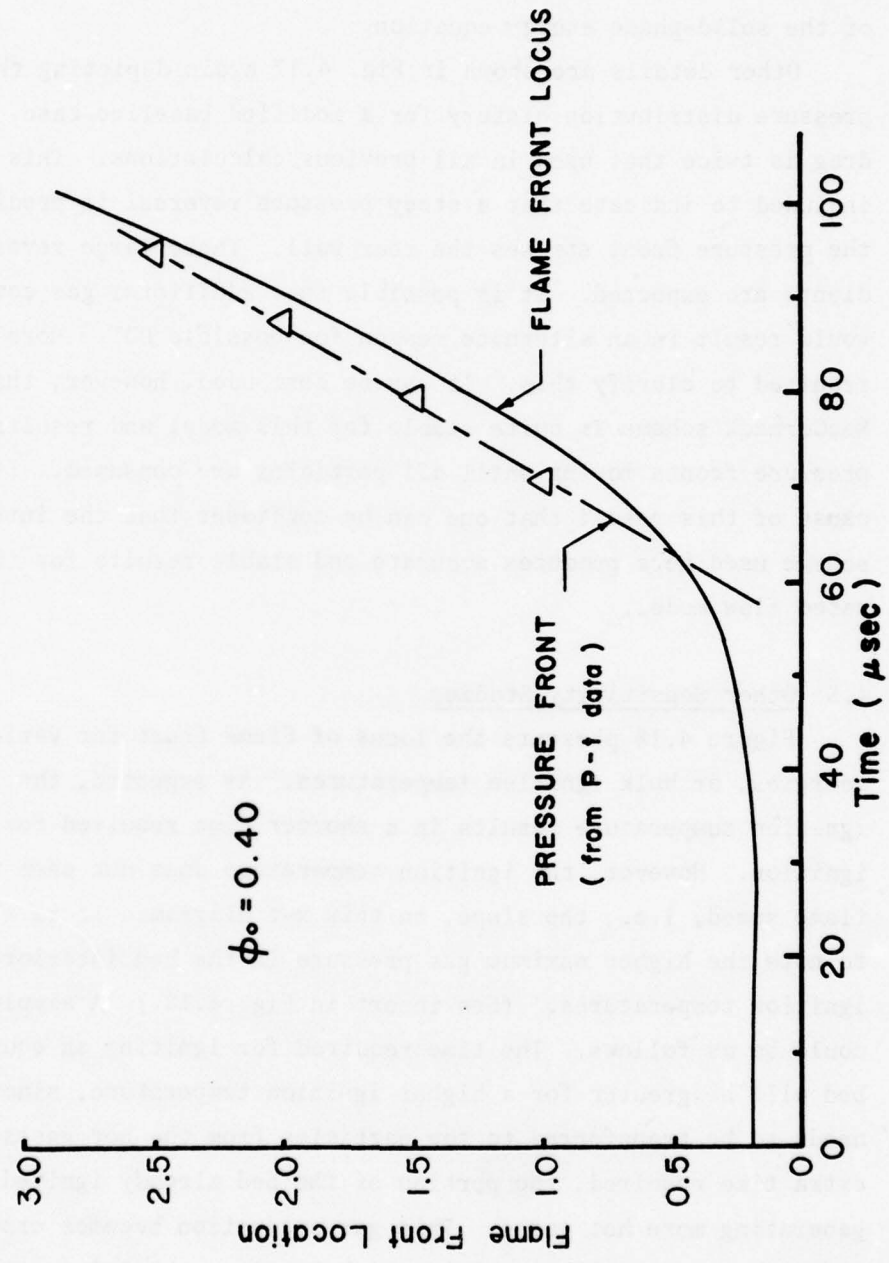

Figure 4.16 Flame front locus and pressure wave front, indicating conditions for possible DDT.

shock supported by a combustion region. Also, the flame front accelerates from a speed of 1.9 mm/μsec at x = 2 inches to about 2.5 mm/μ-sec at x = 2.75 inches. It is concluded that a search for possible DDT should include a thorough study of this alternate form of the solid-phase energy equation.

Other details are shown in Fig. 4.17 again depicting the pressure distribution history for a modified baseline case. Here the drag is twice that used in all previous calculations. This figure is included to indicate that a steep pressure reversal is predicted after the pressure front strikes the rear wall. These large reverse gradients are expected. It is possible that additional gas compression would result in an alternate reason for possible DDT. More work is required to clarify this. It can be concluded, however, that the MacCormack scheme is quite stable for this model and results indicate pressure fronts moving until all particles are consumed. It is because of this result that one can be confident that the integration scheme used here produces accurate and stable results for the separated flow model.

4.5 Other Sensitivity Studies

Figure 4.18 presents the locus of flame front for various ignition energies, or bulk ignition temperatures. As expected, the lower bulk ignition temperature results in a shorter time required for complete bed ignition. However, the ignition temperature does not seem to affect the flame speed, i.e., the slope, on this x-t diagram. It is also interesting to note the higher maximum gas pressure in the bed interior for higher ignition temperatures. (See insert in Fig. 4.18.) A simple explanation could be as follows. The time required for igniting an equal length of bed will be greater for a higher ignition temperature, since more energy needs to be transferred to the particles from the hot gases. In this extra time required, the portion of the bed already ignited keeps on generating more hot gases. This gas production becomes especially significant for propellants with a high burning rate index (n = 0.9). We can conclude that, at the conditions being studied here, the ignition energy (or temperature) variation is not necessarily of primary importance for setting up transition to detonation. Of course, for quantitative analysis, such as a detonation run-up length the ignition

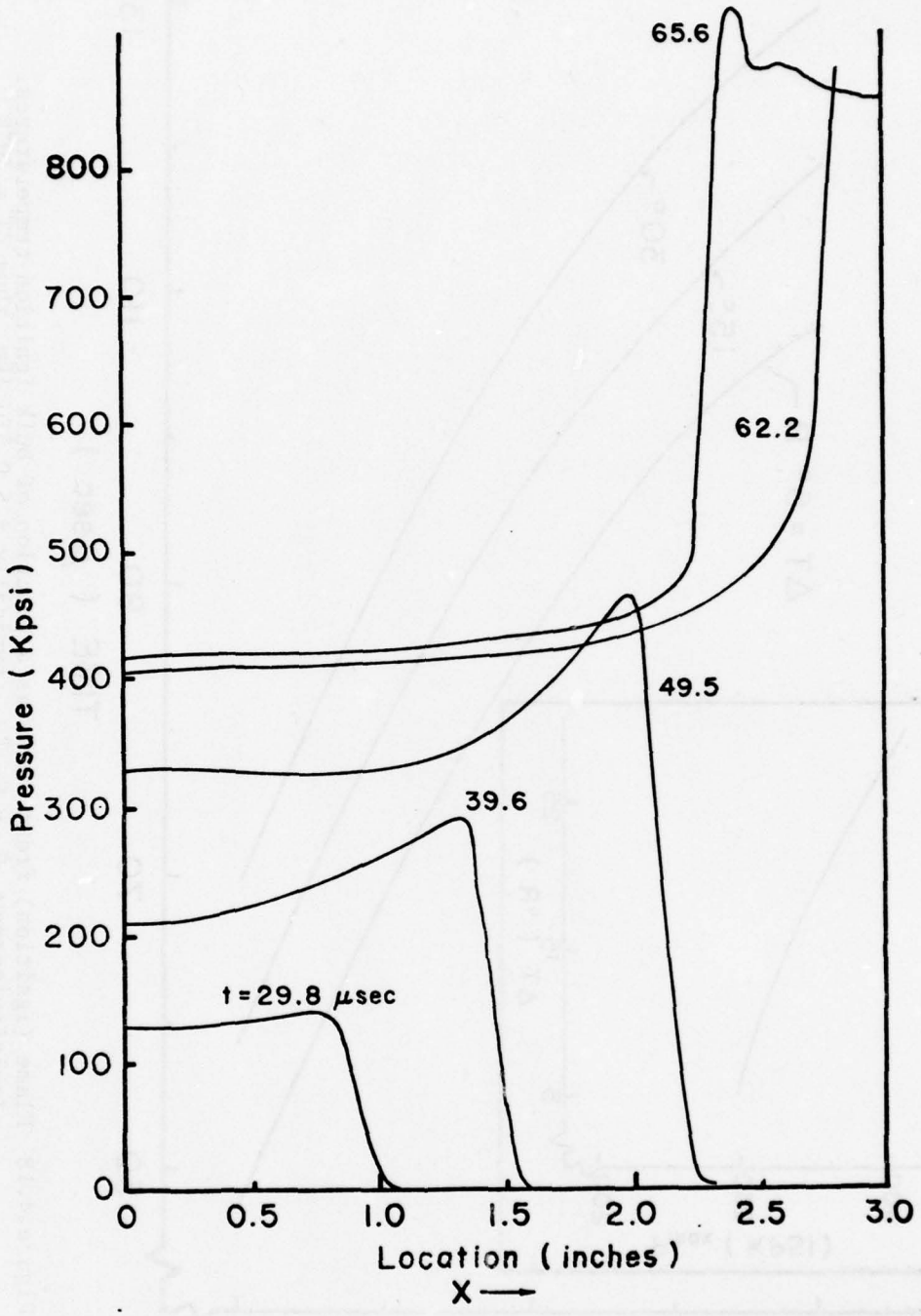

Figure 4.17 Pressure distribution history, indicating strong pressure wave reversal after the pressure front reflects from rear wall. [Viscous inter-phase drag assumed here is twice that used for calculations shown in Fig. 4.1.]

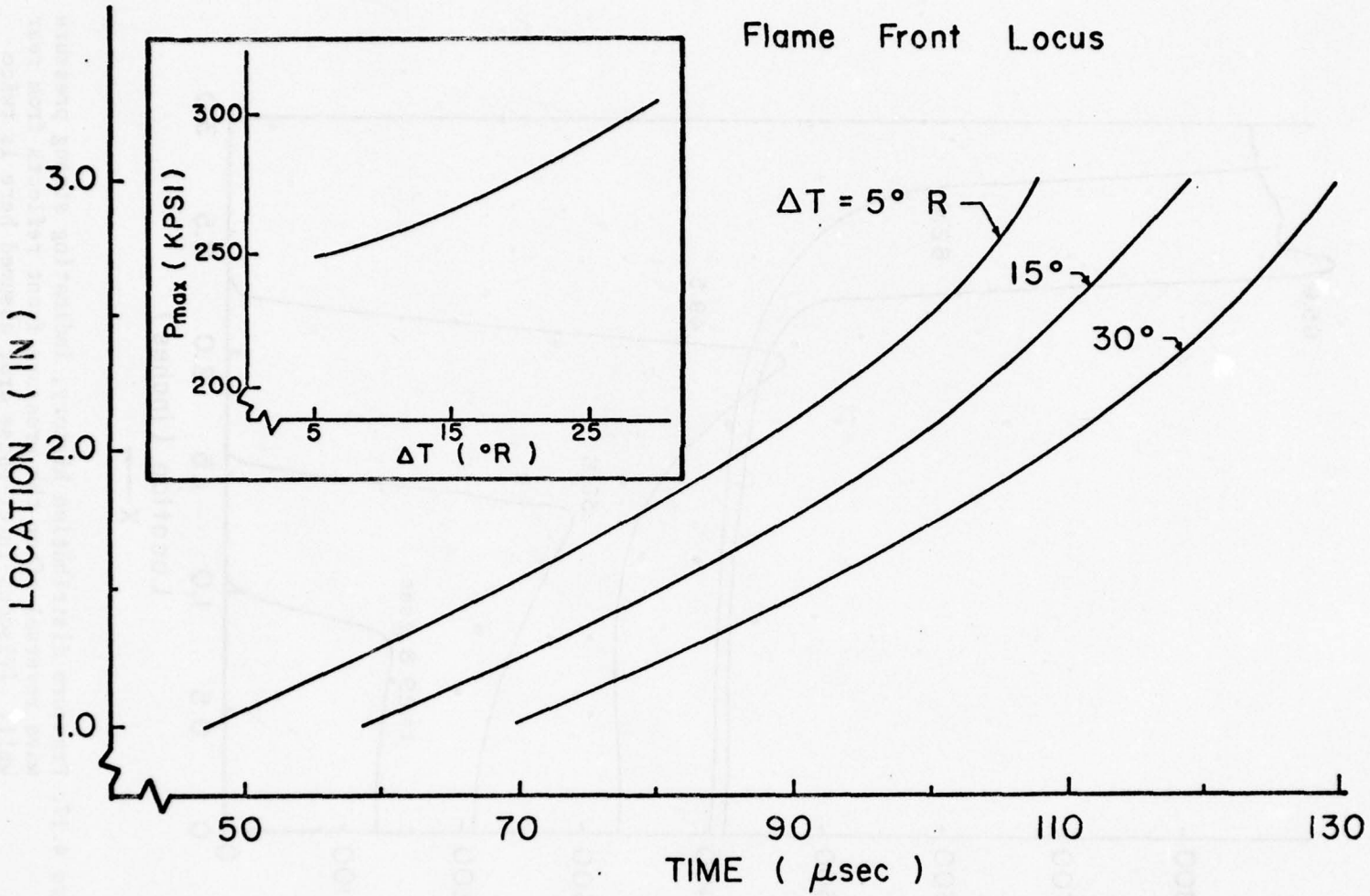

Figure 4.18 Flame (ignition) front locus as a function of bulk ignition temperatures. (Ignition energy, $E_I = C_{V_p} T_{P_I}$, typically = 5.0 BTU/lbm, thus $\Delta T = 30°R$ represents 10.0 BTU/lbm, while $\Delta T = 5°R$ indicates 1.67 BTU/lbm.)

temperature (energy) should be specified as accurately as possible.

Figure 4.19 depicts the effect of drag correlation on the flame locus. In general, the drag coefficient, C_D, modifying the function f_{gp} has minimum effect on either the time required for complete bed ignition or the flame speeds. But it is interesting to note that the full Ergun's drag (C_D = 1) did not compute for this separated flow model. It was observed that, even with C_D = 5.0, only 50% of the bed was ignited before the flow gradients, in particular the pressure gradient, became unrealistically large, and the program became unstable. A larger value of C_D means a lower drag. For lower drag conditions, the particles are not accelerated enough to cause localized compaction, and hence the maximum pressures predicted were significantly lower. Or, corresponding to lower drag, the gases will travel faster and convective heat transfer is more rapid with the pressure more uniform.

Figure 4.20 shows the pressure distribution in a three-inch bed at one typical instant. Here $\overline{H}$ is defined as the ratio of actual gas-solid heat transfer coefficient to that calculated by the Denton formula. The lower the value of $\overline{H}$, the less heat will be transferred from hot gases to the particles. That is, for smaller values of $\overline{H}$, less energy will be removed from the gas phase and transferred to the particle phase. As a result of retention of energy content in the gas phase, the pressure predicted at the equal time will be higher. It seems apparent that both the interphase viscous drag correlation, f_{pg}, and the interphase heat transfer correlation, h_{pg}, are sensitive functions of the dynamic flow being modelled here. There is no data available that indicates whether any of the formulas used here, generally developed from cold-flow, steady, low-pressure experiments are applicable to the transient high pressure conditions being studied here.

Figure 4.21 depicts the flame front (ignition) locus again for three different heat transfer coefficients, $\overline{H}$. Note that the greater the gas-particle heat transfer, the greater the time required for the complete bed ignition. It seems an extension of the previous explanation. Higher $\overline{H}$ means more energy will be transferred to the particle phase from the gas phase. Thus, the gas phase energy available for convecting towards the unignited particles will be less and, consequently, the time required for the complete bed ignition will be more. However, there does

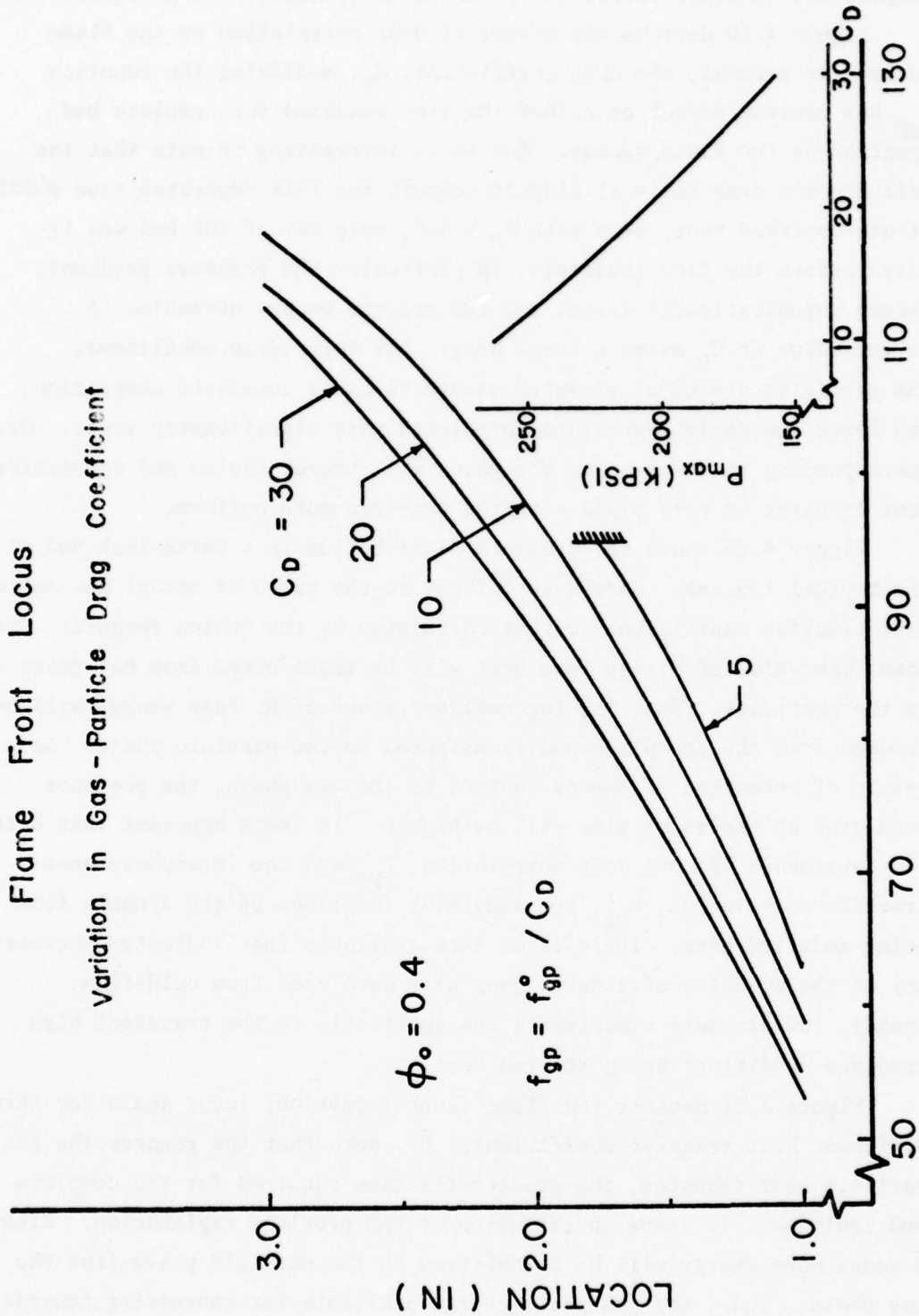

Figure 4.19 Flame (ignition) front locus as a function of the interphase momentum (drag) correlation of Ergun, reduced by a constant value, C_D.

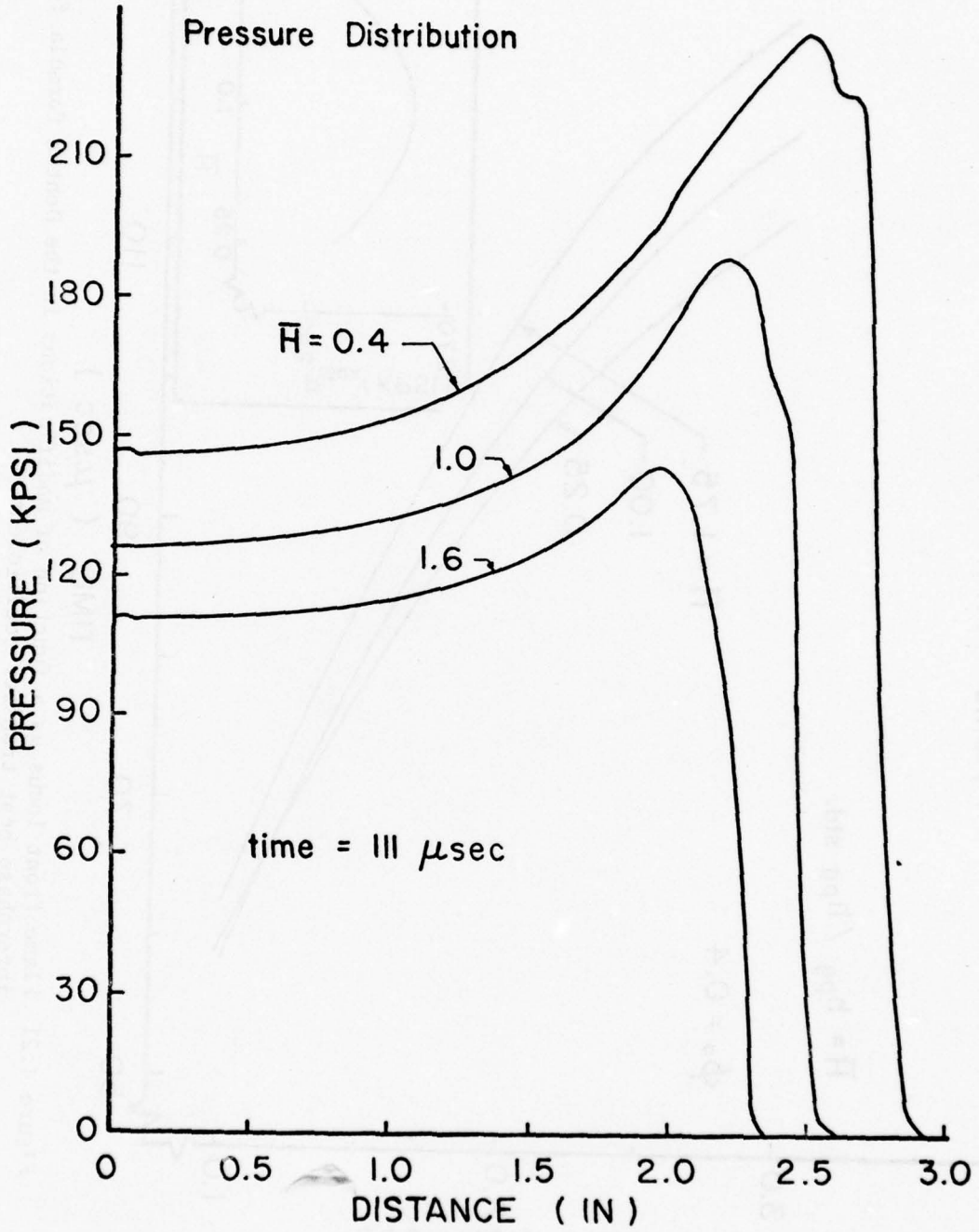

Figure 4.20 Pressure distribution at a fixed time (t = 111 μsec) for three different heat transfer coefficients, modifying Denton's formula.

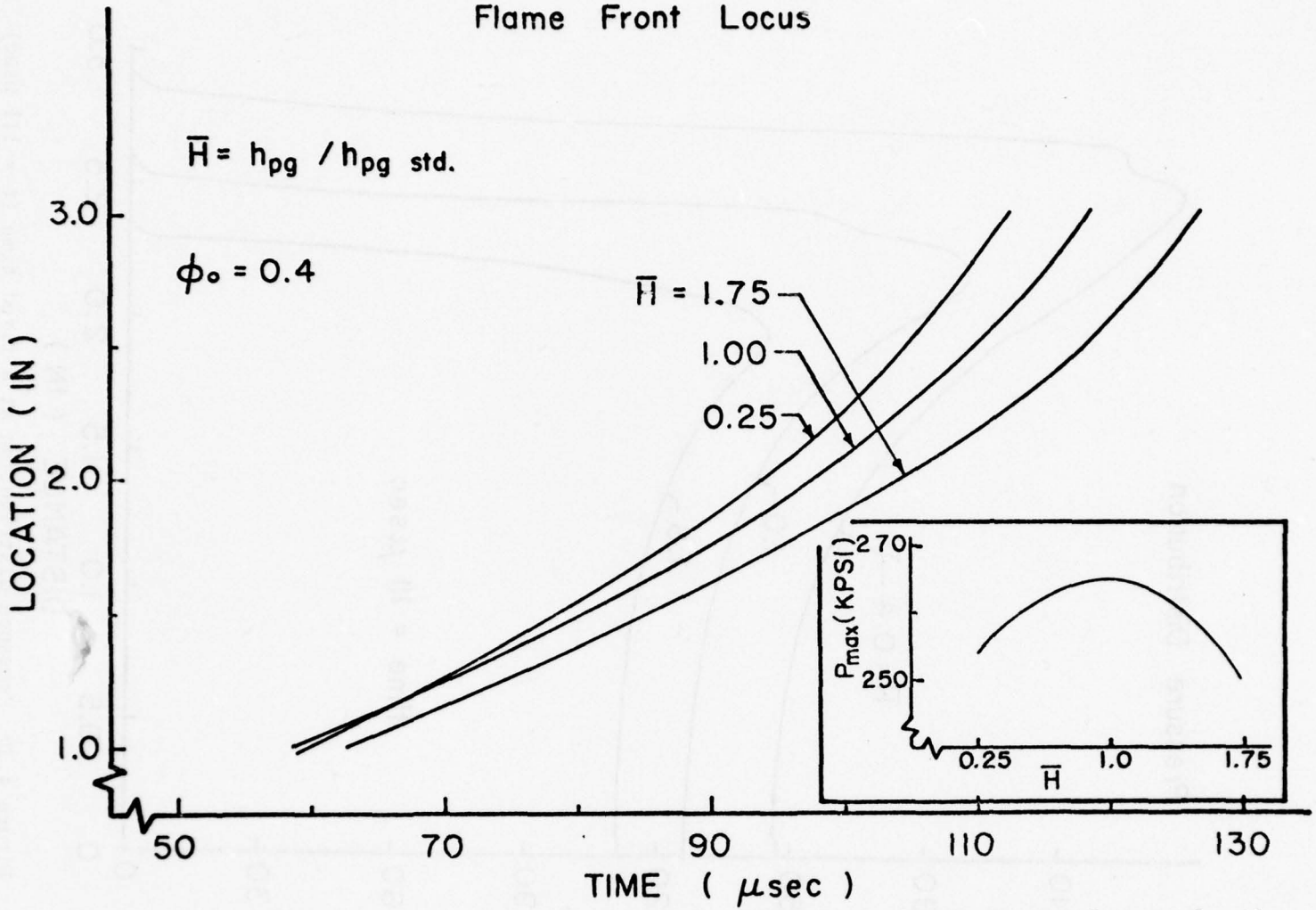

Figure 4.21 Flame front locus as a function of modifications in the Denton formula for the interphase heat transfer coefficient.

not seem to be any change in relative flame acceleration for various heat transfer coefficients. Additionally, the predicted maximum pressure (see insert) for various heat transfer coefficients fails to provide insight into the dynamic behavior during the convection process.

Figure 4.22 shows the flame front locus for alternative forms of the propellant burning rate law. An attempt was made to make the rate sensitive to the particle temperature, as shown by the equation given in the figure. Even though the temperature sensitivity index, assumed here to be 1/4, is somewhat arbitrary, it was felt that some form of temperature sensitivity of rate law should be accounted for, since propellants are known to burn more rapidly as their mean (storage) temperature is increased. This is a first attempt in that direction. As expected, the more sensitive the rate law is to the particle temperature, the faster the whole bed is ignited. This seems logical since a more temperature-sensitive burning rate law generates more hot gases which will be convected forward to produce higher gradients. This also explains the higher maximum bed interior pressure for the more temperature-sensitive burning rate law, as shown in the insert of the figure.

Finally, Fig. 4.23 shows the flame front loci for various coefficients multiplying the particle-particle interaction law. In general, it shows that the lower the particle-particle interaction, the sooner the whole bed is ignited. The particle-particle interaction law used here is the one employed by Kuo et al. [22], where the nominal value $K = 6.94 \times 10^4$ lbf/in^2 was utilized. Large values of the particle-particle interaction indicate that the bed would resist the further compaction more severely. Correspondingly, for the case of 10 K, apparently the bed resistance to compaction is so high that before the complete bed is ignited the numerical code goes unstable due to resulting excessively high gradients. The flame locus does not show any interesting flame accelerations or any significant change in the total bed ignition time. As with the interphase heat and momentum correlations, there seems to be only a limited range of these formulations which allow (with our computational scheme) for well-behaved solutions which lead to complete ignition of a given length of granulated propellant.

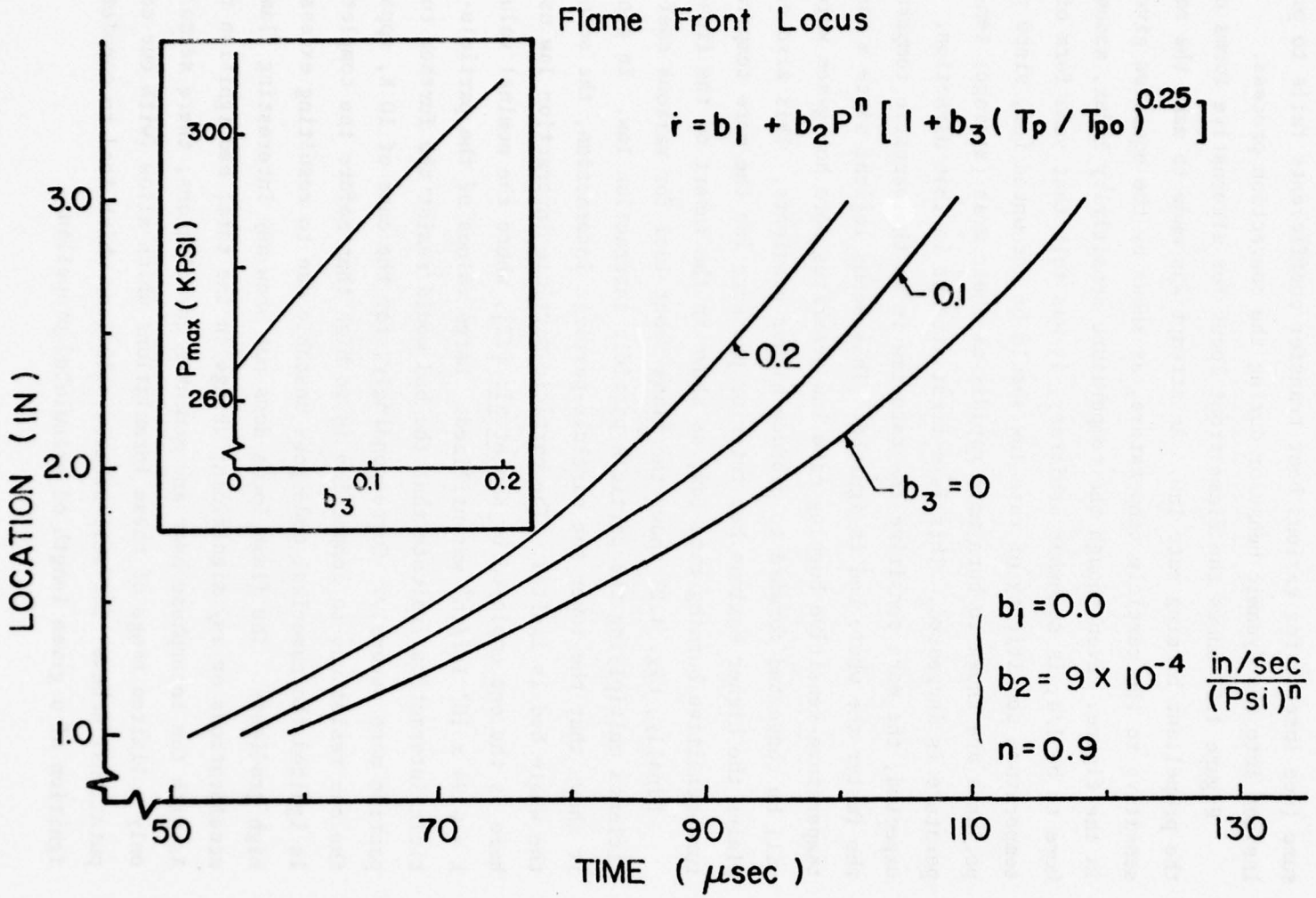

Figure 4.22 Flame front locus as a function of propellant burning rate sensitive to the bulk temperature of the solid.

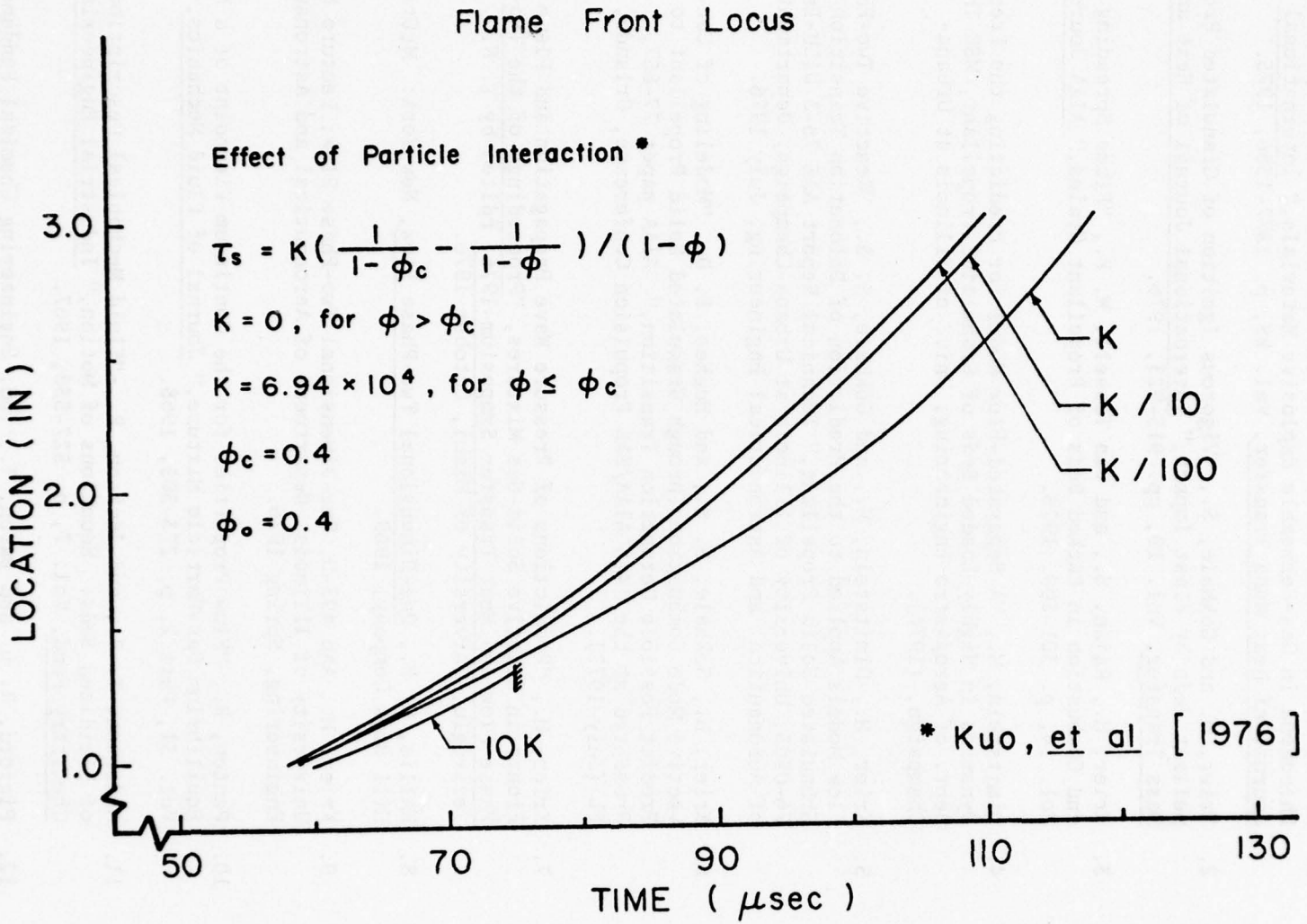

Figure 4.23 Flame (ignition) front locus for variations in the amount of particle-particle interaction, resisting propellant compaction.

REFERENCES

1. Krier, H. and Van Tassell, W. F.,"Combustion and Flame Spreading Phenomena in Gas-Permeable Explosive Materials," International Journal of Heat Mass Transfer, Vol. k8, p. 1377-1386, 1975.

2. Krier, H. and Gokhale, S., "Vigorous Ignition of Granulated Propellant Beds by Blast Impact," International Journal of Heat and Mass Transfer, Vol. 19, pp. 915-923, 1976.

3. Krier, H., Rajan, S., and Van Tassell, W. F., "Flame Spreading and Combustion in Packed Beds of Propellant Grains," AIAA Journal, Vol. 14, p. 301-309, 1976.

4. Dimitstein, M., "A Separated-Flow Model for Predicting the Pressure Dynamics in Highly Loaded Beds of Granulated Propellant, MSE Thesis, Dept. of Aero/Astro Engineering; Univ. of Illinois at Urbana-Champaign, (1976).

5. Krier, H., Dimitstein, M., and Gokhale, S. S., "Reactive Two-Phase Flow Models Applied to the Prediction of Detonation Transition in Granulated Solid Propellant," Technical Report AAE 76-3 UILU-Eng 76-0503, University of Illinois at Urbana-Champaign, Department of Aeronautical and Astronautical Engineering, July 1976.

6. Krier, H., Gokhale, S. S., and Hughes, E. D., "Modeling of Convective Mode Combustion Through Granulated Solid Propellant to Predict Possible Detonation Transition," AIAA paper 77-857, Presented at the 14th AIAA/SAE Propulsion Conference, Orlando, FL (July 1977).

7. Krier, H., "Predictions of Pressure Wave Propagation and Flame Fronts in Reactive Solid-Gas Mixtures, "Proceedings of the Two-Phase Flow and Heat Transfer Symposium-1976, Edited by T. N. Veziroglu, University of Miami, October 1976.

8. Wallis, G. B., One-Dimensional Two-Phase Flow, New York: McGraw-Hill Book Company, 1969.

9. Krier, H., AAE 493-D, One-Dimensional Two-Phase Flow; Lecture Notes, University of Illinois, Department of Aeronautical and Astronautical Engineering, Spring 1976.

10. Panton, R., "Flow Properties for the Continuum Viewpoint of a Non-Equilibrium Gas-Particle Mixture," Journal of Fluid Mechanics, Vol. 31, Part 2, p. 273-303, 1968.

11. Anderson, T. B., and Jackson, R., "Fluid Mechanical Description of Fluidized Beds: Equations of Motion," Industrial Engineering Chemistry Fund, Vol. 7, p. 527-538, 1967.

12. Pigford, R. L. and Baron, T., Ind. Engineering Chemical Fundamentals, Vol. 4, pp. 81-89 (1965).

13. Green, A. E. and Naghdi, P. M., "On Basic Equation for Mixtures," Quarterly Journal Mechanical and Applied Math, Vol. 22, Part 4, pp. 427-438, 1969.

14. Crowe, C. T., "Conservation Equations for Vapor-Droplet Flows," Proceedings of the 1976 Heat Transfer and Fluid Mechanics Institute, Stanford, California: Stanford University Press, 1976.

15. Solbrig, C. W., Mortensen, G. A., and Lyczkowski, R. W., "An Unequal Phase Velocity, Unequal Phase Temperature Theory Applied to Two-Phase Blowdown from a Horizontal Pipe," Proceedings of the 1976 Heat Transfer and Fluid Mechanics Institute, Stanford, Cali-California: Stanford University Press, 1976.

16. Hughes, E. D., "Field Balance Equations for Two-Phase Flows in Porous Media, "Proceedings of the Two-Phase Flow and Heat Transfer Symposium-1976, Edited by T. N. Veziroglu, University of Miami, October 1976.

17. Kuo, K. K. and Summerfield, M., "High Speed Combustion of Mobile Granular Solid Propellants," Fifteenth Symposium on Combustion, The Combustion Institute, Pittsburgh, Pennsylvania, pp. 515-525, August 1974.

18. Gough, P., "Fundamental Investigation of the Interior Ballistics of Guns," Space Corporation Report SRC-R-74, 1974.

19. Nigmatulin, R. I., "Methods of a Continuous Medium for the Description of Multiphase Mixtures," Soviet J. Fluid Mechanics, Vol. 2, No. 5, p. 33 (1967).

20. Gidaspow, D., Fifth International Heat Transfer Conference, Vol. 7, p. 163 (1974).

21. Zuber, N., Chem. Eng. Science, Vol. 19, p. 897 (1964).

22. Kuo, K. K., Koo, J. H., Davis, T. R., and Coates, G. R., "Transient Combustion in Mobile Gas-Permeable Propellants," Acta Astronautica, Vol. 3, pp. 573-591 (1976).

23. Culick, F. E. C., "Conservation Equations for a Reacting Two-Phase Flow Based on Continuum Theory," Summary notes for Workshop presented at 12th JANNAF Combustion Meeting, Newport, Rhode Island, August 1975.

24. Soo, S. I., Int. J. Multiphase Flow, Vol. 3, p. 79 (1976).

25. Ames, W. F., Nonlinear Partial Differential Equations in Engineering, New York: Academic Press, pp. 416-461, 1965.

26. Warming, R. F., Kutler, P., and Lomax, H., "Second and Third Order Non-centered Difference Schemes for Nonlinear Hyperbolic Equations," AIAA Journal, Vol. 11, No. 2, pp. 189-195, February 1973.

27. Rudinger, G., Nonsteady Duct Flow: Wave-Diagram Analysis. New York, Dover Publications, Inc., pp. 55-56, 1969.

28. Dwyar, H., Allen, R., Ward, M., Karnopp, D., and Margolis, D., "Shock Capturing Finite Difference Methods for Unsteady Gas Transfer," AIAA Paper No. 74-521, Presented at AIAA 7th Fluid and Plasma Dynamics Conference, Palo, Alto, CA, June 1974.

29. Roache, P. J., Computational Fluid Dynamics. Albuquerque, New Mexico: Hermos Publishers, pp. 261-271, 1972.

30. See Ames, W. F., Nonlinear Partial Differential Equations in Engineering. New York: Academic Press, 1965.

31. Hung, C. M. and MacCormack, R. W., "Numerical Solutions of Supersonic and Hypersonic Laminar Compression Corner Flows," AIAA Journal, Vol. 14, No. 4, pp. 475-481, April 1976.

32. Denton, W. H., "General Discussion on Heat Transfer," Institution of Mechanical Engineers and American Society of Mechanical Engineers, London, p. 370, 1951.

33. Ergun, S., "Fluid Flow Through Packed Columns," Chemical Engineering Progress, Vol. 48, pp. 89-96, 1952.

34. Kuo, K. K., and Nydegger, C. C., "Cold Flow Resistance Measurement and Correlation in a Packed Bed of WC-870 Spherical Propellants," to be published (1976).

35. Bernecker, R. R. and Price, D., "Studies in the Transition to Detonation in Granular Explosives," Combustion and Flame 22, Parts I-II, pp. 111-129 (1974); Part III, pp. 161-170 (1974).

36. Gipson, R. W. and Maček, A., "Flame Fronts and Compression Waves During Transition from Deflagration to Detonation in Solids," Eighth Symposium on Combustion, Williams & Wilkins Co., Baltimore, MD (1962), pp. 847-854.

APPENDIX A: DERIVATION OF THE TWO-PHASE CONSERVATION EQUATIONS WITH SEPARATE-FLOW CONCEPT

The following is a summary of the key steps generally used to derive the six field-balance conservation equations. Some of the details were presented in a graduate course, AAE 493, taught by Professor H. Krier, on the subject of one-dimensional two-phase flow. The key assumptions are:

1) The gas phase and the solid phase are treated separately.
2) The motion of the two phases is coupled through interaction terms.
3) Each phase is treated as a continuum.
4) Solid particles are large compared to molecules.

Conservation of Mass

(a) Gas Phase Continuity

Consider a control volume with gas flowing through it.

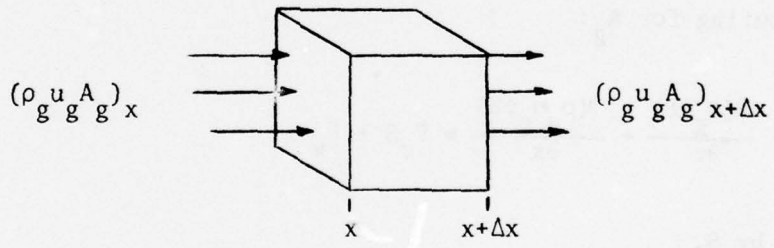

Increase of mass inside = mass added to control volume in time t

$$\frac{\partial(\rho_g A_g \Delta x)}{\partial t} = (\rho_g u_g A_g)_x - (\rho_g u_g A_g)_{x+\Delta x} + \Gamma_c S \Delta x + \Gamma_w \Delta x \qquad (1)$$

where

ρ_g = density of the gas

A_g = cross-sectional area of gas phase

u_g = velocity of the gas

Γ_c = gas source due to combustion of solid particles, = Γ_g

Γ_w = gas source due to combustion of walls

S = total cross-sectional area of control volume

Note that Γ_c is defined as mass per total volume per unit time. Also Γ_w is defined as mass per unit length per unit time.

Now divide by Δx (which is not a function of time) and let $\Delta x \to 0$.

$$\frac{\partial(\rho_g A_g)}{\partial t} = - \frac{\partial(\rho_g u_g A_g)}{\partial x} + \Gamma_c S + \Gamma_w \quad . \tag{1a}$$

Now use the definition of porosity to further simplify:

$$\phi = \frac{A_g \Delta x}{S \Delta x} = \frac{A_g}{S} \quad - - \rightarrow \quad A_g = \phi S$$

$$1-\phi = \frac{S-A_g}{S} = \frac{A_p}{S} \quad - - \rightarrow \quad A_p = (1-\phi)S$$

Substituting for A_g:

$$\frac{\partial(\rho_g \phi S)}{\partial t} + \frac{\partial(\rho_g u_g \phi S)}{\partial x} = \Gamma_c S + \Gamma_w \tag{1b}$$

Divide by S,

$$\frac{\partial(\phi \rho_g)}{\partial t} + \frac{1}{S} \frac{\partial(\phi \rho u_g S)}{\partial x} = \Gamma_c - \frac{\Gamma_w}{S} \tag{1c}$$

Let $\rho_1 = \phi \rho_g$ and expand partial derivatives.

$$\frac{\partial(\rho_1)}{\partial t} + \frac{1}{S}\left[\rho_1 u_g \frac{\partial S}{\partial x} + \rho_1 S \frac{\partial u_g}{\partial x} + u_g S \frac{\partial \rho_1}{\partial x}\right] = \Gamma_c + \frac{\Gamma_w}{S} \tag{1d}$$

Rearranging the term, the final form is written in the manner most useful for implementation in a finite difference scheme, that is,

$$\frac{\partial \rho_1}{\partial t} = -\rho_1 \frac{\partial u_g}{\partial x} - u_g \frac{\partial \rho_1}{\partial x} - \frac{\rho_1 u_g}{S} \frac{\partial S}{\partial x} + \Gamma_c + \frac{\Gamma_w}{S} \tag{2}$$

(b) Solid Phase Continuity

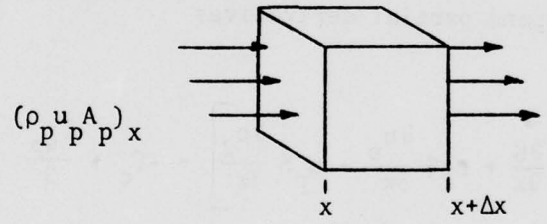

$$\frac{\partial (\rho_p A_p \Delta x)}{\partial t} = (\rho_p u_p A_p)_x - (\rho_p u_p A_p)_{x+\Delta x} + \Gamma_p S \Delta x + \Gamma_{wp} \Delta x \tag{3}$$

where

ρ_p = density of the solid particles

A_p = cross-sectional area of the particles

u_p = velocity of the particles

Γ_p = mass rate loss of particles; must equal $-\Gamma_c$

Γ_{wp} = particle source from walls

Note that Γ_p is defined as mass per total volume per unit time. Also Γ_{wp} is defined as mass per unit length per unit time. Again divide by Δx and let $\Delta x \to 0$.

$$\frac{\partial(\rho_p A_p)}{\partial t} = - \frac{\partial(\rho_p u_p A_p)}{\partial x} + \Gamma_p S + \Gamma_{wp} \tag{3a}$$

Substituting for A_p from the previous page

$$\frac{\partial[\rho_p(1-\phi)S]}{\partial t} + \frac{\partial[\rho_p u_p(1-\phi)S]}{\partial x} = \Gamma_p S + \Gamma_{wp} \tag{3b}$$

Divide by S and employ the relation $\Gamma_p = - \Gamma_c$

$$\frac{\partial[(1-\phi)\rho_p]}{\partial t} + \frac{1}{S} \frac{\partial[(1-\phi)\rho_p u_p S]}{\partial x} = - \Gamma_c + \frac{\Gamma_{wp}}{S} \tag{3c}$$

Let $\rho_2 = (1-\phi)\rho_p$ and expand partial derivatives

$$\frac{\partial(\rho_2)}{\partial t} + \frac{1}{S}\left[\rho_2 u_p \frac{\partial S}{\partial x} + \rho_2 S \frac{\partial u_p}{\partial x} + u_p S \frac{\partial \rho_2}{\partial x}\right] = -\Gamma_c + \frac{\Gamma_{wp}}{S} \tag{3d}$$

Rearranging terms yields the final form of the equation

$$\boxed{\begin{aligned} \frac{\partial \rho_2}{\partial t} = & - \rho_2 \frac{\partial u_p}{\partial x} \\ & - u_p \frac{\partial \rho_2}{\partial x} \\ & - \frac{\rho_2 u_p}{S} \frac{\partial S}{\partial x} \\ & - \Gamma_c \\ & - \frac{\Gamma_{wp}}{S} \end{aligned}} \tag{4}$$

Conservation of Momentum

(a) Gas Phase Balance

Once again consider the control volume with mass flowing through it.

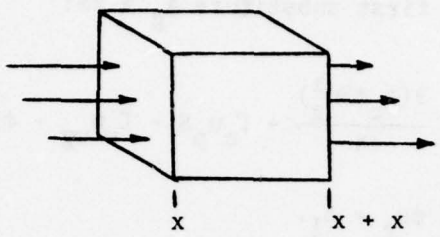

Time rate of increase of momentum inside the control volume.

The sum of the forces acting on the control volume. These include:

Momentum flux through entrance and exit.

Interaction forces.

Pressure gradient force.

Forces associated with mass addition or loss.

Thus

$$\frac{\partial(\rho_g A u_g)}{\partial t} = -\frac{\partial(\rho_g A u^2)}{\partial x} + \Gamma_c u_p S - \Gamma_w u_{wg} - A_g \frac{\partial P}{\partial x} - \overline{F}S \qquad (5)$$

Note that it is assumed the pressure gradient force acts only on the area A_g. It is also assumed that since the gas is formed at a velocity equal to the particle velocity, there is a source of gas momentum per unit area equal to $\Gamma_c u_p$. Of course the solid phase must have a sink of momentum equal to that amount. Also, here,

u_{wg} = x - component of the velocity of the gas leaving the control volume.

$\bar{F}$ = viscous interaction force between the gas and the solid particles.

To simplify Eq. (5) first substitute $A_g = \phi S$:

$$\frac{\partial(\rho_g \phi S u_g}{\partial t} = - \frac{\partial(\rho_g \phi S u_g^2)}{\partial x} + \Gamma_c u_p S - \Gamma_w u_{wg} - \phi S \frac{\partial P}{\partial x} - \bar{F} S \tag{5a}$$

Divide by S and let $\phi \rho_g = \rho_1$.

$$\frac{\partial(\rho_1 u_g)}{\partial t} + \frac{1}{S} \frac{\partial(\rho_1 S u_g^2)}{\partial x} = \Gamma_c u_p - \frac{\Gamma_w u_{wg}}{S} - \phi \frac{\partial P}{\partial x} - \bar{F} \tag{5b}$$

Now expand the partial derivatives:

$$\rho_1 \frac{\partial u_g}{\partial t} + u_g \frac{\partial \rho_1}{\partial t} + \frac{1}{S} \left[2\rho_1 S u_g \frac{\partial u_g}{\partial x} + \rho_1 u_g^2 \frac{\partial S}{\partial x} - S u_g \frac{\partial \rho_1}{\partial x} \right] \tag{5c}$$

$$= \Gamma_c u_p - \frac{\Gamma_w u_{wg}}{S} - \phi \frac{\partial P}{\partial x} - \bar{F}$$

To further simplify this equation, take the gas continuity equation (2) and multiply it by u_g

$$u_g \frac{\partial \rho_1}{\partial t} = -\rho_1 u_g \frac{\partial u_g}{\partial x} - u_g^2 \frac{\partial \rho_1}{\partial x} - \frac{\rho_1 u_g^2}{S} \frac{\partial S}{\partial x} + u_g \Gamma_c + \frac{u_g \Gamma_w}{S} \tag{2*}$$

Subtract Eq. (2*) from Eq. (5c) to get

$$\rho_1 \frac{\partial u_g}{\partial t} + \rho_1 u_g \frac{\partial u_g}{\partial x} = \Gamma_c (u_p - u_g) - \frac{\Gamma_w}{S} (u_{wg} + u_g) - \phi \frac{\partial P}{\partial x} - \bar{F} \tag{5d}$$

Rearranging the terms, one finally obtains

$$\frac{\partial u_g}{\partial t} = - u_g \frac{\partial u_g}{\partial x} - \frac{\phi}{\rho_1} \frac{\partial P}{\partial x} + \frac{\Gamma_c}{\rho_1}(u_p - u_g) - \frac{\Gamma_w}{\rho_1 S}(u_{wg} + u_g) - \frac{\bar{F}}{\rho_1} \tag{6}$$

(b) Solid Phase Momentum Balance

Remembering the assumption that the particles act as a continuum, the solid phase momentum equation can be written as follows.

$$\frac{\partial(\rho_p A_p u_p)}{\partial t} = - \frac{\partial(\rho_p A_p u_p^2)}{\partial x} - \Gamma_c u_p S - A_p \frac{\partial \tau_p}{\partial x} + \bar{F}S \tag{7}$$

Note that here it is assumed the pressure gradient force acts only on the area A_p and particle source from the walls has been neglected. To simplify Eq. (7), first substitute $A_p = (1-\phi)S$

$$\frac{\partial[\rho_p(1-\phi)Su_p]}{\partial t} = - \frac{\partial[\rho_p(1-\phi)Su_p^2]}{\partial x} - \Gamma_c u_p S - (1-\phi)S \frac{\partial \tau_p}{\partial x} + \bar{F}S \tag{7a}$$

Divide by S and let $(1-\phi)\rho_p = \rho_2$

$$\frac{\partial(\rho_2 u_p)}{\partial t} + \frac{1}{S} \frac{\partial(\rho_2 S u_p^2)}{\partial x} = - \Gamma_c u_p - (1-\phi) \frac{\partial \tau_p}{\partial x} + \bar{F} \tag{7b}$$

Now expand the partial derivatives:

$$\rho_2 \frac{\partial u_p}{\partial t} + u_p \frac{\partial \rho_2}{\partial t} + \frac{1}{S}\left[2\rho_2 S u_p \frac{\partial u_p}{\partial x} + \rho_2 u_p^2 \frac{\partial S}{\partial x} + S u_p^2 \frac{\partial \rho_2}{\partial x}\right]$$

$$= - \Gamma_c u_p - (1-\phi) \frac{\partial \tau_p}{\partial x} + \bar{F} \qquad (7c)$$

To further simplify Eq. (7c), multiply the solid phase continuity Eq. (4) by u_p.

$$u_p \frac{\partial \rho_2}{\partial t} = - \rho_2 u_p \frac{\partial u_p}{\partial x} - u_p^2 \frac{\partial \rho_2}{\partial x} - \frac{\rho_2 u_p^2}{S} \frac{\partial S}{\partial x} - \Gamma_c u_p \qquad (4^*)$$

Subtract Eq. (4*) from Eq. (7c) to get

$$\rho_2 \frac{\partial u_p}{\partial t} + \rho_2 u_p \frac{\partial u_p}{\partial x} = - (1-\phi) \frac{\partial \tau_p}{\partial x} + \bar{F} \qquad (7d)$$

Divide by ρ_2 and rearrange terms:

$$\boxed{\frac{\partial u_p}{\partial t} = - u_p \frac{\partial u_p}{\partial x} - \frac{(1-\phi)}{\rho_2} \frac{\partial \tau_p}{\partial x} + \frac{\bar{F}}{\rho_2}} \qquad (8)$$

Conservation of Energy

(a) Gas Phase Energy Balance

The first law of thermodynamics for a control volume provides that

$$\rho_g A_g q_e = F u_p S + \Phi S + \frac{\partial}{\partial t}[\rho_g A_g (E_g + u_g^2/2)] + \frac{\partial}{\partial x}\left[\rho_g A_g \left(E_g + \frac{u_g^2}{2} + \frac{p_g}{\rho_g}\right) u_g\right]$$

$$- \Gamma_c S \left[E_g^{chem} + \frac{u_p^2}{2}\right] \qquad (9)$$

Note: 1. The walls are neglected as a source or sink of gas.

2. $E_g = \int c_v dT = c_v T$ (calorically perfect gas)

3. $q_e = \frac{\partial}{\partial x}\left(-K \frac{\partial T}{\partial x}\right)$ (heat conduction)

4. E_g^{chem} = heat of combustion

5. $\Gamma_c S \frac{u_p^2}{2}$ = kinetic energy added because gases are generated with the velocity u_p.

6. Φ = interphase energy transfer from gas to particles and interphase dissipation work

$$= \dot{q}_{pg} + \frac{\partial}{\partial x}\{\tau_{xx} u_g (1-\alpha)\}$$

$$\dot{q}_{pg} = h(T_g - T_p)(1-\alpha)(S/V)_p$$

To simplify Eq. (9), substitute $A_g = \phi S$ and divide by S.

$$\phi \rho_g q_e = F u_p + \Phi + \frac{\partial}{\partial t}\left[\phi \rho_g \left(E_g + \frac{u_g^2}{2}\right)\right] + \frac{1}{S}\frac{\partial}{\partial x}\left[\phi \rho_g S \left(E_g + \frac{u_g^2}{2} + \frac{p_g}{\rho_g}\right) u_g\right] - \Gamma_c \left[E_g^{chem} + \frac{u_p^2}{2}\right] \tag{9a}$$

Let $\rho_1 = \phi \rho_g$ and expand terms.

$$\rho_1 q_e = F u_p + \Phi + \rho_1 \frac{\partial}{\partial t}\left(E_g + \frac{u_g^2}{2}\right) + \left(E_g + \frac{u_g^2}{2}\right)\frac{\partial \rho_1}{\partial t} + \frac{1}{S}\left\{\rho_1 u_g S \frac{\partial}{\partial x}\left(E_g + \frac{u_g^2}{2} + \frac{P_g}{\rho_g}\right) + \rho_1 u_g \left(E_g + \frac{u_g^2}{2} + \frac{P_g}{\rho_g}\right)\frac{\partial S}{\partial x} + \rho_1 S \left(E_g + \frac{u_g^2}{2} + \frac{P_g}{\rho_g}\right)\frac{\partial u_g}{\partial x} + u_g S \left(E_g + \frac{u_g^2}{2} + \frac{P_g}{\rho_g}\right)\frac{\partial \rho_1}{\partial x}\right\} - \Gamma_c \left[E_g^{chem} + \frac{u_p^2}{2}\right] \tag{9b}$$

Divide by ρ_1 and form substantial derivatives

$$q_e = \frac{Fu_p}{\rho_1} + \frac{\Phi}{\rho_1} + \frac{D}{Dt}\left(E_g + \frac{u_g^2}{2}\right) + u_g \frac{\partial}{\partial x}\left(\frac{P_g}{\rho_g}\right)$$

$$+ \frac{(E_g + u_g^2/2)}{\rho_1} \frac{D\rho_1}{Dt} + \frac{u_g P_g}{\rho_1 \rho_g} \frac{\partial \rho_1}{\partial x} - \frac{\Gamma_c}{\rho_1}\left[E_g^{chem} + \frac{u_g^2}{2}\right]$$

$$+ \frac{u_g}{S}\left(E_g + \frac{u_g^2}{2} + \frac{P_g}{\rho_g}\right)\frac{\partial S}{\partial x} + \left(E_g + \frac{u_g^2}{2} + \frac{P_g}{\rho_g}\right)\frac{\partial u_g}{\partial x} \qquad (9c)$$

In order to further simplify Eq. (9c), multiply the gas continuity Eq. (2) by $\frac{(E_g + u_g^2/2)}{\rho_1}$ to get

$$\frac{\left(E_g + \frac{u_g^2}{2}\right)}{\rho_1}\frac{D\rho_1}{Dt} = -\left(E_g + \frac{u_g^2}{2}\right)\frac{\partial u_g}{\partial x} - \left(E_g + \frac{u_g^2}{2}\right)\frac{u_g}{S}\frac{\partial S}{\partial x} + \frac{(E_g + u_g^2/2)}{\rho_1}\Gamma_c \qquad (2^{**})$$

(Remember it is now assumed that $\Gamma_w = 0$.)

Now add Eq. (2**) to Eq. (9c)

$$q_e = \frac{Fu_p}{\rho_1} + \frac{\Phi}{\rho_1} + \frac{D}{Dt}\left(E_g + \frac{u_g^2}{2}\right) + u_g \frac{\partial}{\partial x}\left(\frac{P_g}{\rho_g}\right) + \frac{u_g P_g}{\rho_1 \rho_g}\frac{\partial \rho_1}{\partial x}$$

$$- \frac{\Gamma_c}{\rho_1}\left(E_g^{chem} + \frac{u_p^2}{2} - E_g - \frac{u_g^2}{2}\right) + \frac{u_g P_g}{S\rho_g}\frac{\partial S}{\partial x} + \frac{P_g}{\rho_g}\frac{\partial u_g}{\partial x} \qquad (9d)$$

Now multiply the gas momentum Eq. (6) by u_g to get:

$$u_g \frac{Du_g}{Dt} = - \frac{u_g \phi}{\rho_l} \frac{\partial P}{\partial x} + \frac{\Gamma_c u_g}{\rho_l} (u_p - u_g) - \frac{u_g \overline{F}}{\rho_l} \tag{6*}$$

Add Eq. (6*) to Eq. (9d) and rearrange to get:

$$\frac{D(E_g)}{Dt} = \frac{F(u_g - u_p)}{\rho_l} - \frac{\Phi}{\rho_l} + q_e + \frac{\Gamma_c}{\rho_l} \left(E_g^{chem} + \frac{u_p^2}{2} \right)$$

$$- \frac{\Gamma_c}{\rho_l} \left(E_g - \frac{u_g^2}{2} + u_g u_p \right) - \frac{u_g P_g}{S \rho_g} \frac{\partial S}{\partial x} - \frac{P_g}{\rho_g} \frac{\partial u_g}{\partial x}$$

$$- u_g P_g \frac{\partial}{\partial x} \left(\frac{1}{\rho_g} \right) - \frac{u_g P_g}{\rho_l \rho_g} \frac{\partial \rho_l}{\partial x} \tag{9e}$$

The last two terms can be combined as follows:

$$- u_g P_g \frac{\partial}{\partial x} \left(\rho_g^{-1} \right) = \frac{u_g P_g}{\rho_g^2} \frac{\partial \rho_g}{\partial x}$$

$$- \frac{u_g P_g}{\rho_l \rho_g} \frac{\partial \rho_l}{\partial x} = - \frac{u_g P_g \phi}{\phi \rho_g \rho_g} \frac{\partial \rho_g}{\partial x} - \frac{u_g P_g}{\rho_l} \frac{\partial \phi}{\partial x}$$

Rewrite Eq. (9e), substituting for q_e and Φ.

$$\frac{\partial E_g}{\partial t} = - u_g \frac{\partial E_g}{\partial x}$$

$$- \frac{P_g}{\rho_g} \frac{\partial u_g}{\partial x}$$

$$- \frac{u_g P_g}{S\rho_g} \frac{\partial S}{\partial x}$$

$$- \frac{u_g P_g}{\rho_l} \frac{\partial \phi}{\partial x}$$

$$+ \frac{F(u_g - u_p)}{\rho_l}$$

$$- \frac{1}{\rho_l} \frac{\partial}{\partial x} \{\tau_{xx} u_g \phi\}$$

$$- \frac{\bar{h}(T_g - T_s)\phi}{\rho_l} \left(\frac{S}{V}\right)_p$$

$$+ \frac{1}{\rho_l} \frac{\partial}{\partial x} \left(-k \frac{\partial T}{\partial x}\right)$$

$$+ \frac{\Gamma_c}{\rho_l} \left(E_g^{chem} - \frac{u_p^2}{2}\right)$$

$$- \frac{\Gamma_c}{\rho_l} \left(E_g - \frac{u_g^2}{2} + u_g u_p\right) \qquad (10)$$

The heat conduction term was deleted in the code used here because it was negligible compared to other forms of heat transfer.

(b) Solid Phase Energy Balance

Expressed in a form similar to the gas phase, the solid phase energy balance is

$$\rho_p A_p \dot{q}_p = - Fu_p S - \Phi S + \frac{\partial}{\partial t}\left[\rho_p A_p (E_p + u_p^2/2)\right] + \frac{\partial}{\partial x}\left[\rho_p A_p u_p \left(E_p + \frac{u_p^2}{2} + \frac{P_g}{\rho_p}\right)\right] - \Gamma_c S\left[E_p^{chem} - \frac{u_p^2}{2}\right] \qquad (11)^*$$

Note the signs on the terms $Fu_p S$ and ΦS are opposite those in the gas phase energy equation because the overall mixture equation (gas + solid) cannot have such source terms. For this derivation the following form for the particle enthalpy has been assumed.

$$H_p = E_p + \frac{u_p^2}{2} + \frac{P_g}{\rho_p}$$

That is, the "continuum" particles act like a gas.

To simplify Eq. (11), substitute $A_p = (1-\phi)S$ and divide by S.

$$\rho_p(1-\phi)\dot{q}_p = - Fu_p - \Phi + \frac{\partial}{\partial t}\left[\rho_p(1-\phi)(E_p + u_p^2/2)\right] - \frac{1}{S}\frac{\partial}{\partial x}\left[\rho_p(1-\phi)Su_p\left(E_p + \frac{u_p^2}{2} + \frac{P_g}{\rho_p}\right)\right] - \Gamma_c\left[E_p^{chem} - \frac{u_p^2}{2}\right] \qquad (11a)$$

Let $\rho_2 \equiv (1-\phi)\rho_p$ and expand terms.

---

*Generally, E_p^{chem} would be a negative number, representing the latent heat of the solid.

$$\rho_2 \dot{q}_p = - Fu_p - \Phi + \rho_2 \frac{\partial}{\partial t}\left(E_p + \frac{u_p^2}{2}\right) + \left(E_p + \frac{u_p^2}{2}\right)\frac{\partial \rho_2}{\partial t}$$
$$+ \rho_2 u_p \frac{\partial}{\partial x}\left(E_p + \frac{u_p^2}{2} + \frac{P_g}{\rho_p}\right) + \frac{\rho_2 u_p}{S}\left(E_p + \frac{u_p^2}{2} + \frac{P_g}{\rho_p}\right)\frac{\partial S}{\partial x}$$
$$+ u_p\left(E_p + \frac{u_p^2}{2} + \frac{P_g}{\rho_p}\right)\frac{\partial \rho_2}{\partial x} + \rho_2\left(E_p + \frac{u_p^2}{2} + \frac{P_g}{\rho_p}\right)\frac{\partial u_p}{\partial x}$$
$$- \Gamma_c\left[E_p^{chem} - \frac{u_p^2}{2}\right] \qquad (11b)$$

Rearrange terms to get substantial derivatives.

$$\rho_2 q_p = - Fu_p - \Phi + \rho_2 \frac{D(E_p + u_p^2/2)}{Dt} + \left(E_p + \frac{u_p^2}{2}\right)\frac{D\rho_2}{Dt}$$
$$+ \rho_2 u_p \frac{\partial}{\partial x}\left(\frac{P_g}{\rho_p}\right) + u_p \frac{P_g}{\rho_p}\frac{\partial \rho_2}{\partial x} - \Gamma_c\left(E_p^{chem} - \frac{u_p^2}{2}\right)$$
$$+ \frac{\rho_2 u_p}{S}\left(E_p + \frac{u_p^2}{2} + \frac{P_g}{\rho_p}\right)\frac{\partial S}{\partial x} + \rho_2\left(E_p + \frac{u_p^2}{2} + \frac{P_g}{\rho_p}\right)\frac{\partial u_p}{\partial x} \qquad (11c)$$

To further simplify this equation multiply the solid phase continuity Eq. (4) by $(E_p + u_p^2/2)$.

$$(E_p + u_p^2/2)\frac{D\rho_2}{Dt} = - \rho_2 (E_p + u_p^2/2)\frac{\partial u_p}{\partial x} - \frac{\rho_2 u_p}{S}(E_p + u_p^2/2)\frac{\partial S}{\partial x} - \Gamma_c (E_p + u_p^2/2) \qquad (4^{**})$$

Add Eq. (4**) to Eq. (11c).

$$\rho_2 \dot{q}_p = - Fu_p - \Phi + \rho_2 \frac{D}{Dt}(E_p + u_p^2/2) - \frac{\rho_2 P_g}{\rho_p}\frac{\partial u_p}{\partial x}$$

$$+ \rho_2 u_p \frac{\partial}{\partial x}\left(\frac{P_g}{\rho_p}\right) + u_p\left(\frac{P_g}{\rho_p}\right)\frac{\partial \rho_2}{\partial x} - \Gamma_c\left[E_p + E_p^{chem}\right]$$

$$+ \frac{\rho_2 u_p P_g}{S\rho_p}\frac{\partial S}{\partial x} \qquad (11d)$$

This equation can be further simplified by multiplying the solid phase momentum Eq. (8) by $\rho_2 u_p$.

$$\rho_2 u_p \frac{Du_p}{Dt} = - (1-\phi)u_p \frac{\partial \tau_p}{\partial x} + \bar{F}u_p \qquad (8^*)$$

Now add Eq. (8*) to Eq. (11d).

$$\rho_2 \dot{q}_p = - \Phi + \rho_2 \frac{DE_p}{Dt} + \frac{\rho_2 P_g}{\rho_p}\frac{\partial u_p}{\partial x}$$

$$+ \frac{u_p P_g}{\rho_p}\frac{\partial \rho_2}{\partial x} + (1-\phi)u_p \frac{\partial P_g}{\partial x} - (1-\phi)u_p \frac{\partial \tau_p}{\partial x}$$

$$- \Gamma_c\left[E_p + E_p^{chem}\right] + \frac{\rho_2 u_p P_g}{S\rho_p}\frac{\partial S}{\partial x} \qquad (11e)$$

Rearrange terms, remembering that $\frac{\partial}{\partial x}\left(\frac{1}{\rho_p}\right) = 0$ and assuming $\dot{q}_p = 0$.

$$\frac{\partial E_p}{\partial t} = - u_p \frac{\partial E_p}{\partial x}$$

$$- \frac{(1-\phi)P_g}{\rho_2} \frac{\partial u_p}{\partial x}$$

$$- \frac{u_p P_g}{\rho_2} \frac{\partial (1-\phi)}{\partial x}$$

$$- \frac{(1-\phi)u_p}{\rho_2} \frac{\partial P_g}{\partial x}$$

$$+ \frac{(1-\phi)u_p}{\rho_2} \frac{\partial \tau_p}{\partial x}$$

$$+ \frac{\Gamma_c}{\rho_2}\left[E_p + E_p^{chem}\right]$$

$$- \frac{u_p P_g}{S\rho_p} \frac{\partial S}{\partial x}$$

$$+ \frac{\Phi}{\rho_2} \qquad (12)$$

An alternate form of the particle phase energy equation can be derived by assuming $H_p = E_p + u_p^2/2$. With this assumption the particle phase energy balance is

$$\rho_p A_p \dot{q}_p = - Fu_p S - \Phi_p S + \frac{\partial}{\partial t}[\rho_p A_p (E_p + u_p^2/2)]$$

$$+ \frac{\partial}{\partial x}[\rho_p A_p u_p (E_p + u_p^2/2)] - \Gamma_c S[E_p^{chem} - u_p^2/2] \qquad (13)$$

Substitute $A_p = (1-\phi)S$, $\rho_2 \equiv (1-\phi)\rho_p$, divide by S and expand terms.

$$\rho_2 \dot{q}_p = - F u_p - \Phi_p + \rho_2 \frac{\partial (E_p + u_p^2/2)}{\partial t}$$

$$+ (E_p + u_p^2/2) \frac{\partial \rho_2}{\partial t} + \rho_2 u_p \frac{\partial (E_p + u_p^2/2)}{\partial x}$$

$$+ \rho_2 (E_p + u_p^2/2) \frac{\partial u_p}{\partial x} - \rho_2 u_p \frac{(E_p + u_p^2/2)}{S} \frac{\partial S}{\partial x}$$

$$+ u_p (E_p + u_p^2/2) \frac{\partial \rho_2}{\partial x} - \Gamma_c [E_p^{chem} - u_p^2/2] \qquad (13a)$$

Once again simplify by adding Eq. (4**) to Eq. (13a).

$$\rho_2 \dot{q}_p \approx - F u_p - \Phi_p + \rho_2 \frac{DE_p}{Dt} + \rho_2 u_p \frac{Du_p}{Dt} - \Gamma_c [E_p + E_p^{chem}] \qquad (13b)$$

Simplify further by adding Eq. (8*) to Eq. (13b).

$$\rho_2 \dot{q}_p \approx - \Phi_p + \rho_2 \frac{DE_p}{Dt} - (1-\phi) u_p \frac{\partial \tau_p}{\partial x} - \Gamma_c [E_p + E_p^{chem}]$$

Rearrange terms with $\dot{q}_p = 0$ to get the following result.

$$\frac{\partial E_p}{\partial t} \approx - u_p \frac{\partial E_p}{\partial x} + \frac{(1-\phi) u_p}{\rho_2} \frac{\partial \tau_p}{\partial x} + \frac{\Gamma_c}{\rho_2} [E_p + E_p^{chem}] + \frac{\Phi_p}{\rho_2} \qquad (14)$$

A third form of the particle phase energy equation can be derived from the assumption $H_p = E_p$. With this assumption a drop in the particle kinetic energy cannot change the particle temperature. The solid phase energy balance is

$$\rho_p A_p \dot{q}_p = - Fu_p S - \Phi_p S + \frac{\partial}{\partial t} [\rho_p A_p E_p]$$

$$+ \frac{\partial}{\partial x} [\rho_p A_p u_p E_p] - \Gamma_c S[E_p^{chem} - u_p^2/2] \qquad (15)$$

Substitute $A_p = (1-\phi)S, \rho_2 \equiv (1-\phi)\rho_p$, divide by S and expand terms.

$$\rho_2 \dot{q}_p = - Fu_p - \Phi_p + \rho_2 \frac{\partial E_p}{\partial t} + E_p \frac{\partial \rho_2}{\partial t} + \rho_2 u_p \frac{\partial E_p}{\partial s}$$

$$+ \rho_2 E_p \frac{\partial u_p}{\partial x} + \frac{\rho_2 u_p E_p}{S} \frac{\partial S}{\partial x} + u_p E_p \frac{\partial \rho_2}{\partial x}$$

$$- \Gamma_c [E_p^{chem} - u_p^2/2] \qquad (15a)$$

Simplify by multiplying the particle continuity equation by E_p.

$$E_p \frac{D\rho_2}{Dt} = - \rho_2 E_p \frac{\partial u_p}{\partial x} - \frac{\rho_2 u_p E_p}{S} \frac{\partial S}{\partial x} - E_p \Gamma_c \qquad (4***)$$

Add Eq. (4***) to Eq. (15a)

$$\rho_2 \dot{q}_p = - Fu_p - \Phi_p + \rho_2 \frac{DE_p}{Dt} - \Gamma_c [E_p^{chem} + E_p - u_p^2/2] \qquad (15b)$$

Divide by ρ_2 and rearrange terms.

$$\frac{\partial E_p}{\partial t} = - u_p \frac{\partial E_p}{\partial x} + \frac{F u_p}{\rho_2} + \frac{\Gamma_c}{\rho_2}[E_p + E_p^{chem} - u_p^2/2] + \frac{\Phi_p}{\rho_2} \qquad (16)$$

It was not necessary to use the particle phase momentum equation to put this last form of the energy equation in operator form.

Notice that the three forms of the particle energy equation (Eqs. 12, 14, 16) are significantly different!

APPENDIX B: CONSTITUTIVE RELATIONS

As stated in Chapter Two the solution of the conservation equations requires some knowledge of the physical laws that govern the rate and interaction processes involved. In some cases use of these laws was extrapolated to areas not within their stated domain. The applicability of some of these laws is discussed by Krier and Van Tassell.[1]

A general criterion for particle ignition assumes ignition to have occurred when the surface temperature of a particle reaches a critical value. In order to determine the surface temperature, Kuo et al.[22] solve the heat conduction equation for the particle and do not employ a particle energy equation. Although this approach may define ignition appropriately, Krier[7] argues strongly that any separated flow model must satisfy a mixture energy equation which is the sum of separate phase energy equations (Eqs. 10, 12). To predict ignition he expresses a solid phase energy balance (Eq. 11) and defines a mean "bulk temperature," as being an average temperature of the solid. Ignition occurs when this "bulk temperature" reaches a critical value called T_{ign} which is less than the surface critical temperature. This latter approach was taken here and a value of 560°R for T_{ign} was used.

The convective heat transfer between the hot gases and the solid particles was described using Denton's formula.[32] That is

$$\bar{h}_{gp} = 0.65\left(\frac{K_g}{d_p}\right)\left[\frac{\rho_g|u_p - u_g|\phi d_p}{\mu_g}\right]^{0.7} \cdot P_r^{0.33} \qquad (B.1)$$

There is some question whether the same formula should be used for inter-phase heat transfer before and after ignition of the particles. It seems reasonable

to believe that the flow field around burning particles differs from that around inert particles, and that these differences act to change (reduce) heat transfer. Because of this effect on the boundary layer by the generation process, the above heat transfer coefficient was reduced after ignition, usually to 10% of its actual value.

Two laws for drag between the particles and gases were used. One was Ergun's correlation[33]

$$\overline{F} = \frac{\rho_g (u_g - u_p)\left|u_g - u_p\right| (1-\phi)}{d_p \phi}\left[\frac{150(1-\phi)}{Re_p} + 1.75\right] \quad (B.2)^*$$

and the other was a correlation devised by Kuo and Nydegger[34]

$$\overline{F} = \frac{\mu (u_g - u_p)(1-\phi)^2}{d_p^2 \phi}\left[276.23 + 5.05\left(\frac{Re_p}{1-\phi}\right)^{.87}\right] \quad (B.3)$$

Here the Reynold's number, Re_p, was calculated based on the radius of a solid particle.

$$Re_p = \frac{2 r_p \rho_g \phi \left|u_p - u_g\right|}{\mu_g} \quad (B.4$$

In the course of this work it proved desirable to reduce both of these drag laws by a constant fraction. Justification for this reduction is based on the application of these laws to regions outside their stated domain, use of three dimensional laws to a one-dimensional problem, and uncertainty in the correct gas viscosity.

For the burning rate law the simple pressure dependent relation was employed.

$$\dot{r} = b_1 + b_2 (P_g)^n \quad (B.5)$$

---

*Eq. (B.2) therefore defines $f_{gp} = \overline{F}/(u_g - u_p)$.

The production rate of gases from solid particles, per total volume of the bed, is therefore given by

$$\Gamma_g = (1-\phi)\rho_p \dot{r}\left(\frac{S}{V}\right)_p = \frac{(1-\phi)\rho_p \dot{r}}{d_p/6} \tag{B.6}$$

where $\left(\frac{S}{V}\right)_p$ is the surface area to volume ratio for a single particle.

The expression for axial normal stress between particles was that used by Kuo and Summerfield,[17] that is

$$-\tau_p = \begin{cases} (1-\phi)^{-1}\{K[(1-\phi_c)^{-1} - (1-\phi)^{-1}]\} & \text{if } \phi \leq \phi_c \\ 0 & \text{if } \phi > \phi_c \end{cases} \tag{B.7}$$

where $\phi_c = .4$ and $K = 6.94 \times 10^4$ lbf/in^2. The constant, ϕ_c, is a critical porosity above which the particles do not touch.

The last relation of concern in the program has to do with the variation of viscosity with temperature. Ideally, a relation using both temperature and pressure should be used since with the extremely high pressure encountered it is natural to assume that viscosity would be affected. Unfortunately no such relation could be found. Two expressions were employed which vary viscosity as a function of temperature alone. They are

$$\mu = \mu_o\left(\frac{T_g}{T_o}\right)^{.65}$$

and

$$\mu = \mu^* \frac{(T_g/537)^{1.5}}{(T_g+198)} \tag{B.8}$$

where μ_o and T_o are viscosity and temperature at initial conditions and μ^* is not a viscosity but a parameter with units of lbm - °R/in-sec. When

calculating a heat transfer coefficient between gas and particles, an average temperature $[(T_g + T_p)/2]$ was used instead of just T_g in the second expression to calculate an appropriate viscosity.

APPENDIX C: CALCULATION OF THE SOUND SPEED IN THE TWO-PHASE MIXTURE

In order to calculate the sound speed of the mixture, the sound speed in each phase must be known.

Convention: 1 - indicates gas phase

2 - solid phase

$$C_1 = \sqrt{\gamma RT}$$

$$= \sqrt{1.25 \left\{ \frac{1.9869 \frac{\text{BTU}}{\text{lb-mole } ^\circ\text{R}}}{22.6 \frac{\text{lbm}}{\text{lb-mole}}} \right\} 5960^\circ\text{R} \left(9336 \frac{\text{in-lbf}}{\text{BTU}} \right) 386 \frac{\text{lbm-in}}{\text{lbf-sec}^2}}$$

$$= 48{,}572 \text{ in/sec}$$

$$C_2 = \sqrt{K_2/\rho_2}$$

$$= \sqrt{\frac{200 \times 10^3 \frac{\text{lbf}}{\text{in}^2}}{.571 \times 10^{-1} \frac{\text{lbm}}{\text{in}^2}} \left(386 \frac{\text{lbm-in}}{\text{lbf-sec}^2} \right)}$$

$$= 36{,}770 \text{ in/sec}$$

$$\rho_1 \approx 1.0 \times 10^{-2} \text{ lbm} \qquad \rho_2 \approx .571 \times 10^{-1} \text{ lbm}$$

$$\alpha = \frac{V_2}{V_{\text{total}}} = 1-\phi = .6 \qquad 1-\alpha = \frac{V_1}{V_{\text{total}}} = \phi = .4$$

Now the sound speed of the mixture can be calculated using the following formula from Wallis [8].

$$\frac{1}{C^2} = \left[\alpha\rho_2 + (1-\alpha)\rho_1\right]\left[\frac{\alpha}{\rho_2 C_2^2} - \frac{1-\alpha}{\rho_1 C_1^2}\right]$$

$$= 9.46 \times 10^{-10} \text{ sec}^2/\text{in}^2$$

$$C = 32{,}500 \text{ in/sec}$$

UNIVERSITY OF ILLINOIS

RECENT AERONAUTICAL AND ASTRONAUTICAL
ENGINEERING DEPARTMENT TECHNICAL REPORTS

Technical Report Number	Title	Author	Journal Publication
AAE 62-1	An Introduction to Viscoelastic Analysis	H. H. Hilton	Engineering Design for Plastics, Reinhold Publ. Corp., N.Y., 199-276 (1964).
AAE 62-2	A Method of Characteristics Analysis of Detonation Stability	R. A. Strehlow	
AAE 63-1	On Non-Stationary White Noise	Y. K. Lin	J. Acoust. Soc. Amer. 36:82-84 (1964).
AAE 63-2	Formulation and Evaluation of Approximate Analogies for Transient Temperature Dependent Linear Viscoelastic Media	H. H. Hilton and J. R. Clements	Proc. Conf. on Thermal Loading and Creep, Inst. Mech. Eng., London, 6.17-6.24(1964).
AAE 63-3	Free Vibrations of Continuous Skin-Stringer Panels with Non-Uniform Stringer Spacing and Panel Thickness	Y. K. Lin, T. J. McDaniel, B. K. Donaldson, C. F. Vail and W. J. Dwyer	AFML-TR-64-347, Wright-Patterson AFB (1965).
AAE 64-1	Random Vibrations of a Myklestad Beam	Y. K. Lin	AIAA J., 2:1448-1451 (1964).
AAE 64-2	On Detonation Initiation	R. A. Strehlow	AIAA J., 2:783-784 (1964).
AAE 64-3	A Theoretical Investigation of a Restrictive Model for Detonation Initiation	R. B. Gilbert	AIAA J., 4:1777-1783 (1966).

RECENT AERONAUTICAL AND ASTRONAUTICAL ENGINEERING DEPARTMENT TECHNICAL REPORTS (continued)

Technical Report Number	Title	Author	Journal Publication
AAE 64-4	Transfer Matrix Representation of Flexible Airplanes in Gust Response Study	Y. K. Lin	J. of Aircraft, 2:116-121 (1965).
AAE 64-5	Dynamic Characteristics of Continuous Skin-Stringer Panels	Y. K. Lin	Acoustical Fatigue in Aerospace Structures, Syracuse Univ. Press, 163-184 (1965).
AAE 64-6	Experimental Study of the Growth of Transverse Waves in Detonations	R. Liaugminas	See AAE 66-3
AAE 64-7	Nonstationary Excitation and Response in Linear Systems Treated as Sequences of Random Pulses	Y. K. Lin	Journal of the Acoustical Society of America, 38: 453-460 (1965).
AAE 65-1	Transverse Waves in Detonations	R. A. Strehlow and F. Dan Fernandes	Combustion and Flame, 9:109-119 (1965).
AAE 65-2	A Summary of Linear Viscoelastic Stress Analysis	H. H. Hilton	Solid Rocket Structural Integrity Abstracts, 2: 1-56 (1965).
AAE 65-3	Approximate Correlation Function and Spectral Density of the Random Vibration of an Oscillator with Non-Linear Damping	Y. K. Lin	AFMK-TR-66-62, Wright Patterson AFB (1966).
AAE 65-4	Investigation of the Flow Properties Downstream of a Shock Wave Propagating into a Convergent Duct	R. E. Cusey	See AAE 65-6

AD-A049 499 ILLINOIS UNIV AT URBANA-CHAMPAIGN DEPT OF AERONAUTICA--ETC F/G 21/9.2
MODELING OF CONVECTIVE MODE COMBUSTION THROUGH GRANULATED PROPE--ETC(U)
OCT 77 H KRIER, J A KEZERLE AFOSR-77-3115

UNCLASSIFIED AAE-77-17 AFOSR-TR-78-0007 NL

2 OF 2
AD
A049499

END
DATE FILMED
3-78
DDC

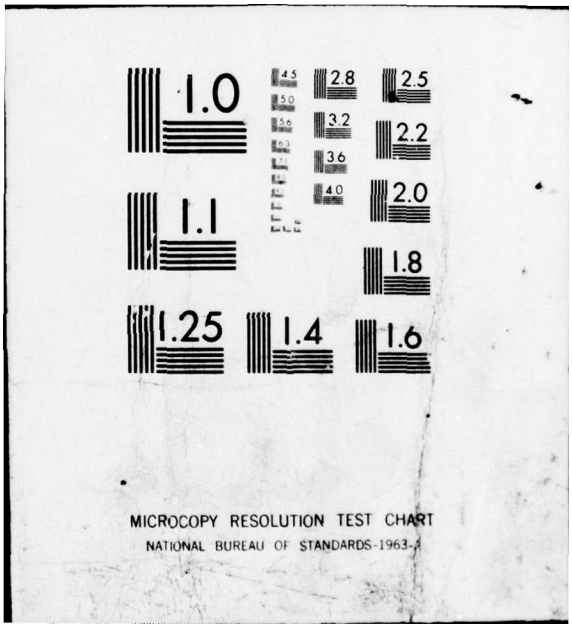
1.0
1.1
1.25
1.4
1.6
1.8
2.0
2.2
2.5
2.8
3.2
3.6
4.0
4.5
5.0
5.6
MICROCOPY RESOLUTION TEST CHART
NATIONAL BUREAU OF STANDARDS-1963-A

RECENT AERONAUTICAL AND ASTRONAUTICAL ENGINEERING DEPARTMENT TECHNICAL REPORTS (continued)

Technical Report Number	Title	Author	Journal Publication
AAE 65-5	A Method for the Determination of the Matrix of Impulse Response Functions with Special Reference to Applications in Random Vibration Problems	Y. K. Lin	AFFDL-TR-66-80, Wright Patterson AFB, 743-751 (1966).
AAE 65-6	Convergent Channel Shock Tube for Detonation Initiation Studies	A. J. Crooker	"Detonation and Initiation Behind an Accelerating Shock Wave" by R. A. Strehlow, A. J. Crooker, R. E. Cusey, Comb and Flame, 11:339-351 (1967).
AAE 66-1	A Comparison of Experimental and Theoretical Transverse Wave Spacings in Detonation	R. H. Watson	See AAE 66-3
AAE 66-2	A Simple Model for the Mechanism of Detonation	J. R. Eyman	See AAE 66-3
AAE 66-3	Transverse Wave Structure in Detonations	R. A. Strehlow, R. Liaugminas, R. H. Watson and J. R. Eyman	11th Symposium (International) on Combustion, Mono Book Corp. Baltimore, Md., (1967).
AAE 66-4	A Real Gas Analysis Using an Acoustic Model for the Transverse Wave Spacing in Detonations	R. E. Maurer	AIAA Journal, 7: 323-328, (1969).
AAE 67-1	Shock Tube Studies in Exothermic Systems	R. A. Strehlow	Phys. Fluids, 12: 96-100, (1969).

RECENT AERONAUTICAL AND ASTRONAUTICAL ENGINEERING DEPARTMENT TECHNICAL REPORTS (continued)

Technical Report Number	Title	Author	Journal Publication
AAE 67-2	Shock Tube Chemistry	R. A. Strehlow	Progress in High Temperature Physics and Chemistry, Pergamon Press, N.Y., 2: 127-176 (1968).
AAE 67-3	Structural Failure Criteria for Solid Propellants Under Multiaxial Stresses	A. R. Zak	J. Spacecraft, 5: 265-269 (1968)
AAE 67-4	Structural Analysis of Realistic Solid Propellant Materials	A. R. Zak	J. Spacecraft, 5: 270-275 (1968).
AAE 67-5	Characteristics of Transverse Waves in Detonations of H_2, C_2H_2, C_2H_4 and CH_4 - Oxygen Mixtures	C. D. Engel	AIAA Journal, 7: 492-496 (1969).
AAE 68-1	A Review of Shock Tube Chemistry	R. A. Strehlow	Progress in High Temperature Physics and Chemistry, Pergamon Press, N.Y., 2: 1-146 (1969).
AAE 68-2	On the Interpretation of Molecular Beam Data	A. Klavins	A. Klavins and L. H. Sentman Rev. Sci. Instr., 41: 1560-1567 (1970).
AAE 68-3	Detonative Mach Stems	R. A. Strehlow H. O. Barthel	
AAE 68-4	On the Strength of Transverse Waves and Geometrical Detonation Cell Model for Gas Phase Detonations	J. R. Biller	R. A. Strehlow and J. R. Biller Comb. and Flame, 13: 577-582, (1970).
AAE 68-5	The MISTRESS User Manual	H. H. Hilton	
AAE 69-1	The Chemical Shock Tube - Implications of Flow Non-Idealities	R. A. Strehlow R. L. Belford	

RECENT AERONAUTICAL AND ASTRONAUTICAL ENGINEERING DEPARTMENT TECHNICAL REPORTS (continued)

Technical Report Number	Title	Author	Journal Publication
AAE 69-2	Phenomenological Investigation of Low Mode Marginal Planar Detonations	A. J. Crooker	Acta Astronautica, 1:303-315(1974).
AAE 69-3	Multi-Dimensional Detonation Wave Structure	R. A. Strehlow	Astronautica Acta, 15:345-358(1970).
AAE 69-4	An Experimental and Analytical Investigation of a Two-Dimensionally Stiffened Panel	A. R. Zak C. E. French	AFML-TR-68-390, Wright-Patterson AFB,(1969).
AAE 69-5	On the Kinetic Equations for a Dilute, Short Range Gas	T. J. Forster L. H. Sentman	with A.D. Grimm, Proc. Ninth International Symposium on Rarefied Gas Dynamics, A3.1-3.8 (1974).
AAE 69-6	The Sawtooth Column of the Supersonic Electric Arc in Sulfur Hexafluoride	C. E. Bond	AIAA J., 9: 510-512 (1971).
AAE 69-7	Theoretical and Experimental Analysis of Stiffened Panels Under Dynamic Conditions	A. R. Zak R. N. Yurkovich J. H. Schmidt	J. of Aircraft, 3: 149-155 (1971).
AAE 70-1	On the Interaction Between Chemical Kinetics and Gas-Dynamics in the Flow Behind a Cylindrical Detonation Front	S. Rajan	
AAE 70-2	Preliminary Studies on the Engineering Applications of Finite Difference Solutions of the Navier-Stokes Equations	W. F. Van Tassell	
AAE 70-3	Some Aspects of the Surface Boundary Condition in Kinetic Theory	A. Klavins	Proc. of International Symposium on Rarefied Gas Dynamics, Pisa, Italy (1970).

RECENT AERONAUTICAL AND ASTRONAUTICAL ENGINEERING DEPARTMENT TECHNICAL REPORTS (continued)

Technical Report Number	Title	Author	Journal Publication
AAE 70-4	A Study of the Transient Behavior of Fuel Droplets during Combustion: Theoretical Considerations for Aerodynamic Stripping	H. Krier	
AAE 70-5	On the Solid Body Model for an Accelerating Electric Arc	F. Klett	
AAE 71-1 UILU-ENG 71 0501	Detonative Mach Stems	R. A. Strehlow H. O. Barthel	
AAE 71-2 UILU-ENG 71 0502	An Investigation of Transient Phenomena in Detonations	R. J. Stiles	with R. A. Strehlow, A. A. Adamczyk, Astronautica Acta, 17: 509-527 (1972)
AAE 71-3 UILU-ENG 71 0503	On the Role of Tangential Velocity Changes in the Scattering of a Molecular Beam from A Solid Surface	C. C. Chrisman L. H. Sentman	Chemical Physics Letters, 26:407-413(197
AAE 72-1 UILU-ENG 72 0501	Unconfined Vapor Cloud Explosions - An Overview	R. A. Strehlow	Fourteenth Symposium on Combustion, 1189-1200 (1973).
AAE 72-2 UILU-ENG 72 0502	Application of Illiac IV Computer to Numerical Solutions of Structural Problems	H. H. Hilton A. R. Zak J. J. Kessler P. C. Rockenbach	
AAE 72-3 UILU-ENG 72 0503	On the Measurement of Energy Release Rates In Vapor Cloud Explosions	R. A. Strehlow L. D. Savage G. M. Vance	Combustion Science and Technology, 6: 307-312 (1972).

RECENT AERONAUTICAL AND ASTRONAUTICAL ENGINEERING DEPARTMENT TECHNICAL REPORTS (continued)

Technical Report Number	Title	Author	Journal Publication
AAE 72-4 UILU-ENG 72 0504	A Performance Comparison of Several Numerical Minimization Algorithms	J. E. Prussing	
AAE 73-1 UILU-ENG 73 0501	Stresses and Damping in the Matrix of a Composite Material	A. R. Zak	
AAE 73-2 UILU-ENG 73 0502	Early Burning Anomalies in the XM 645 Flechette Cartridge	H. Krier D. R. Hall	BRL Rept. No. 104 (1973).
AAE 73-3 UILU-ENG 73 0503	Equivalent Explosive Yield of the Explosion in the Alton Southern Gateway Yard, East St. Louis, Ill., January 22, 1972	R. A. Strehlow	
AAE 73-4 UILU-ENG 73 0504	Failure Studies of Gaseous Detonations	R. J. Salm	Acta Astronautica (in press).
AAE 73-5 UILU-ENG 73 0505	An Investigation of Hydrogen-Oxygen-Argon Detonations	J. R. Biller	
AAE 73-6 UILU-ENG 73 0506	Interior Ballistic Predictions Using Data From Closed and Variable-Volume Simulators	H. Krier S. A. Shimpi M. J. Adams	Proc. 11th JANNAF Combustion Meeting, CPIA Publ. 261:17-30(1974).
AAE 73-7 UILU-ENG 73 0507	Theory of Rotationally Symmetric Laminar Premixed Flames	G. M. Vance H. Krier	Comb. and Flame J., 22: 365-375 (1974).
AAE 73-8 UILU-ENG 73 0508	Burning of Fuel Droplets at Elevated Pressures	J. H. Rush H. Krier	Comb. and Flame J., 22: 377-382 (1974).
AAE 73-9 UILU-ENG 73 0509	An Impact Ignition Model for Solid Propellants	H. Krier H. H. Hilton O. Olorunsola D. L. Reuss	BRL Rept. No. 1707 (1974).

RECENT AERONAUTICAL AND ASTRONAUTICAL ENGINEERING DEPARTMENT TECHNICAL REPORTS (continued)

Technical Report Number	Title	Author	Journal Publication
AAE 73-10 UILU-ENG 73 0510	Optimal Multiple-Impulse Direct Ascent Fixed-Time Rendezvous	J. E. Prussing L. R. Gross	AIAA J., 12, 885-889 (1974).
AAE 73-11 UILU-ENG 73 0511	The Structure and Stability of Detonation Waves	R. A. Strehlow	
AAE 74-1 UILU-ENG 74 0501	Model of Flame Spreading and Combustion Through Packed Beds of Propellant Grains	H. Krier W. F. Van Tassell S. Rajan J. T. Ver Shaw	BRL Report No. 147 (1974). Int. J. Heat-Mass Transfer, 1377-86 (1975).
AAE 74-2 UILU-ENG 74 0502	On the Nature of Non-Ideal Blast Waves	R. A. Strehlow A. A. Adamczyk	WSS/CI Paper No. 74-12, Pullman, Wash. (1974).
AAE 74-3 UILU-ENG 74 0503	Viscous Incompressible Flow in Spiral Channels	W. F. VanTassell	
AAE 74-4 UILU-ENG 74 0504	Frequency Response Functions of a Disordered Periodic Beam	J. N. Yang Y. K. Lin	J. Sound and Vibration 38: 317-340 (1975).
AAE 74-5 UILU-ENG 74 0505	Predicting Uniform Gun Interior Ballistics: Part I. An Analysis of Closed Bomb Testing	H. Krier S. A. Shimpi	Comb. and Flame J. 25: 229-240 (1975).
AAE 74-6 UILU-ENG 74 0506	Predicting Uniform Gun Interior Ballistics: Part II. The Interior Ballistic Code	H. Krier M. J. Adams	Proc. 11th JANNAF Comb. Meeting, CPIA Publ. 261: 17-30 (1974).
AAE 74-7 UILU-ENG 74 0507	Predicting Uniform Gun Interior Ballistics: Part III. The Concept and Design of the Dynagun Ballistic Simulator	H. Krier J. W. Black	Proc. 11th JANNAF Comb. Meeting, CPIA Publ. 261: 31-43(1974).
AAE 74-8 UILU-ENG 74 0508	Process of Fluidization During Porous Solid Propellant Combustion	H. Krier J. T. Ver Shaw	AIAA Paper 75-242 (1975).
AAE 74-9 UILU-ENG 74 0509	An Analysis of Flame Propagation Through Coal Dust-Air Mixtures	J. L. Krazinski H. Krier	AIAA Paper 74-1111 (1974).

RECENT AERONAUTICAL AND ASTRONAUTICAL ENGINEERING DEPARTMENT TECHNICAL REPORTS (continued)

Technical Report Number	Title	Author	Journal Publication
AAE 74-10 UILU-ENG 74 0510	An Interior Ballistics Prediction of the M549 Rocket Assisted Projectile	H. Krier S. Shimpi E. Meister	
AAE 75-1 UILU-ENG 75 0501	Dynamically Induced Thermal Stresses in Composite Material, Structural Panels	A. Zak W. Drysdale	
AAE 75-2 UILU-ENG 75 0502	Numerical Analysis of Laminated, Orthotropic Composite Structures	A. R. Zak	
AAE 75-3- UILU-ENG 75 0503	The Characterization and Evaluation of Accidental Explosions	R. A. Strehlow W. E. Baker	NASA CR 134779 (June 1975). Also Progr. Energy & Comb Sc. (in press).
AAE 75-4 UILU-ENG 75 0504	Program Manual for the Eppler Airfoil Inversion Program	W. G. Thomson	
AAE 75-5 UILU-ENG 75 0505	Design of High Lift Airfoils with a Stratford Distribution by the Eppler Method	W. G. Thomson	
AAE 75-6 UILU-ENG 75 0506	Prediction of Flame Spreading and Pressure Wave Propagation in Propellant Beds	H. Krier	AIAA J. (in press)
AAE 75-7 UILU-ENG 75 0507	Vigorous Ignition of Granulated Beds by Blast Impact	H. Krier S. Gokhale	Int. J. Heat-Mass Transfer (in press)
AAE 75-8 UILU-ENG 75 0508	Solid Propellant Burning Evaluation with the Dynagun Ballistic Simulator	H. Krier T. G. Nietzke M. J. Adams J. W. Black E. E. Meister	
AAE 75-9 UILU-ENG 75 0509	Structural Reliability & Minimum Weight Analysis for Combined Random Loads & Strengths	H. H. Hilton	AIAA J. (in press)

RECENT AERONAUTICAL AND ASTRONAUTICAL ENGINEERING DEPARTMENT TECHNICAL REPORTS (Continued)

Technical Report Number	Title	Author	Journal Publication
AAE 75-10 UILU-ENG 75 0510	Linear Viscoelastic Analysis with Random Material Properties	H. H. Hilton J. Hsu J. S. Kirby	
AAE 76-1 UILU-ENG 76 0501	Two Degree of Freedom Flutter of Linear Visco-elastic Wings in Two Dimensional Flow	C. F. Vail H. H. Hilton	In press AIAA J.
AAE 76-2 UILU-ENG 76 0502	An Error Analysis of Computerized Aircraft Synthesis	V. V. Volodin H. H. Hilton	In press J. of Aircraft
AAE 76-3 UILU-ENG 76 0503	Reactive Two-Phase Flow Models Applied to the Prediction of Detonation Transition in Granulated Propellant	H. Krier M. Dimitstein S. S. Gokhale	
AAE 76-4 UILU-ENG 76 0504	Transient Temperature Response of Charring Composite Slabs	J. E. Prussing H. Krier	
AAE 76-5 UILU-ENG 76 0505	Nonlinear Response of Laminated Composite Material Cylindrical Shells	A. R. Zak J. N. Craddock	
AAE 76-6 UILU-ENG 76 0506	An Investigation of Blast Waves Generated from Non-Ideal Energy Sources	A. A. Adamczyk	
AAE 77-1 UILU-ENG 77 0501	Nonlinear Dynamic Analysis of Flat Laminated Plates by the Finite Element Method	A. R. Zak	
AAE 77-2 UILU-ENG 77 0502	An Investigation of Blast Waves Generated by Constant Velocity Flames	R. T. Luckritz	
AAE 77-3 UILU-ENG 77 0503	On the Blast Waves Produced by Constant Velocity Combustion Waves	R. A. Strehlow R. D. Luckritz	
AAE 77-4 UILU-ENG 77 0504	Direct Initiation of Detonation by Non-Ideal Blast Waves	R. J. Cesarone	
AAE 77-5 UILU-ENG 77 0505	The Blast Wave Generated by Constant Velocity Flames	S. A. Shimpi R. A. Strehlow	

RECENT AERONAUTICAL AND ASTRONAUTICAL ENGINEERING DEPARTMENT TECHNICAL REPORTS (Continued)

Technical Report Number	Title	Author	Journal Publication
AAE 77-6 UILU-ENG 77 0506	Exploratory Studies of Flame and Explosion Quenching	R. A. Strehlow L. C. Sorenson L. D. Savage H. Krier	
AAE 77-7 UILU-ENG 77 0507	The Trajectory of a Liquid Droplet Injected Into the Wake of an Aircraft in Ground Effect	M. B. Bragg	
AAE 77-8 UILU-ENG 77 0508	Comparison of Viscoelastic and Structural Damping in Flutter	H. H. Hilton	
AAE 77-9 UILU-ENG 77 0509	The Blast Wave Generated by Constant Velocity Flames	R. A. Strehlow R. T. Luckritz A. A. Adamczyk S. Shimpi	
AAE 77-10 UILU-ENG 77 0510	Wind Energy: History, Economics, and the Vertical Wind Turbine	T. R. Richards	
AAE 77-11 UILU-ENG 77 0511	Final Report: Low Speed Airfoil Study	A. I. Ormsbee	
AAE 77-12 UILU-ENG 77 0512	Final Report: Propeller Study, Part I, Introduction and Overview	A. I. Ormsbee	
AAE 77-13 UILU-ENG 77 0513	Final Report: Propeller Study, Part II, The Design of Propellers for Minimum Noise	C. J. Woan	
AAE 77-14 UILU-ENG 77 0514	Final Report: Propeller Study, Part III, Experimental Determination of Thrust & Torque on the YO-3A Aircraft	S. A. Siddiqi K. R. Sivier A. I. Ormsbee	
AAE 77-15 UILU-ENG 77 0515	Direct Initiation of Detonation	R. A. Strehlow H. O. Barthel	

RECENT AERONAUTICAL AND ASTRONAUTICAL ENGINEERING DEPARTMENT TECHNICAL REPORTS (Continued)

Technical Report Number	Title	Author	Journal Publication
AAE 77-16 UILU-ENG 77 0516	The Effects of Energy Distribution Rates and Density Distribution on Blast Wave Structure	R. A. Strehlow L. H. Sentman	
AAE 77-17 UILU ENG 77 0517	Modeling of Convective Mode Combustion Through Granulated Propellant to Predict Transition to Detonation	H. Krier J. A. Kezerle	